NORTHWESTERN UNIVERSITY

Wave Chaos in Elastodynamic Scattering

A DISSERTATION
SUBMITTED TO THE GRADUATE SCHOOL
IN PARTIAL FULFILLMENT OF THE REQUIREMENTS

for the degree

DOCTOR OF PHILOSOPHY

Field of Physics

by Niels Søndergaard

EVANSTON, ILLINOIS

June 2001

ABSTRACT

Wave Chaos in Elastodynamic Scattering

Niels Søndergaard

The exact scattering resonances are calculated for a system of several cylindrical cavities in plane strain elastodynamics. A basis of scattering states is constructed and the scattering determinant is found. The high frequency limit is investigated by studying the Green's function for one cavity. In the high frequency limit the spectrum is dominated by infinitely many periodic orbits, each orbit consisting of classical particle trajectory segments with varying polarizations, and surface wave segments, with contributions of longer orbits decreasing in importance with the orbit length.

Acknowledgements

The author is grateful to the Danish Research Academy for the Ph.D. fellowship and to the Northwestern University for hospitality and partial support; to the Niels Bohr Institute for computational resources, to the administrative staff at the physics office, to his thesis advisor Predrag Cvitanović, to Andreas Wirzba for invaluable theoretical and computational insights, to Gergely Palla and Gabor Vattay for a nice stay in Budapest, to Clive Ellegaard, Mark Oxborrow and Kristian Schaadt for their beautiful experimental measurements, to Christel Chandre for patient critical reading of the text, to Priya, Erhai, Yueheng , Anton, Atakan, Juana and Fernando for good times and finally to my dear family.

Contents

1 Introduction **1**
- 1.1 Deterministic chaos . . . 1
- 1.2 Quantum chaos . . . 3
- 1.3 Symbolic dynamics . . . 7
- 1.4 Experimental elastodynamics . . . 7
- 1.5 Wave chaos in elastodynamics . . . 9

2 Elastodynamics **12**
- 2.1 Displacement and stress . . . 12
- 2.2 Navier-Cauchy equation . . . 14
- Resumé . . . 16

3 Multi-cavity scattering problem **17**
- 3.1 Elastodynamics . . . 17
- 3.2 Boundary integral equations . . . 18
- 3.3 Formal tools . . . 19
- 3.4 Calculation of boundary integrals . . . 21
- 3.5 Scattering from one cavity . . . 27
- 3.6 Factorization of the spectral determinant . . . 27
- 3.7 Fredholm theory and shadowing . . . 30
- Resumé . . . 31

4 High frequency limit **32**
- 4.1 One cavity resonances . . . 33
- 4.2 Green's function in the presence of a single cavity . . . 37
- Resumé . . . 54

5 Numerics **55**
- 5.1 One-cavity . . . 55
- 5.2 Multi-cavity . . . 56
- Resumé . . . 61

6 Summary and outlook **62**
- 6.1 What is new in this thesis . . . 63
- 6.2 Outlook . . . 63

A Counting elasticity tensor parameters **65**

B Green's function using scattering states **67**
B.1 Asymptotic behavior at infinity 67
B.2 Derivation using transverse gradient 68

C Translation matrices and their composition **71**

D Calculation of boundary integrals **73**

E Traction matrices **77**

F Symmetry factorization **79**

G Wigner's time delay **82**
G.1 Delay of plane wave 82
G.2 Excess level density 84
G.3 Cluster delay and symmetries 84

H Ray matrices **86**
H.1 Refraction and reflection 86
H.2 Flight differential 90

Bibliography **91**

List of Figures

1.1 Sensitivity to initial conditions. 2

2.1 Continuous medium; notation. 13
2.2 Refraction of S, P waves. 15

3.1 Two cavities geometry. 17
3.2 Three cavities geometry. 18
3.3 Scattering zone; definitions of boundaries. 22

4.1 Rayleigh scattering resonances. 34
4.2 T-R-T ray contribution to the Green's function. 54

5.1 A_1 scattering resonances. 57
5.2 Time delays for the two cavity; frequency domain. 58
5.3 Time spectrum 59
5.4 Two-cavity fundamental domain 60

H.1 Differential shadow of a beam 87
H.2 Curvature for a convex scatter 88

Chapter 1

Introduction

The goal of the research described in this thesis is to formulate an approximate short-wavelength theory of wave chaos in elastodynamics, paralleling the Gutzwiller semiclassical periodic orbit theory of quantal spectra of systems whose classical dynamics is chaotic.

We start by providing the background needed to understand the terms used in the above sentence: chaos, wave chaos, Gutzwiller semiclassical periodic orbit theory. In this we follow the exposition of ref. [1]. The stage set, in sect. 1.5 we turn to the work to be undertaken here.

1.1 Deterministic chaos

A deterministic system is a system whose present state is fully determined by its initial conditions, in contradistinction to a stochastic system, for which the initial conditions determine the present state only partially, due to noise, or other external circumstances beyond our control. A deterministic system with sufficiently complicated dynamics can fool us into regarding it as a stochastic one; disentangling the deterministic from the stochastic is the main challenge in many experimental situations. So, what is "chaos"?

In a game of pinball two trajectories that start out very close to each other separate exponentially with time, and in a finite (and in practice, a very small) number of bounces their separation $\delta\mathbf{x}(t)$ attains the magnitude of L, the characteristic linear extent of the whole system, fig. 1.1. This property of *sensitivity to initial conditions* can be quantified as

$$|\delta\mathbf{x}(t)| \approx e^{\lambda t}|\delta\mathbf{x}(0)|$$

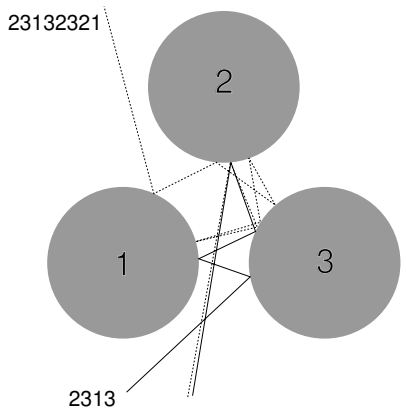

Figure 1.1: Sensitivity to initial conditions: two pinballs that start out very close to each other separate exponentially with time.

where λ, the mean rate of separation of trajectories of the system, is called the *Lyapunov exponent*. For any finite accuracy δx of the initial data, the dynamics is predictable only up to a finite *Lyapunov time*

$$T_{\rm Lyap} \approx -\frac{1}{\lambda} \ln |\delta x/L| \,, \tag{1.1}$$

despite the deterministic laws that rule the pinball motion.

A positive Lyapunov exponent does not in itself lead to chaos. One could try to play 1- or 2-disk pinball game, but it would not be much of a game; trajectories would only separate, never to meet again. What is also needed is *mixing*, the coming together again and again of trajectories. While locally the nearby trajectories separate, the interesting dynamics is confined to a globally finite region of the phase space and thus of necessity the separated trajectories are folded back and can re-approach each other arbitrarily closely, infinitely many times. The number of distinct trajectories with n bounces can be quantified as

$$N(n) \approx e^{hn}$$

where the topological *entropy* h is the growth rate of the number of topologically distinct trajectories.

When a physicist says that a certain system exhibits "chaos", he means that the system obeys deterministic laws of evolution, but that the outcome is highly sensitive to small uncertainties in the specification of the initial state. The word "chaos" has in this context taken on a narrow technical meaning. If a deterministic system is locally unstable (positive Lyapunov exponent) and globally mixing (positive entropy), it is said to be *chaotic*.

In a chaotic system any open ball of initial conditions, no matter how small, will in finite time overlap with any other finite region and in this sense spread over the extent of the entire asymptotically accessible phase space. Once this is grasped, the focus

of theory shifts from attempting precise prediction of individual trajectories (which is impossible) to description of the geometry of the space of possible outcomes, and evaluation of averages over this space.

Confronted with a potentially chaotic dynamical system, we analyze it through a sequence of three distinct stages; diagnose, count, measure. I. First we determine the intrinsic *dimension* of the system – the minimum number of degrees of freedom necessary to capture its essential dynamics. Step II; we *count* and *classify* all possible topologically distinct trajectories of the system into a hierarchy whose successive layers require increased precision and patience on the part of the observer. If successful, we can proceed with step III: investigate the *weights* of the different pieces of the system.

When should we be mindful of chaos? The solar system is "chaotic", yet we have no trouble keeping track of the annual motions of planets. The rule of thumb is this; if the Lyapunov time (1.1), the time in which phase space regions comparable in size to the observational accuracy extend across the entire accessible phase space, is significantly shorter than the observational time, we need methods that will be developed here. That is why the main successes of the theory are in statistical mechanics, quantum mechanics, and questions of long term stability in celestial mechanics. At this time the theory is in practice applicable only to systems with a low intrinsic *dimension* of the system – the minimum number of degrees of freedom necessary to capture its essential dynamics.

1.2 Quantum chaos

What happens quantum mechanically, that is, if we scatter waves rather than point-like pinballs? Were the game of pinball a closed system, quantum mechanically one would determine its stationary eigenfunctions and eigenenergies. For open systems one seeks instead for complex resonances or scattering phase shifts. The imaginary part of the eigenenergy describes the rate at which the quantum wave function leaks out of the central multiple scattering region whereas the phase shift measures whether the wave function gets drawn into or expelled from the scattering zone.

A fundamental concept in physics is the spectrum. The spectrum, for instance an energy- or frequency spectrum, can be seen, can be measured, and that information gives direct knowledge of the object upon which we perform a measurement. We may say that the spectrum is a fingerprint of the object. A large part of physics consists in developing theories that can explain or even predict new spectra. Even though few have seen a hydrogen atom, its spectroscopy gives us a very detailed understanding of its structure.

In the beginning of quantum mechanics de Broglie explained the spectrum of the hydrogen atom in a very elegant way by considering standing electron waves

on a circular orbit around the nucleus. However, this naive picture of quantizing integrable systems could not explain the spectra of many-electron atoms even as simple as the helium atom. On formalizing this theory one could in principle (and also in practice with the advent of computers) calculate many energy spectra. Some of the formalization with Schrödinger's wave mechanics and Heisenberg's matrix theory was at the expense of understanding, and an explanation of the actual form of the spectra was not given. During the last quarter of the century, however, a new theory, quantum chaos, has emerged which is much more descriptive since it includes classical dynamics in a very direct way.

Quantum chaos is mainly concerned with the wave nature of the quantum particles. In this project we will work on a generalization of the traditional free quantum particle in a box by studying a similar object in elastodynamics. Generalizations to different wave types like electromagnetic fields in optics are possible as well. Experimental studies of these systems in terms of concepts of quantum chaos are already in progress, whereas a further development is needed with regard to theory.

As an example of experimental results we mention the eigenfrequencies of optical cavity resonators (laser) and the transport properties related to certain integrated optical components (photonics). These devices are inspired by the developments in mesoscopic physics, where the transport and conductivity in electron "billiards" are investigated. New insights about these systems are gained in terms of quantum chaos concepts.

What do we actually mean by the Bohr correspondence principle if classically the dynamics is chaotic? Can such systems be quantized? During the last two decades significant progress has been made in answering this question *quantatively*. The two main approaches are the *random matrix theory* and the *periodic orbit theory*.

1.2.1 Random matrix theory

The random matrix theory was originally invented by Wigner [4] to treat complicated spectra of nuclear physics. The theory is based on the realist assumption that for a many-body system with complicated interactions the complete Hamiltonian is not known. Therefore one studies statistical properties of measured spectra, comparing the results to what would be expected were the Hamiltonian a random operator. Empirically it appears that the dimensionality of the problem does not have to be very high for a reasonable agreement with the predictions of the random matrix theory. In fact, the quantum spectrum of just one particle in a box of generic shape seems to already agree with the random matrix predictions.

Up to this day, the random matrix hypothesis remains just that - a hypothesis - and no proof that it follows from chaotic dynamics has been devised as yet. We shall not pursue the random matrix approach in this thesis.

1.2.2 Periodic orbit theory

The random matrix theory is a mathematical statement of what a spectrum would look like were it completely random - it uses almost no information about any particular given physical system.

In contrast, the periodic orbit theory aims to compute *the* spectrum for *the* physical system studied. The classical periodic orbit theory is an exact theory that yields all averages and correlations that can be extracted from a given classical chaotic dynamical system [1]. The semi-classical periodic orbit theory of quantum systems derived by Gutzwiller [31] in 1970 expresses quantum quantities such as the spectral density in terms of sums over classical unstable periodic orbits [34]. In quantum mechanics the periodic orbit theory arose from studies of (eminently applicable) semiconductors, and the unstable periodic orbits have been measured in experiments on the very paradigm of Bohr's atom, the hydrogen atom, in strong external fields.

Rederiving this theory here would take us too far afield - we refer the reader to [1], and limit ourselves to stating the relevant key formulas. Technically, the theory is formulated in terms of the *Gutzwiller trace formula*

$$\mathrm{Tr}\, G_{sc}(E) = \frac{1}{i\hbar} \sum_p T_p \sum_{r=1}^{\infty} \frac{1}{|\det(1-\mathbf{J}_p^r)|^{1/2}} e^{r(\frac{i}{\hbar}S_p - \frac{i\pi}{2}m_p)} \,. \tag{1.2}$$

Here $S_p = S_p(E)$ is the action evaluated along the prime cycle p, the single, shortest traversal of a periodic orbit. $\mathbf{J}$ is the monodromy matrix computed on a surface of section transverse to the orbit within the constant energy shell $E = H(q,p)$. The Maslov index $m_p = m_p(E)$ counts the number of changes of sign of the matrix of second derivatives evaluated along the prime periodic orbit p. The sum is over all prime cycles p and their rth repeats, as any repeat of a periodic orbit is also a periodic orbit. The action and the Maslov index are additive along the trajectory, so for rth repeat they simply get multiplied by r. The monodromy matrix of the rth repeat of a prime cycle p is (by the chain rule for derivatives) $\mathbf{J}_p^r$, where $\mathbf{J}_p$ is the prime cycle monodromy matrix. In deriving the formula one assumes that $\mathbf{J}_p$ has no marginal eigenvalues, that the the periodic orbits are isolated and do not form families, unlike the case of integrable systems or in the KAM tori of systems with mixed phase space, so the formula is valid only for the hyperbolic and elliptic periodic orbits.

In practice, all quantum chaos calculations take the stationary phase approximation to quantum mechanics (the Gutzwiller trace formula, possibly improved by including tunneling periodic trajectories, diffraction corrections, *etc*) as the point of departure. Once the stationary phase approximation is made, what follows is *classical* in the sense that all quantities used in periodic orbit calculations - actions, stabilities, geometrical phases - are classical quantities. While various periodic orbit formulas are formally equivalent, practice shows that some are preferable to others. Three classes of periodic orbit formulas are frequently used:

1. *Trace formulas.* Easy to derive, in actual calculations the Gutzwiller trace formulas (1.2) are hard to use for anything other than the leading eigenvalue estimates, as they tend to be divergent in the region of physical interest.

2. *Ruelle or dynamical zeta functions*

$$1/\zeta(s) = \prod_p (1 - t_p), \qquad t_p = \frac{1}{\sqrt{|\Lambda_p|}} e^{\frac{i}{\hbar} S_p - i\pi m_p/2} \ . \tag{1.3}$$

Here t_p is the quantum amplitude associated with a given prime cycle, Λ_p is the product over expanding stability eigenvalues of $\mathbf{J}_p$, and the product is over all prime cycles p.

3. *Selberg-type zeta functions, Fredholm determinants, spectral determinants, functional determinants* are the natural objects for spectral calculations. The *semi-classical zeta function*

$$\Delta(E) = \exp\left(- \sum_p \sum_{r=1}^{\infty} \frac{1}{r} \frac{e^{ir(S_p/\hbar - m_p\pi/2)}}{|\det(\mathbf{1} - \mathbf{J}_p^r)|^{1/2}} \right) \tag{1.4}$$

is formally equivalent to the trace formula (1.2) and follows from it by simple manipulations. Its Selberg-type zeta function infinite product representation for Hamiltonian systems with 2 degrees of freedom is

$$\Delta(E) = \prod_p \prod_{k=0}^{\infty} \left(1 - \frac{e^{iS_p/\hbar - i\pi m_p/2}}{|\Lambda_p|^{1/2} \Lambda_p^k} \right) \ .$$

The billiards that we shall study here belong to this class of quantum systems. For hyperbolic systems both the dynamical zeta functions and the spectral determinants have good convergence and are powerful tools for determination of quantum mechanical resonances. Most periodic orbit calculations are based on cycle expansions of such determinants.

Similar zeta functions have already been derived much earlier [26] for the special case of spectral determinants of Laplace operators on spaces of constant negative curvature, with the spectral determinants expressed in terms of the closed, periodic geodesics. For the deterministic dynamical flows and number theory, zeta functions are exact. The quantum-mechanical ones, derived by the Gutzwiller approach, are at best only the stationary phase approximations to the exact quantum spectral determinants, and for quantum mechanics an important conceptual problem arises already at the level of derivation of zeta functions; how accurate are they, and can the periodic orbit theory be systematically improved?

1.3 Symbolic dynamics

At first using orbits in calculations may seem like a hopeless task since in general there are infinitely many unstable periodic orbits. The key tool in dealing with this infinity of orbits is the concept of symbolic dynamics borrowed from the theory of dynamical systems and ergodic theory [34, 1]. The idea is to associate to each trajectory a unique bi-infinite symbolic sequence $...a_{-2}\,a_{-1}\,a_0.a_1\,a_2\,...$, and vice versa, establish that there is one and only one trajectory for a given bi-infinite symbolic sequence. This is especially valuable when the symbols can be chosen from a finite alphabet subjected to a finite number of rules (grammar). Here periodic orbits have periodic symbolic sequences (e.g. a period three orbit is denoted $\overline{a_1\,a_2\,a_3}$). Calculations of zeta functions are organized in terms of increasing word lengths of such orbits. As the length of the words included in a cycle expansion of (1.4) is increased, an increase in the convergence of the quantum resonance estimates is observed. This convergence can be characterized as super-exponential in the most optimal cases, meaning that the number of significant digits one gains is not fixed at say two but grows at each step. Thus symbolic dynamics is not only useful for classifying and finding the orbits, it can also be numerically effective.

In quantum mechanical applications this rather brave semi-classical periodic orbit quantization accomplishes something altogether remarkable; putting together all ingredients that make the pinball game unpredictable, it yields surprisingly accurate helium quantum spectrum [5]. Even though the cycle expansion was based on the *semiclassical approximation* which is expected to be good only in the classical large energy limit, the eigenenergies are good to 1% all the way down to the ground state.

Gutzwiller's semiclassical quantization has been applied to the helium atom, the anisotropic Kepler problem, the hydrogen atom in a magnetic field and to the wave scattering for the scalar Helmholtz equation from several discs. However, the method does not appear to be generally valid. The convergence is severely degraded for generic dynamical systems whose phase space is mixed between chaotic and integrable. It has been seen that for *intermittent* systems the zeta functions may develop branch points [42].

1.4 Experimental elastodynamics

Having sketched the broad historical backdrop, we are ready to turn to the beautiful experimental work that motivates our undertaking.

Why elastodynamics? Besides the experimental accessibility and the high quality experimental spectra new and interesting features show up: The ray splitting and surface waves. The elastodynamic wave equation describes the propagation of waves with two different wave speeds. When a plane wave hits a boundary, two or more

plane waves are emitted at different angles. In the high-frequency limit this leads to a so-called branching Hamiltonian system. The surface waves are important as they can propagate without attenuation along the boundaries. Thus, compared to electrodynamics and quantum mechanics of scalar fields we have to take into account radically different periodic orbits.

While the surface waves can already be seen in the simpler case of the scalar Helmholtz equation with *impedance* conditions $\frac{\partial u}{\partial n} = -ikZu$ [15], our goal in the following is to address the problem of physical elastodynamics with *free* boundary conditions, the conditions experimentally realized in the highest Q-value ($5 \cdot 10^6$ for a quartz sphere) measurements up to date. Here there are some clear advantages in studying elastodynamics in for example experiments with quartz compared to the more conventional systems in atomic physics, micro-wave cavities and electronical nanostructures. In spite that elastodynamic experiments are usually performed on macroscopic systems the spectra are remarkably good with sharp and well-defined resonance lines. The quality factor, the Q-value is introduced as a measure of the "goodness" of a resonance. The Q-value is defined as the ratio between the line with and the resonance frequency. Thus the Q-value of quartz is about 10^6 whereas for a typical mesoscopic experiment its approximately 20. This means roughly that a sound beam is reflected inside quartz resonator millions of times before it fades away, whereas the electron wave dies out after only 20 reflections. Another advantage is the low dimensional phase space which greatly reduces the number of orbits and the numerical work in finding them. A third advantage is the low degree of non-linearity in the elastodynamic wave equation. Hence, the eigenmodes are almost un-coupled, and the theoretical complications found in strongly correlated electronic systems are avoided. Nor should it be underestimated from a practical point of view that elastodynamic experiments tend to be much simpler and cheaper than their counterparts in atomic physics, helium-cooled microwave cavities and electronic nano-devices.

1.4.1 Tests of the random matrix theory

So far the predictions of the random matrix theory have been tested on the resonance spectra for a large number of different classically chaotic systems, with good qualitative agreement. The common belief is that the classically chaotic billiards should have spectral statistics different from the classically integrable billiards, and that is borne out by experiments. Hence from the spectrum alone it appears that one can determine whether or not a system is chaotic or integrable.

A particularly strong test of these predictions comes from the experiments of Oxborrow *et al.* [23] on quartz resonators. These experiments are remarkable for the high Q-value of the resonances, of order $10^5 - 10^6$. This stands in sharp contrast with the nuclear physics and the room temperature microwave experiments for which the Q-values are orders of magnitude lower, typically ~ 100. Thus in elastodynamics

highly accurate spectra can be measured, with the attendant spectral statistics of unparalleled quality.

1.4.2 Tests of the periodic orbit theory

In quantum mechanics the atomic physics measurements of Welge *et al.* [32] and the theoretical investigations of Wintgen *et al.* [33] gave a dramatic demonstration of the underlying periodic orbit structure of spectra of hydrogen in strong external fields. Up to this day there has been no experimental verification of the corresponding periodic orbit theory in elastodynamics. This unsatisfactory state of affairs is, of course, the *raison d'etre* for the entire theoretical effort described in this thesis.

1.5 Wave chaos in elastodynamics

Elastodynamics in crystals is described by linear partial differential equations [17, 21]. For bulk vibrations these equations are vectorial, and in general three different modes of polarization are found. When a wave of a given polarization hits a boundary this results for free boundary conditions in normally three new outgoing waves, the so-called wave split phenomenon. Another property of acoustic waves is the extraordinary refraction, i.e. the fact that the phase velocity is in general not parallel to the group velocity. Finally there is also the possibility of surface waves. Thus compared to the Schrödinger equation in quantum mechanics the acoustic wave equation exhibits new features.

1.5.1 What is known so far?

Exact results

At first we should have the corresponding exact scattering spectrum. This work has already been done in the case of one cavity [12, 13]. However, for multiple cavities the exact S-matrix cannot be written down in closed form. We will use the of S-matrix formalism and follow the strategy of Wirzba's [2] derivation for the scalar Helmholtz equation with Dirichlet conditions. For the experimental elastodynamics (resonator in vacuum) purposes, the boundary should be taken as *free*. Next we shall derive a factorization of the spectral determinant in a coherent part among different scatters and incoherent parts for individual scatters.

Wirzba's approach [2] is based on the partial wave expansions and the Sommerfeld-Watson transformation. In the multi-scattering case it has been shown that also creeping along different scatters matters. Thus for low frequencies these orbits have

to be included also. We expect similar effects in elastodynamics. This we shall study for the two cavity system. The surprise is that while the classical two disc system has only one unstable orbit, the semiclassical case has infinitely many orbits of Rayleigh type and is in this sense chaotic. This will go beyond the usual classical notions of symbolic dynamics since the Rayleigh and creeping orbits are essentially complex orbits. They reside in the complexified phase space and do not sit on the classical object, the chaotic repeller. One may speculate that complex orbits are exactly what is needed in a more general theory. How complex orbits enter, however, is not clear at all for general systems.

Geometrical theory of wave elastodynamics

Keller and collaborators have treated surface waves and diffraction in a more general setting [15, 16]. From only a few assumptions diffraction constants and propagation segments are derived. By studying a limited number of examples, wedges, points, creeping around discs ... enough knowledge about general diffraction is gathered. This theory is often called the *geometrical theory of diffraction*. In particular concerning surface waves using a WKB expansion the curvature correction to the Rayleigh wave speed has been found [25, 20]. Therefore surfaces with varying curvature can be treated.

Concerning the special case of one disc respective cavity, the individual scatter, there is already a sophisticated theory in terms of orbits. The main tool is the Sommerfeld-Watson transformation which transforms slowly converging sums of partial waves to a fast converging sum over *complex creeping* orbits [22]. Creeping here refers to circumferential orbits. This transformation is used in the high frequency limit. For instance consider the scattering of visible light from an $a = 1$ mm diameter drop of water. Here one finds that one has to use approximately $\beta = ka \sim 5000$ partial waves. Now similar results are obtained using just a few creeping orbits ($\beta \approx 1$ requires only four). Nussenzweig [22] reports, for example, that for $\beta = ka > 100$ the error is better than 1 ppm. This technique was first used by Watson in the study of the transmission of radio waves around the earth. Later it was applied in high energy physics, where it goes under the name of the method of Regge poles [6]. Similar calculations have been done in elastodynamics [19]. Here practical applications are in the study of cavities and other defects in materials and in seismography. The different polarizations and Rayleigh waves render the calculations more complicated than the scalar case. We shall derive a spectral determinant for one cavity as a product over creeping orbits and Rayleigh orbits. The quantization is particularly simple with phase matching on just one periodic orbit. Here creeping orbits constantly leaks out rays leading to a loss of amplitude. This is then incorporated by using a complex wave number leading to scattering resonances with finite lifetime. This effect is also seen for the Rayleigh wave because of the curvature.

Periodic orbit theory

There is already a candidate for quantization in elastodynamics based on the work by Couchmann and Ott [10] which studied a closed system, the stadium billiard. Their article is mainly devoted to the "classical" behavior associated to elastodynamics in the high frequency limit focusing on wave splitting. Apparently not much work has been done on these branching Hamiltonian systems. In particular whether suitable Fredholm determinants are entire and similar questions. The thesis of Couchmann describes the random matrix properties of these systems and contains a derivation of a Gutzwiller trace formula for the spectral density.

1.5.2 What is new in this thesis?

We shall present a derivation of the exact scattering determinant for a system of several cylindrical cavities. From this object we shall extract spectral quantities focusing on mainly the phase shift and the associated Wigner time delay. Our analysis will show that the results for this wave problem are strongly influenced by its classical ray dynamics. Here the new feature are periodic orbits with surface segments on the boundaries of the cavities. These surface pieces are of Rayleigh type and are only slightly attenuated for high frequencies. In particular already a system of two cavities will have infinitely many orbits leading not only to chaotic classical behavior but also to very complex wave behavior.

1.5.3 Organization of the thesis

We review the requisite theory of elasticity and derive the linearized elasticity wave equation in chapter 2. In chapter 3 we formulate the scattering problem for a set of cylindrical cavities in an infinite elastodynamic medium. In chapter 4 we study the scattering resonances in the high frequency limit for the cases of a single cavity. We extract from the Green's function in the presence of a cavity the diffraction constants corresponding to geometrical reflection, refraction and Rayleigh creeping waves. Numerical investigations of the Wigner time delay are carried out in chapter 5. A summary and outlook for future work is given in chapter 6.

While elastodynamics is a well founded, well studied classical theory, and the required derivations are technically straightforward, due to the tensorial structure of elastodynamics the intermediate steps are frequently rather heavy going for a casual reader. Whenever permissible I have relegated such details to appendices. The independent components of the isotropic elasticity tensor are counted in appendix A. The decomposition of the Green's function in scattering states is described in appendix B, and appendices C–E contain computational details of the scattering problem. Appendix G is on the Wigner time delay and finally appendix H is on ray matrices for a system with wave splitting.

Chapter 2

Elastodynamics

In this chapter we will state a few basic results from linear elastodynamics [17, 27, 19]. A reader familiar with the subject can profitably skip this chapter. We consider an elastodynamic body with constant mass density ρ. The Einstein repeated index summation convention is assumed throughout.

2.1 Displacement and stress

Consider a deformation of an elastodynamic body, Fig. 2.1(a): The local change of position of a particle is given by the *displacement* vector field, $\mathbf{u}$.

$$x_i' = u_i(x) + x_i \,. \tag{2.1}$$

Some deformations have no effect on the local energy density at the point x. For instance, a global parallel translation or a rotation does not matter, only local variations corresponding to $u_{j;i}\partial_i u_j$ matter, since the former displacements do not deform the body. Furthermore, as a local rotation around a given point preserves distances in a neighborhood of this point, the medium in this neighborhood is not stretched. A local rotation is measured by the $(curl\mathbf{u})_i = \epsilon_{ijk}\,\partial_j u_k = \frac{1}{2}\epsilon_{ijk}\,(\partial_j u_k - \partial_k u_j)$. Thus we do not attribute any significance to the antisymmetric part of $\partial_i u_j$. To show this consider the line element (squared distance) between two infinitesimally close points after a deformation sketched in Fig. 2.1(b):

$$\begin{aligned} dx'^2 &= d(\mathbf{x}+\mathbf{u})^2 = dx^2 + 2\,d\mathbf{x}\cdot d\mathbf{u} + du^2 \\ &= dx^2 + 2\frac{\partial u_i}{\partial x_k} dx_i dx_k + O(du^2) \\ &= dx^2 + 2u_{ik} dx_i dx_k \,, \end{aligned} \tag{2.2}$$

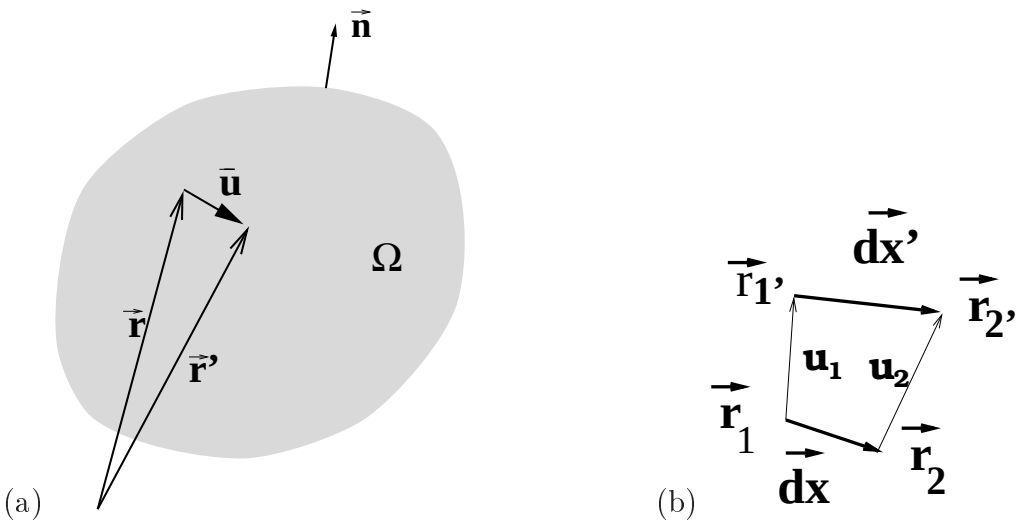

Figure 2.1: The continuous medium; definition of (a) the displacement vector, outward normal to the boundary; (b) deformation in the neighborhood of two points.

where we have defined the *strain* field:

$$u_{ij} = \frac{1}{2}(u_{i;j} + u_{j;i})\,, \qquad u_{j;i} = \frac{\partial u_j}{\partial x_i}\,. \tag{2.3}$$

We see that the distance depends solely on the symmetric part of $\nabla \mathbf{u}$.

To the kinematic strain field corresponds a dynamic field, the stress field. This may be introduced in the following way: Taylor expanding the potential energy density to leading order in the strain field we find:

$$U = \frac{1}{2} c_{ijkl} u_{ij} u_{kl}\,. \tag{2.4}$$

There is no linear term since that would describe an unstable medium and we can always assume a vanishing constant term. This expansion is the generalization of the energy of a spring as a function of the displacement. The displacement is now replaced by the strain field. In a general medium the spring constant corresponds to a suitable four-tensor,*the elasticity tensor*. A generalized force, the *stress* field, is given by Hooke's law:

$$\sigma_{ij} = \frac{\partial}{\partial u_{ij}} U = c_{ijkl} u_{kl}\,. \tag{2.5}$$

Thus the pressure in the direction "i" coming from the element of area with normal along "j" is given by σ_{ij}. The pressure at the boundary is referred to as the *traction* $t(u)$:

$$t_i = \sigma_{ij} n_j\,. \tag{2.6}$$

Here n refers to the normal vector. The symmetries of elasticity tensor follow from (2.3–2.4):

$$c_{ijkl} = c_{jikl} = c_{ijlk} = c_{klij} \,. \tag{2.7}$$

A most general tensor in three dimensions with these symmetries has 21 independent components. However, if further symmetry is present the elasticity tensor will have fewer independent components. In the isotropic case the elasticity tensor reduces to

$$c_{ijkl} = \lambda\delta_{ij}\delta_{kl} + \mu(\delta_{ik}\delta_{jl} + \delta_{il}\delta_{jk}) \,, \tag{2.8}$$

where λ and μ are the *Lamé* constants. For a more detailed discussion see Appendix A.

2.2 Navier-Cauchy equation

We shall now derive the wave equation for elastodynamics, restricting ourselves to the linearized elasticity.

Consider Newton's second law on an infinitesimal volume element. The total force will come from the boundaries. Thus per unit volume, the force in the direction "i" is $\sigma_{ij;j}$. The mass times the acceleration of a volume element is $\rho\frac{\partial^2 u_i}{\partial t^2}$ with ρ the local mass density. Hence the Newton equation of motion for elastodynamics is

$$\rho\frac{\partial^2 u_i}{\partial t^2} = \sigma_{ij;j} = c_{ijkl}u_{l;jk} \,. \tag{2.9}$$

In the isotropic case (2.8) this reduces to:

$$\begin{aligned} \rho\frac{\partial^2 \mathbf{u}}{\partial t^2} &= \mu\Delta(\mathbf{u}) + (\lambda+\mu)\nabla(\nabla\cdot\mathbf{u}) \\ \rho\frac{\partial^2 u_i}{\partial t^2} &= \mu u_{i;kk} + (\lambda+\mu)u_{k;ki} \,. \end{aligned} \tag{2.10}$$

In the frequency domain, with $\mathbf{u} = \mathbf{u}(\mathbf{r})e^{i\omega t}$ this is called the *Navier-Cauchy equation*:

$$\mu\Delta(\mathbf{u}) + (\lambda+\mu)\nabla(\nabla\cdot\mathbf{u}) + \rho\omega^2\mathbf{u} = 0 \,. \tag{2.11}$$

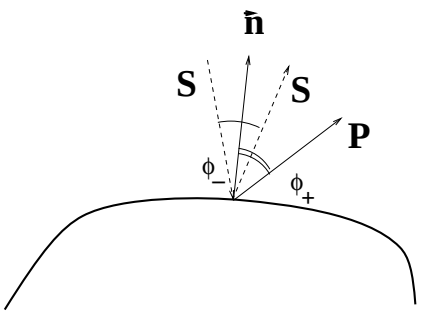

Figure 2.2: Refraction of S, P waves.

Inserting plane waves one derives the existence of transversal and longitudinal polarized waves with wave speeds

$$c_T = \sqrt{\frac{\mu}{\rho}}\,, \qquad c_L = \sqrt{\frac{\lambda + 2\mu}{\rho}}. \tag{2.12}$$

In what follows these waves will be referred to as *shear* and *pressure* waves, S and P. This nomenclature is motivated by their representation in terms of *potentials*. (As we shall see in what follows, P and S could also stand for *primary* and *secondary* waves, referring to the *difference* in their arrival times.) Write

$$\begin{aligned} \mathbf{u}_L &= \nabla\phi \\ \mathbf{u}_T &= \nabla \times \vec{\psi}\,. \end{aligned} \tag{2.13}$$

A fundamental theorem in vector analysis [9] states that any three-dimensional vector field can be uniquely decomposed in terms of such fields:

$$u = u_L + u_T\,. \tag{2.14}$$

Inserting into the Navier-Cauchy equation we see that the potentials satisfy a scalar and a vectorial Helmholtz equation:

$$\begin{aligned} \Delta\phi + k_L^2\phi &= 0, \qquad k_L = \omega/c_L \\ \Delta\vec{\psi} + k_T^2\vec{\psi} &= 0, \qquad k_T = \omega/c_T \end{aligned} \tag{2.15}$$

The longitudinal waves correspond to irrotational waves and transverse waves to incompressible waves ("curl" respective "div" vanishes). Hence the longitudinal waves are often referred to as pressure waves and the transverse as shear waves. It follows from (2.12) that the pressure waves propagate faster than the shear waves.

The two kinds of waves are the full solution to the wave mechanics in an infinite isotropic medium of constant density.

In the presence of an infinite half space boundary there is also a third kind of wave, the surface *Rayleigh wave* propagating with a complex wave vector with no energy loss. An ansatz that leads to the Rayleigh wave solution assumes that the displacement field decays exponentially into the medium. Choosing z as the coordinate normal to the boundary, going into the medium for positive z, we write down a plane wave solution:

$$\mathbf{u}(x,y,z) = \mathbf{a}\, e^{i(k_x x + k_y y) - k_z z}\,, \tag{2.16}$$

with $\mathbf{a}$ is a constant polarization vector.

The physically relevant boundary condition is the *free* boundary condition with vanishing traction (2.6)

$$\mathbf{0} = \mathbf{t} = \sigma \cdot \mathbf{n} = (\lambda \nabla \cdot \mathbf{u}\, \mathbf{1} + \mu(\nabla \mathbf{u} + (\nabla \mathbf{u})^{\mathbf{t}})) \cdot \mathbf{n}\,. \tag{2.17}$$

Inserting the wave vector (2.16) into the boundary condition and the wave equation one verifies that such a wave indeed exists with the polarization entirely in the plane of the boundary. The wave propagates with a velocity c_R, slightly slower than the shear wave and much slower than the pressure wave. c_R^2 is the real root of

$$\left(\frac{c_L}{c_T}\right)^2 \left(2\left(\frac{c_T}{c_R}\right)^2 - 1\right)^2 - 4\left(\frac{c_T c_L}{c_R^2}\right)\sqrt{\left(\left(\frac{c_L}{c_R}\right)^2 - 1\right)\left(\left(\frac{c_T}{c_R}\right)^2 - 1\right)} = 0\,. \tag{2.18}$$

In a semi-infinite medium with a free plane boundary Rayleigh waves propagate without energy loss. The geometrical theory to be developed below will piece together ray trajectories from shear, pressure and Rayleigh wave segments. The Rayleigh waves along curved boundaries will suffer some radiation loss. In contradistinction to the relatively unimportant creeping waves of quantum mechanics with Dirichlet boundary conditions, the elastodynamic surface Rayleigh waves will turn out to be the dominant effect in the elastodynamic scattering.

Résumé

After an introduction to continuum mechanics the elastodynamic wave equation was derived. It supports two different waves P, S in the bulk each propagating with its own velocity. In case of a semi-infine medium, the Rayleigh surface waves are an additional class of solutions of great physical importance.

Chapter 3

Multi-cavity scattering problem

In the following we shall describe the solution of the scattering problem in an infinite domain with several infinite parallel cylindrical cavities. This is referred to as scattering off cavities in elastodynamics and scattering off discs in the scalar case. We shall assume the free boundary condition, with vanishing traction $t(u) = 0$; The scattering problem will be solved using boundary integral identities derived via Betti's equivalent of the Green's theorem.

3.1 Elastodynamics

So far we have discussed the general three-dimensional elasticity. Now we will restrict our study to a family of cases where it is possible to reduce the dimensionality to two.

This two-dimensional situation is realized if one considers scattering from parallel infinite "bore holes" with each cavity axis normal to a given fixed plane. A wave with the polarization confined to this plane will never flip its polarization and develop components normal to this plane. Furthermore, a polarization parallel to the cavity axes will never mix with the plane strain fields. This field has only one degree of freedom and its scattering is described by a scalar field. We shall restrict our study

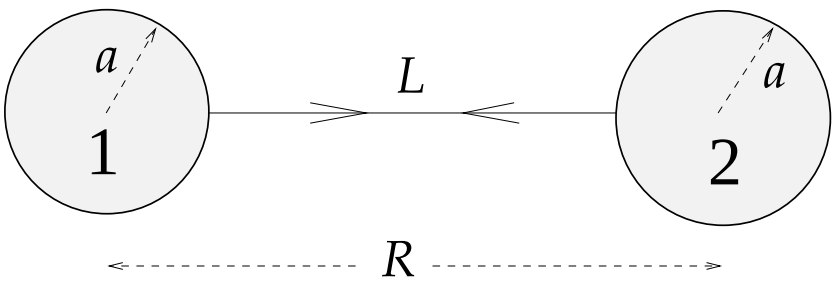

Figure 3.1: Two cavities geometry (A. Wirzba) [3].

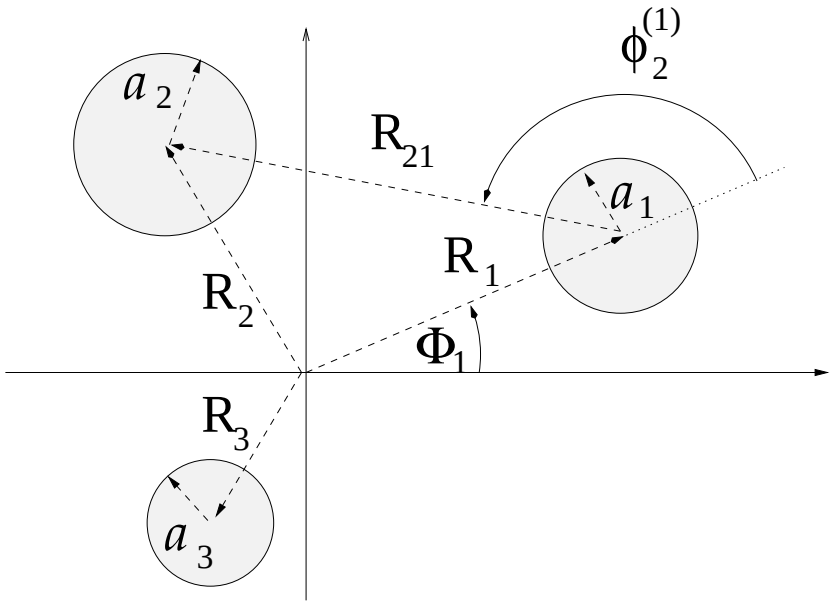

Figure 3.2: Three cavities geometry (modified from Wirzba).

to the normally incident waves (as opposed to the more general *oblique* case) and limit ourselves entirely to the *plane strain* case.

3.2 Boundary integral equations

In elastodynamics the following identity replaces *Green's theorem*. This relation is often referred to as Betti's third identity [11]. To make the notation more compact, in what follows we shall often drop the coordinate dependence in vector fields, $u = u(s)$ and $v = v(s)$. For elastodynamics the differential operator $\Delta^*_{il} = c_{ijkl}\partial_j\partial_k$ is the generalized Laplacian, and the traction boundary operator t replaces the normal derivative:

$$\int (u \cdot \Delta^*(v) - v \cdot \Delta^*(u))\, dV = \int (u \cdot t(v) - t(u) \cdot v)\, ds \tag{3.1}$$

This identity follows by integration by parts. We have suppressed all indices to keep the notation simple. Remark that the *clamped* boundary condition for (3.1) is $u = 0$, and the *free* boundary - relevant to experiments with elastodynamic resonators in vacuum - corresponds to $t(u) = 0$.

We define the *frequency domain* Green's function as the solution of

$$(\boldsymbol{\Delta}^*{}_r + \rho\omega^2\, \mathbf{1}) \cdot \mathbf{G}(\mathbf{r}, \mathbf{r}') = \delta(r - r')\mathbf{1}. \tag{3.2}$$

We shall specialize to two spatial dimensions, isotropic medium case. The Green's function is now a matrix since the elastodynamic wave equation is vectorial. One can derive the form of the frequency dependent Green's function by standard methods described in [11]. The result is (in tensor form)

$$\mathbf{G}(\mathbf{r},\mathbf{0}) = \frac{1}{4i\mu}\left(H_0^{(1)}(k_T r)\mathbf{1} + \frac{1}{k_T^2}\nabla\otimes\nabla(H_0^{(1)}(k_T r) - H_0^{(1)}(k_L r))\right) \tag{3.3}$$

Inserting the Green's function $v = G(s, X)$ into the integral relation we find in general Somigliana's identity [11]:

$$c(X)u(X) = \int (u(s)\cdot t(G(s,X)) - t(u(s))\cdot G(X,s))\, ds. \tag{3.4}$$

Here $c(X) = 0/1$ if X is outside/inside the elastic body. This gives us two relations. Also a third relation may be derived if the point X is precisely at the boundary. Thus for a *smooth* boundary one finds in all dimensions $c(X) = 1/2$. In two dimensions $c(X)$ is a function taking the value

$$\frac{\Delta\theta}{2\pi}, \tag{3.5}$$

where $\Delta\theta$ is the angle subtended at X. This gives the values also at *corners* and can be generalized to higher dimensions. See [11] for further discussion.

3.3 Formal tools

Below we shall state some facts that facilitate the calculation of the scattering matrix.

3.3.1 Basis functions

Our choice of basis functions has been inspired by previous work [19, 20]. In general we shall denote a basis function with the symbol ψ, distinguishing outgoing waves $\psi^{(+)}$, in going $\psi^{(-)}$ and regular waves $\psi^{\wedge}$. By regular we mean a wave which is not singular at the origin. Our scatterers will be cylindrical so the appropriate basis functions will be generated from Bessel and Hankel functions. These basis functions will be generated from the basis potentials $H_l^{(1)/(2)}(kr)e^{il\theta}$ and $J_l(kr)e^{il\theta}$ solving the Helmholtz equations (2.15) by action of ∇ and $\nabla\times(\hat{\mathbf{z}}\,\cdot)$. This gives us a basis since each vector function uniquely decomposes into an incompressible and an irrotational part and that the potential functions are chosen from a complete set, the partial waves. Further we shall denote by "$\sim$" the replacement of $e^{il\theta}$ with $e^{-il\theta}$. We reserve "$*$" to mean complex conjugation. We remark that the basis functions are of dimension length^{-1}.

Orthogonality relations

These basis functions satisfy orthogonality relations on boundaries. In particular, at the disc at infinity we find using the asymptotic expansion of Hankel functions:

$$\int_{\partial_\infty} (t(\psi_l^{(+)})\psi_m^{(-)} - t(\psi_m^{(-)})\psi_l^{(+)})\, ds = 8i\rho\omega^2\delta_{l,-m}(-1)^l \tag{3.6}$$

and

$$\int_{\partial_\infty} (t(\psi_l^{(\pm)})\psi_m^{(\pm)} - t(\psi_m^{(\pm)})\psi_l^{(\pm)})\, ds = 0\,. \tag{3.7}$$

Hence:

$$\int_{\partial_\infty} (t(\psi_l^{(+)})\psi_m^{\wedge} - t(\psi_m^{\wedge})\psi_l^{(+)})\, ds = 4i\rho\omega^2\delta_{l,-m}(-1)^l \tag{3.8}$$

3.3.2 Green's function expansion in normal modes

We can construct an expansion similar to the partial wave expansion for the scalar case. There one chooses regular functions at the origin and outgoing functions at infinity. Here we write a similar expansion of the Green's function and insert it in the boundary integral relations above. Using the orthogonality relation (3.8) on a solution $\psi^{(-)}$ the overall normalization is fixed.

Thus we may expand the Green's function as

$$\begin{aligned} \mathbf{G}(\mathbf{x},\mathbf{y}) &= \frac{1}{4i\rho\omega^2}\sum_n \psi_{\mathbf{n}}^{\wedge\sim}(\mathbf{r}_<)\otimes\psi_{\mathbf{n}}^{(+)}(\mathbf{r}_>) \\ &= \frac{1}{4i\rho\omega^2}\sum_{l=-\infty}^{\infty}[\psi_{\mathbf{l}}^{\wedge\sim}(\mathbf{r}_<)]\cdot[\psi_{\mathbf{l}}^{(+)}(\mathbf{r}_>)]^{\mathbf{t}}\,, \end{aligned} \tag{3.9}$$

where $r_< = min(x,y)$ and $r_> = max(x,y)$. Here n in the first line is a multi-index containing angular momentum and polarization indices. Further the basis function is a geometric vector. For a derivation see appendix B. The next line is in matrix form and introduces the *displacement matrix*:

$$[\psi_n] = \begin{pmatrix} (P_n)_1 & (S_n)_1 \\ (P_n)_2 & (S_n)_2 \end{pmatrix}\,, \tag{3.10}$$

which for angular momentum n contains the vectorial components $1,2$ of the pressure and shear basis function. Below we shall often suppress geometrical and polarization indices.

Translations

For different cylinders the natural basis functions may be defined centered at different positions. To relate such basis sets we introduce translation operators (inspired by [40, 41] who introduced such operators in three dimensions). These operators translate the underlying coordinate plane but not the basis functions. We shall work with several coordinate systems: a global system and one local for each scatter. We write a basis function at system S' in terms of those at system S. Here $S, S' \in \{G, j, j'\}$ refer to global respectively local coordinate systems.

Thus for instance to go from a global to a local coordinate system for an outgoing state we have:

$$\psi_n^{(+)}(X^{(G)}) = \sum_{l=-\infty}^{\infty} T_{nl}^{+Gj} \psi_l^{\wedge}(X^{(j)}) \tag{3.11}$$

with

$$T_{nl}^{+Gj} = (-1)^l H_{n-l}^{(1)}(kR_j) e^{i(n\phi_j^{(G)} - l\phi_G^{(j)})} \,. \tag{3.12}$$

Other combinations are possible. See appendix C for further details. In the above the wave vector k is chosen according to whether a pressure or shear state is considered.

Composition

Products of the translation operators will again lead to translation operators. The tool used is the addition theorem for Bessel functions [35]. Thus

$$\mathbf{T}^{+jG} \cdot \mathbf{T}^{\wedge Gj} = \mathbf{1} \tag{3.13}$$

as particular example.

3.4 Calculation of boundary integrals

We now proceed with the calculation of the S-matrix using the definitions above and (3.4). We assume the scattering zone surrounded by a large disc with a radius going to infinity, fig. 3.3.

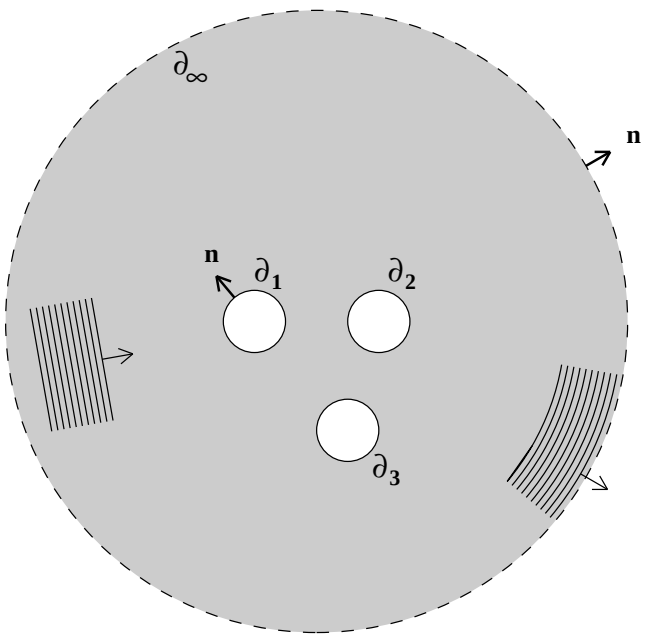

Figure 3.3: We imagine the scattering zone enclosed in a disc with a radius going to infinity. The white zones are voids in the medium. Boundaries are denoted with a ∂. An incoming plane wave and its scattered field are sketched.

Consider an incoming *plane* wave as potential. This can be written as a sum over the regular Bessel functions,

$$e^{i\mathbf{k}\cdot\mathbf{r}} = \sum_{l=-\infty}^{\infty} J_l(kr)e^{il\theta} = \sum_l \frac{1}{2}(H_l^{(2)}(kr)e^{il\theta} + H_l^{(1)}(kr)e^{il\theta})\,. \tag{3.14}$$

On the level of the wave function the last part corresponds to ingoing and outgoing states. In the presence of scattering we modify the outgoing part with the *scattering matrix* $\mathbf{S}$. Thus at infinity the wave function is:

$$u = \sum_{i,l} \frac{1}{2}\, a_i \left(\delta_{il}\psi_l^{(-)} + S_{il}\psi_l^{(+)}\right)\,. \tag{3.15}$$

Here a_i will be referred to as the scattering data at infinity. By convention we keep the factor $1/2$ and do not absorb it in a_i.

At a given cavity j expand the wave function in a Fourier series:

$$u = \sum_m \mathbf{B}_m^{(j)} e^{im\theta} = \sum_m ((B_r^{(j)})_m \hat{\mathbf{r}} + (B_\theta^{(j)})_m \hat{\theta}) e^{im\theta} \tag{3.16}$$

Here $\theta = \theta^{(j)}$ refers to the local coordinate system at the cavity.

In the boundary integrals (3.4) the integration will be over the cavity boundaries ∂_j and the boundary at infinity ∂_∞. Each integral is to be evaluated with respect to a final point X which we shall take in the following either as ending on a cavity or going to infinity. For each of the cavities we shall evaluate the boundary integrals above at a final point infinitesimally inside the cavity. For these integrals the factor is zero. However, in the latter case we constantly stay inside the elastic medium. Hence the factor c in (3.4) above equals unity. Thus for a point $X^{(j)}$ ending on a cavity we define:

$$\begin{aligned} I^j_{j'} &= \int_{\partial_{j'}} ds\, u(s) \cdot t(G(s, X^{(j)})) \\ I^j_\infty &= \int_{\partial_\infty} ds (u(s) \cdot t(G(s, X^{(j)})) - t(u(s)) \cdot G(s, X^{(j)}) \end{aligned} \tag{3.17}$$

with

$$0 = I^j_\infty - (I^j_j + \sum_{j' \neq j} I^j_{j'}) \,. \tag{3.18}$$

For a point $X = r \to \infty$ inside the medium:

$$\begin{aligned} I^r_j &= \int_{\partial_j} ds\, u(s) \cdot t(G(s, X)) \\ I^r_\infty &= \int_{\partial_\infty} ds (u(s) \cdot t(G(s, X)) - t(u(s)) \cdot G(s, X)) \end{aligned} \tag{3.19}$$

similarly

$$u(r) = I^r_\infty - \sum_j I^r_j \,. \tag{3.20}$$

Here the upper index refers to the final point X and the lower to the boundary over which the integration has been performed.

These quantities are stated below. To summarize: $I^j_{j'}, I^j_j, I^r_j, \cdots$ express the field at a given boundary or point generated from another field at the same or a different boundary. For example the field at infinity generates fields at the cavities in the bulk. Details of the calculations are given in appendix D.

3.4.1 From boundaries to boundaries

The inter-cavity integrals are $I^j_j, I^j_{j'}$ and I^j_∞.

We find from cavity j to cavity j:

$$\begin{aligned} I_j^j &= \int_{\partial_j} ds\, u(s)\cdot t(G(s,X^{(j)})) \\ &= \frac{\pi a_j}{2i\rho\omega^2}\sum_l \mathbf{B}_l^{(j)}\cdot \mathbf{t}(\psi_l^{(+)\sim}(a_j,\theta=0))\psi_l^{\wedge}(X^{(j)}) \\ &= \frac{\pi a_j}{2i\rho\omega^2}\,\mathbf{B}_l^{(j)}\cdot[\mathbf{t}(\psi_l^{(+)\sim}(a_j))]\cdot[\psi_l^{\wedge}(X^{(j)})]^t \end{aligned} \tag{3.21}$$

from cavity j' to cavity j:

$$\begin{aligned} I_{j'}^j &= \int_{\partial_{j'}} ds\, u(s)\cdot t(G(s,X^{(j)})) \\ &= \frac{\pi a_{j'}}{2i\rho\omega^2}\sum_{l,n} \mathbf{B}_l^{(j')}\cdot \mathbf{t}(\psi_l^{\wedge\sim}(a_{j'},\theta'=0))T_{ln}^{+j'j}\psi_n^{\wedge}(X^{(j)}) \\ &= \frac{\pi a_{j'}}{2i\rho\omega^2}\,\mathbf{B}_l^{(j')}\cdot[\mathbf{t}(\psi_l^{\wedge\sim}(a_{j'}))]\cdot T_{ln}^{+j'j}\cdot[\psi_n^{\wedge}(X^{(j)})]^t \end{aligned} \tag{3.22}$$

and from disc ∞ to cavity j:

$$\begin{aligned} I_\infty^j &= \int_{\partial_\infty} ds(u(s)\cdot t(G(s,X^{(j)})) - t(u(s))\cdot G(s,X^{(j)}) \\ &= \sum_{m,l} a_m T_{ml}^{\wedge Gj}\psi_l^{\wedge}(X^{(j)}) \\ &= a_m\cdot T_{ml}^{\wedge Gj}\cdot[\psi_l^{\wedge}(X^{(j)})]^t\,. \end{aligned} \tag{3.23}$$

We notice that the above terms are all in the basis of regular solutions $\psi^\wedge$. Thus with respect to this basis we can reformulate the relationship from (3.4)

$$I_\infty^j = I_j^j + \sum_{j'\neq j} I_{j'}^j \tag{3.24}$$

as a matrix equation:

$$\mathbf{a}\cdot\mathbf{C}^{\mathbf{j}} = \sum_{\mathbf{j}'}\mathbf{B}^{\mathbf{j}'}\cdot\mathbf{M}^{\mathbf{j}'\mathbf{j}}\,. \tag{3.25}$$

The first two integrals give the inter-cavity scattering matrix $\mathbf{M}$:

$$\boxed{\mathbf{M}_{nl}^{jj'} = \delta_{jj'}\delta_{ln}\mathbf{1} + (1-\delta_{jj'})\frac{a_j}{a_{j'}}[\mathbf{t}(\psi_n^{\wedge\sim})(a_j)]\cdot\mathbf{T}_{nl}^{+jj'}\cdot[\mathbf{t}(\psi_l^{+\sim})(a_{j'})]^{-1}}\,. \tag{3.26}$$

Here we have normalized the matrix so that it reduces to unity in the case of one cavity only. The summation on the right hand side above is also over the spatial indices. To keep the notation compact the terms in the square brackets refer to two-by-two *traction matrices* containing the columns of the coordinates of $t(P)$ respective. $t(S)$ (Appendix E):

$$[\mathbf{t}(\psi)] = \begin{pmatrix} t(P)_1 & t(S)_1 \\ t(P)_2 & t(S)_2 \end{pmatrix} . \tag{3.27}$$

The coordinates are with respect to some fixed system which we choose to be the global system. This matrix is found from a local expression at disc j by a rotation:

$$[\mathbf{t}(\psi)] := [\mathbf{t}(\psi)]^{(G)} = \mathbf{R}^{Gj} \cdot [\mathbf{t}(\psi)]^{(j)} , \tag{3.28}$$

where say for an outgoing state the latter is

$$[\mathbf{t}(\psi)_m^{+\sim}] \;=\; \begin{pmatrix} t(P_m)_r^{+\sim} & t(S_m)_r^{+\sim} \\ t(P_m)_\theta^{+\sim} & t(S_m)_\theta^{+\sim} \end{pmatrix} = \frac{2\mu}{a^2} \tag{3.29}$$

$$\times \begin{pmatrix} (m^2+m-\frac{1}{2}a^2\beta^2)H_m^{(1)}(a\alpha) - a\alpha H_{m-1}^{(1)}(a\alpha) & i\,m((m+1)H_m^{(1)}(a\beta) - a\beta H_{m-1}^{(1)}(a\beta)) \\ i\,m((m+1)H_m^{(1)}(a\alpha) - a\alpha H_{m-1}^{(1)}(a\alpha)) & a\beta H_{m-1}^{(1)}(a\beta) - (m^2+m-\frac{1}{2}a^2\beta^2)H_m^{(1)}(a\beta) \end{pmatrix}$$

In the second term the angular dependence $e^{\pm il\theta}$ is omitted by setting $\theta = 0$ in the end. This gives the rather complicated third term. Corresponding to in going, outgoing or regular states the traction matrix will contain $H^{(1)}, H^{(2)}, J$. The α and β refer to longitudinal and transverse wave vectors and a the cavity radius.

The rotation matrix is

$$\mathbf{R}^{Gj} = \begin{pmatrix} \cos(\theta_j^{(G)}) & -\sin(\theta_j^{(G)}) \\ \sin(\theta_j^{(G)}) & \cos(\theta_j^{(G)}) \end{pmatrix} . \tag{3.30}$$

Furthermore we have a translation matrix

$$\mathbf{T}_{nl}^{+jj'} = \begin{pmatrix} T_{nl}^{+(P)jj'} & 0 \\ 0 & T_{nl}^{+(S)jj'} \end{pmatrix} \tag{3.31}$$

acting on the various polarizations.

The normalization of $\mathbf{M}$ also influences the matrix that multiplies the scattering data a_i:

$$\mathbf{C}_{ml}^{(j)} = \frac{2i\rho\omega^2}{\pi a_j}\, T_{ml}^{\wedge Gj} \cdot [t(\psi_l^{+\sim})(a_j)]^{-1}. \tag{3.32}$$

3.4.2 From boundaries to infinity

Next we shall consider the integrals from boundaries to a point at infinity I_j^r and I_∞^r:

We find

$$\begin{aligned} I_j^r &= \int_{\partial_j} ds\, u(s) \cdot t(G(s,X)) \\ &= \frac{\pi a_j}{2i\rho\omega^2} \sum_{n,l} \mathbf{B}_n^{(j)} \cdot \mathbf{t}(\psi_n^{\wedge\sim}(a_j, \theta = 0))\, T_{nl}^{+jG} \psi_l^{(+)}(X^{(G)}) \\ &= \frac{\pi a_j}{2i\rho\omega^2}\, \mathbf{B}_n^{(j)} \cdot [\mathbf{t}(\psi_n^{\wedge\sim}(a_j))] \cdot T_{nl}^{+jG} \cdot [\psi_l^{(+)}(X^{(G)})]^t \end{aligned} \tag{3.33}$$

and by orthogonality (3.8)

$$\begin{aligned} I_\infty^r &= \int_{\partial_\infty} ds\, (u(s) \cdot t(G(s,X^{(G)})) - t(u(s)) \cdot G(s,X^{(G)}) \\ &= \sum_i a_i \psi_i^\wedge(X^{(G)}) \\ &= a_i \cdot [\psi_i^\wedge(X^{(G)})]^t\,. \end{aligned} \tag{3.34}$$

From (3.4) we have $\psi(r) = I_\infty^r - \sum_j I_j^r$. Inserting the expansion for the field at infinity and using $\psi^\wedge = \frac{1}{2}(\psi^+ + \psi^-)$ we see that all terms can be written in terms of the outgoing basis function $\psi^{(+)}$. Thus

$$\sum_n a_n S_{nl} = \sum_n \left(a_n \delta_{nl} \mathbf{1} - \sum_j \frac{\pi a_j}{i\rho\omega^2}\, \mathbf{B}_n^{(j)} \cdot \mathbf{t}(\psi_n^{\wedge\sim}(a_j, \theta = 0)) T_{nl}^{+jG} \right) \tag{3.35}$$

or in compact form

$$a_n \cdot S_{nl} = a_n \delta_{nl} \cdot \mathbf{1} - \sum_j \frac{\pi a_j}{i\rho\omega^2}\, \mathbf{B}_n^{(j)} \cdot [\mathbf{t}(\psi_n^{\wedge\sim}(a_j))] \cdot T_{nl}^{+jG}\,. \tag{3.36}$$

Defining the matrix $\mathbf{D}$:

$$D_{nl}^j = -\frac{\pi a_j}{\rho\omega^2}\, [\mathbf{t}(\psi_n^{\wedge\sim}(a_j))] \cdot T_{nl}^{+jG} \tag{3.37}$$

we have the matrix equation:

$$\mathbf{a} \cdot \mathbf{S} = \mathbf{a} \cdot \mathbf{1} - i \sum_{\mathbf{j}} \mathbf{B^j} \cdot \mathbf{D^j}\,. \tag{3.38}$$

Eliminating the scattering data $\mathbf{B}$ at the cavities we find the scattering matrix:

$$\mathbf{S} = \mathbf{1} - i\,\mathbf{C}\cdot\mathbf{M}^{-1}\cdot\mathbf{D}. \tag{3.39}$$

3.5 Scattering from one cavity

For scattering from one cylindrical cavity the S-matrix is of the form:

$$\mathbf{S}^{(1)} = \mathbf{1} - i\,\mathbf{C}\cdot\mathbf{D}\,, \tag{3.40}$$

since the $\mathbf{M}$-matrix reduces to unity.

Here we can position the global coordinate system in the center of the cavity. Therefore we can ignore the translation matrices and find in expanded form

$$\begin{aligned}\mathbf{S}^{(1)}_{lm} &= -\delta_{lm}[\mathbf{t}(\psi_l^{+\sim})(a_j)]^{-1}\cdot[\mathbf{t}(\psi_l^{-\sim})(a_j)] \\ &= -\delta_{lm}[\mathbf{t}(P_l^{+\sim})|\mathbf{t}(S_l^{+\sim})]^{-1}\cdot[\mathbf{t}(P_l^{-\sim})|\mathbf{t}(S_l^{-\sim})]\,.\end{aligned} \tag{3.41}$$

This is the scattering matrix for states with angular dependence $e^{il\theta}$. This result is very similar to the scattering matrix for the scalar Neumann problem. The difference is just that the normal derivative of the basis functions is replaced by the traction. We could also have considered scattering with even and odd states with dependence $\cos(\theta)$ and $\sin(\theta)$ as usually done in the literature. Thus in refs. [19, 18] the scattering problem has been worked out in terms of these states. Our matrix is related to the S-matrix of refs. [19, 18] by a unitary transformation. In the following we shall continue working with the states $e^{il\theta}$.

3.6 Factorization of the spectral determinant

From (3.39) the spectral determinant becomes formally

$$\mathrm{Det}(\mathbf{S}) = \frac{\mathrm{Det}(\mathbf{M} - i\,\mathbf{D}\cdot\mathbf{C})}{\mathrm{Det}(\mathbf{M})}\,. \tag{3.42}$$

We shall show that the numerator factorizes

$$\mathrm{Det}(\mathbf{X}) := \mathrm{Det}(\mathbf{M} - i\,\mathbf{D}\cdot\mathbf{C}) = \mathrm{Det}(\mathbf{M}(\omega^*)^\dagger)\prod_{\mathsf{j}}\det(\mathbf{S}^{(1)}_{\mathsf{j}})\,. \tag{3.43}$$

Thus

$$\mathrm{Det}(\mathbf{S}(\omega)) = \frac{\mathrm{Det}(\mathbf{M}(\omega^*)^\dagger)}{\mathrm{Det}(\mathbf{M}(\omega))} \prod_{\mathbf{j}} \det(\mathbf{S}_{\mathrm{j}}^{(1)}(\omega))\,. \tag{3.44}$$

So there is a factorization in a coherent part among scatters and incoherent parts due to the individual scatters. By inspection of (3.26)-(3.47) one finds that the poles of the one-cavity determinants cancel exactly the poles of the denominator matrix $\mathbf{M}$ of the coherent part. Similarly the poles of $\mathbf{M}^\dagger$ are cancelled by the zeroes of the one-cavity determinant. Hence *the genuine scattering resonances are given by the zeroes of the* $\mathbf{M}$*-matrix.*

To prove the above statements we calculate $\mathbf{D}\cdot\mathbf{C}$:

When $j = j'$:

$$\mathbf{D}_n^j \cdot \mathbf{C}_l^j = -2i[\mathbf{t}(\psi_n^{\wedge\sim})(a_j)] \cdot [\mathbf{t}(\psi_l^{+\sim})(a_j)]^{-1}\delta_{nl} \tag{3.45}$$

and for $j \neq j'$:

$$\begin{aligned}\mathbf{D}_n^j \cdot \mathbf{C}_l^{j'} &= \sum_{m=-\infty}^{\infty}\left(-2i\frac{a_j}{a_{j'}}[\mathbf{t}(\psi_n^{\wedge\sim})(a_j)] \cdot \mathbf{T}_{nm}^{+jG} \cdot \mathbf{T}_{ml}^{\wedge Gj'} \cdot [\mathbf{t}(\psi_l^{+\sim})(a_{j'})]^{-1}\right)\\ &= -2i\frac{a_j}{a_{j'}}[\mathbf{t}(\psi_n^{\wedge\sim})(a_j)] \cdot \mathbf{T}_{nl}^{\wedge jj'} \cdot [\mathbf{t}(\psi_l^{+\sim})(a_{j'})]^{-1}\,.\end{aligned}$$

This gives $\mathbf{X}$:

$$\begin{aligned}\mathbf{X}_{ln}^{jj'} &= -\delta_{jj'}\delta_{ln}[\mathbf{t}(\psi_l^{-\sim})(a_j)] \cdot [\mathbf{t}(\psi_l^{+\sim})(a_j)]^{-1}\\ &\quad -(1-\delta_{jj'})\frac{a_j}{a_{j'}}[\mathbf{t}(\psi_l^{\wedge\sim})(a_j)] \cdot \mathbf{T}_{ln}^{-jj'} \cdot [\mathbf{t}(\psi_n^{+\sim})(a_{j'})]^{-1}\,.\end{aligned} \tag{3.46}$$

On the other hand considering complex conjugate frequencies (corresponding to conjugate k_L and k_T) we get

$$(\mathbf{M}_{-l,\,-n}^{jj'}(\omega^*))^* = \delta_{jj'}\delta_{ln}\mathbf{1} + (1-\delta_{jj'})\frac{a_j}{a_{j'}}[\mathbf{t}(\psi_l^{\wedge\sim})(a_j)] \cdot \mathbf{T}_{ln}^{-jj'} \cdot [\mathbf{t}(\psi_n^{-\sim})(a_{j'})]^{-1}\,. \tag{3.47}$$

These two results differ by the matrix $S^\sim$

$$\mathbf{S}_{ln}^{\sim(1)} = -\delta_{ln}[\mathbf{t}(\psi_l^{-\sim})(a_j)] \cdot [\mathbf{t}(\psi_l^{+\sim})(a_j)]^{-1}\,, \tag{3.48}$$

which clearly has the same determinant as the the one-cavity scattering matrix. However, it does not have the same form as the latter. Why? This comes from our choice of specifying the data on the cavities as vectorial. This gives an **M**-matrix which maps from physical space to physical space. The scattering matrix, however, maps from the state of basis functions into basis functions. Thus with the definitions chosen we do not expect a direct matrix factorization of $\mathbf{X}$ into $\mathbf{M}(\omega^*)^\dagger, \mathbf{S}^{(1)}$ as opposed to the scalar case.

3.6.1 Symmetry factorization

We shall consider cavities arranged in a symmetric fashion (fig. 3.1). For the case of two cylindrical cavities of equal radius the symmetry group is C_{2v}, with the character table 3.1, and for three cylindrical cavities with centers at the vertices of an equilateral triangle the symmetry group is C_{3v} [44].

C_{2v}	E	C_2	σ_x	σ_y
A_1	1	1	1	1
A_2	1	1	-1	-1
B_1	1	-1	1	-1
B_2	1	-1	-1	1

Table 3.1: Character table of C_{2v}.

This symmetry can be exploited to block-diagonalize the scattering matrix and hence factorize the scattering determinant. This will reduce the numerical workload, since the subspace scattering matrices will be of much smaller size. Furthermore the symmetry will manifest itself at a classical level by reducing the number of periodic orbits in the cumulant expansion of the determinant. Below we just state the procedure (for a derivation see Appendix F):

We define for $m \geq 0$:

$$d(m) = \sqrt{2} \text{ for } m > 0 \qquad \text{and } d(0) = 1\,. \tag{3.49}$$

For the two-cavity system where all radii are equal ($= a$) and the angles to the respective centers are $\phi_1^{(2)} = \phi_2^{(1)} = \pi$ we get in terms of two by two matrix entries for $m, n \geq 0$

$$\mathbf{M}_{mn}(\sigma_1, \sigma_2) = \delta_{mn}\mathbf{1} + \frac{\sigma_1}{2}\, d(m)\, d(n)\, [\mathbf{t}(\psi_m^{\wedge\sim})(a)] \cdot \mathbf{T}^+_{mn}(\sigma_2) \cdot [\mathbf{t}(\psi_n^{+\sim})(a)]^{-1}\,, \tag{3.50}$$

where the modified translation matrix is

$$\begin{aligned}\mathbf{T}^{+}_{mn}(\sigma_2) &= (-1)^m \left[\begin{pmatrix} H^{(1)}_{m-n}(\alpha R) & 0 \\ 0 & H^{(1)}_{m-n}(\beta R) \end{pmatrix} \right. \\ &\quad \left. +\sigma_2 (-1)^n \begin{pmatrix} H^{(1)}_{m+n}(\alpha R) & 0 \\ 0 & -H^{(1)}_{m+n}(\beta R) \end{pmatrix} \right] \end{aligned} \tag{3.51}$$

and $\sigma_1, \sigma_2 = \pm 1$ indexing the irreducible representations (table 3.2). We have

C_{2v}	A_1	A_2	B_1	B_2
σ_1	+	+	-	-
σ_2	+	-	+	-

Table 3.2: Sign convention in the reduced inter-cavity matrix.

The matrices are reduced since they no longer carry cavity indices and only non-negative indices of angular momentum are present.

The factorization is quite similar to the scalar cases, just with a minus sign in the lower right corner of the second matrix in the translation part (3.51).

3.7 Fredholm theory and shadowing

In the case of the scalar disc problem the results derived above can be justified rigorously by proving that $\mathbf{M} = \mathbf{1} + \mathbf{A}$ is an operator of the *Fredholm* type with $\mathbf{A}$ a *trace-class* operator. This means that all traces of powers of $\mathbf{A}$ exist and therefore the determinant of $\mathbf{M}$ exists, as defined by its expansion in terms of traces

$$\begin{aligned}\mathrm{Det}\,\mathbf{M} &= \exp\left(-\sum_{n=1}^{\infty} (-1)^n \frac{\mathrm{Tr}\,(\mathbf{A}^n)}{n} \right) \\ &= 1 + \mathrm{Tr}\,\mathbf{A} - \frac{1}{2}(\mathrm{Tr}\,(\mathbf{A}^2) - (\mathrm{Tr}\,\mathbf{A})^2) + \cdots . \end{aligned} \tag{3.52}$$

The Fredholm determinant $F(z) = \mathrm{Det}\,(\mathbf{1} + \mathrm{z}\mathbf{A})$ is analytic in z. Thus the coefficients of z^n, *cumulants*, in the above expansion of $F(z)$ decay faster than exponentially.

For high frequencies these traces can be approximated by sums over classical prime cycles and their repeats, as we shall see below. The fast decay of the Fredholm series means that the cumulant sums must involve large cancellations among the individual

cycles, and that the contributions of long orbits are in part cancelled by products of shorter ones. In the theory of dynamical systems this phenomenon is called *shadowing*. There similar cancellations are seen for spectral determinants of evolution operators in strongly chaotic systems. The cancellations determine the convergence of the spectral determinant and hence the precision at which spectral resonances can be found. At its best the convergence is super-exponential [36]. The above shadowing arguments should be taken with the following consideration in mind: In the high-frequency limit the traces in the Gutzwiller-Voros and the analogous elastodynamic determinants are approximated by sums over periodic orbits. This approximation introduces errors in the Fredholm determinant, so the decay of cumulants is degraded and the region of convergence decreased. However, for the leading quantum resonances the numerical agreement is remarkably good [2]. At this time it is not known to what extent the accuracy of the saddle point approximations can be increased by including all creeping orbits and by taking higher $\hbar$-corrections in the saddle point expansions.

From our preliminary investigations we have reason to believe that also in the elastodynamic setting the $\mathbf{M}$-matrix is a Fredholm operator. We will at this stage not attempt to prove this, but just mention that numerically we see decay of the cumulants and that the expression for the elastodynamic $\mathbf{M}$-matrix is very similar in form to the quantum mechanical result, giving us confidence in our numerical calculations of $\det\mathbf{M}$.

Résumé

In this chapter we have formulated the scattering problem for a system of cylindrical cavities in plane strain elasticity. A basis of scattering states makes it possible to explicitly calculate the elements of the full scattering matrix in analytic form, in terms of Bessel functions. The scattering determinant was shown to factorize into an incoherent and coherent part. We now turn to a study of each of these pieces.

Chapter 4

High frequency limit

In this chapter our goal is to introduce a ray dynamics relevant to our elastodynamic system of cavities. This ray dynamics is derived from the underlying wave equation and its boundary condition by studying a single cavity. We shall follow the recent work by Wirzba [3]. Interestingly, we have to include surface rays of very low attenuation.

For wave systems whose underlying classical dynamics is integrable the high frequency or semi-classical resonances are given by the Bohr-Sommerfeld quantization. For systems with a more complicated classical dynamics, often refered to as chaotic, the quantization is likewise more complicated. Those systems have been investigated using several methods. Originally Gutzwiller [34] found his celebrated trace formula using path-integrals. This approach is a very general one and it might not be impossible to define path integrals also in elastodynamics. Investigations on quantum billiards are mostly based on the saddle point method applied to integral kernels. Typically one derives a boundary integral equation which is then studied near a saddle corresponding to a periodic orbit. Perhaps the fastest way [1] of deriving Gutzwiller's formula is the method of WKB. The path-integral and the WKB are general methods allowing for varying potential, whereas the boundary integral method requires constant potential in the inside of the billiard. Complex orbits seem always to be introduced in a rather ad hoc fashion with exception of the very specialized method of [2] using the Sommerfeld-Watson transformation. As mentioned in the introduction, many problems in scattering theory involve sums over the Bessel functions, special functions which often appear if a rotational symmetry is present. These sums over angular momentum l converge for low frequencies but fail at high frequencies. The Sommerfeld-Watson idea is to complexify the angular momentum and convert the sum into a contour integral. This integral will typically pick up contributions from saddle points and poles. We shall see below that the saddles correspond to free geometric rays and the poles to *surface* rays. Further complications will arise if the integrand contains other singularities such as branch points. In our case we shall focus only on the so-called Rayleigh poles.

In elastodynamics contour integral methods have been used in e.g. [19]:

1. An expansion for the dynamic hoop stress: $\sigma_{\theta\theta}$. For the free boundary all stresses vanish except for the hoop stress. This stress depends on the total field which we can write as a sum over angular momenta. This is then transformed into a sum over creeping waves and a Rayleigh wave.

2. The transient response from cavities: one encounters contributions from P,S and Rayleigh waves.

Here we shall work out the high frequency limit of the *Green's function* in the frequency domain for one cavity following Wirzba. As an introduction to the problem we familiarize ourselves with the known exact results on cavity resonances and their attenuation.

4.1 One cavity resonances

4.1.1 Exact results

What is known about the exact position of the resonances? They have been discussed in [13]. We have reproduced their results, see chapter 5. For the sake of presentation we wish to show the data already now. We have confirmed numerically the resonance spectrum for *polyethylene*. For polyethylene the relevant parameters are $c_L = 1950\,m/s$ and $c_T = 540\,m/s$. The resonances correspond to the poles of the scattering determinant at various integer values of the angular momentum.

We plot the first 120 Rayleigh poles in the fourth quadrant of $k_L a$ in fig. 4.1. For high frequencies there is a band of resonances close to the real axis. The spacing is regular and quite close (within two significant digits) to what one would expect for a wave moving with Rayleigh speed ($c_R = 513\,m/s$) on an infinite flat boundary. However, deviations are not only on the real part but also there now is a small imaginary part. The goal in the following is to describe these deviations.

4.1.2 One cavity determinant

To find the resonances we do not have to use the full spectral determinant (3.41) but just its *denominator*. Thus resonances can be found numerically using (3.29) searching for its zeroes. Our theoretical investigation will use the expression (E.7), where the order of the Hankel functions has a fixed angular momentum l.

We shall study this expression perturbatively in the limit of high frequencies focusing on resonances of the Rayleigh type.

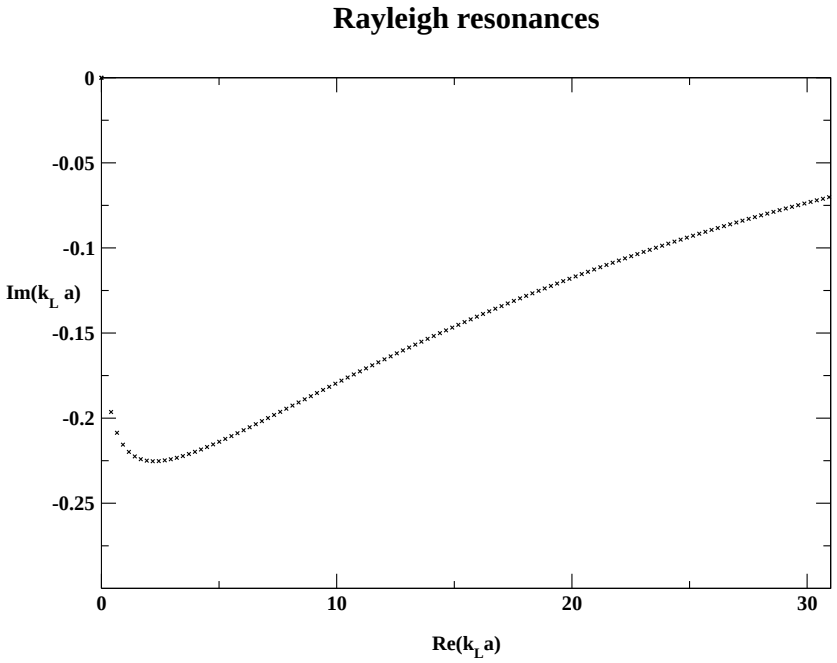

Figure 4.1: The first 120 Rayleigh scattering resonances for polyethylene with a single cavity of radius a. The line of resonances goes asymptotically to the real axis, with high frequencies having vanishingly small attenuation.

First we mention that the Airy expansions of the Hankel functions in the scattering determinant may be used, but seem too complicated for a theoretical description of the Rayleigh resonances. However, for numerical purposes they work well: using two leading terms in the Airy expansion determine the resonances to three significant digits.

This last approach takes two saddles into account and this can also be done using just the Debye expansion but keeping the expontially small term coming from the J_l part of the Hankel function. This is the idea of Viktorov [45] which we shall describe below.

The exponential *Debye* expansion for the Hankel functions:

$$J_l(z) \sim \sqrt{\frac{1}{2\pi Q}} e^{Q - l\,ArcCosh(l/z)} \tag{4.1}$$

$$Y_l(z) \sim -\sqrt{\frac{2}{2\pi Q}} e^{-Q + l\,ArcCosh(l/z)} \tag{4.2}$$

$$H_l^{(1)}(z) = J_l(z) + iY_l(z) \sim -i\sqrt{\frac{2}{2\pi Q}} e^{-Q + l\,ArcCosh(l/z)}, \tag{4.3}$$

with

$$Q = Q(l,z) = \sqrt{l^2 - z^2}\,. \tag{4.4}$$

Here the *order* l is assumed larger than the argument z. Other cases would lead to other resonances, e.g. resonances of Franz type [14] when $l \simeq z$. (4.3) is essentially just the saddle point approximation. We see that $J_l(z)$ is exponentially small and can be omitted from the asymptotic expansion of $H_l^{(1)}(z)$.

For convenience we put

$$q = Q(l, k_L a) \qquad \text{and} \qquad s = Q(l, k_T a)\,. \tag{4.5}$$

Also we shall write the angular momentum in terms of an azimuthal and transverse wave number

$$l = ak_R \equiv \eta a k_T\,. \tag{4.6}$$

Inserting this expansion into (E.7) and defining the determinant D we find to leading order after some manipulation

$$D \sim \det\begin{pmatrix} (l^2 - (a\beta)^2/2) + q & il(1+s) \\ il(1+q) & -(l^2 - (a\beta)^2/2) - s \end{pmatrix}. \tag{4.7}$$

The condition for resonance $D = 0$ gives

$$l^2 qs = ((a\beta)^2/2 - l^2)^2\,. \tag{4.8}$$

Hence we get an equation for the ratio $\eta \simeq c_T/c_R$

$$\eta^2\sqrt{\eta^2 - 1}\sqrt{\eta^2 - (c_T/c_L)^2} = (1/2 - \eta^2)^2\,. \tag{4.9}$$

This is precisely Rayleigh's equation for surface waves on the infinite half plane, as in the high frequency limit we cannot distinguish between a curved surface or a plane. Interestingly there are also other resonances which we associate with the *complex* solutions of Rayleigh's equation which can be rewritten as a cubic equation for η^2 [13]. These resonances are, however, strongly damped and will be omitted in the following.

We find corrections to the ratio η from the curvature of the boundary by inserting the Debye *series* instead:

$$H_l^{(1)}(z) \;=\; J_l(z) + iY_l(z) \sim -i\sqrt{\frac{2}{2\pi Q}}e^{-Q + l\,ArcCosh(l/z)} \tag{4.10}$$

$$
\begin{aligned}
& \times(1-\frac{1}{8}\frac{l}{Q}+\frac{5}{24}(\frac{l}{Q})^3\ldots) \\
H_l^{(1)\prime}(z) \;\sim\; & (-Q/z)(-i\sqrt{\frac{2}{2\pi Q}}e^{-Q+l\,ArcCosh(l/z)} \\
& \times(1+\frac{3}{8}\frac{l}{Q}-\frac{7}{24}(\frac{l}{Q})^3\ldots))\,.
\end{aligned}
\tag{4.11}
$$

Here we expand

$$
\eta=\eta_0+\frac{\eta_1}{\beta a}+\frac{\eta_2}{(\beta a)^2}+\ldots \tag{4.12}
$$

and solve systematically for the unknowns $\eta_1,\eta_2,\ldots$. Analytical expressions soon become cumbersome for the higher corrections and we just state that for our material in consideration we find

$$
\begin{aligned}
\eta_0 &= 1.0525597 \\
\eta_1 &= 2.1436297 \\
\eta_2 &= 26.845142 \\
&\vdots
\end{aligned}
\tag{4.13}
$$

All further corrections can be seen to be real which would seem to imply *no attenuation*. This, however, as we know from fig. 4.1 cannot be.

To proceed one has to include the Debye series for also $J_l(z)$ at some point of approximation near $\eta_0+\frac{\eta_1}{\beta a}$, as in [45]. It has been remarked by Wirzba that for even higher frequencies one should perturb around say $\eta_0+\frac{\eta_1}{\beta a}+\frac{\eta_2}{(\beta a)^2}$ instead, and so on for yet higher frequencies. The reason is that one truncates the Debye series to its smallest term and this truncation happens at higher orders for higher frequencies. On the other hand it appears to be difficult to find a good approximation for intermediate regimes, i.e. up to size parameter $k_L a<25$. This is in contrast to the good convergence in scalar wave mechanics for the Franz resonances.

One can write the resonance condition as

$$
0\approx f(\eta)+e^{-\phi_1(\eta)}h_1(\eta)+e^{-\phi_2(\eta)}h_2(\eta),
$$

where f,ϕ_i and h_i are the functions:

- $h=i(\frac{1}{2}-2\eta_0^2+2qs\eta_0^2+2\eta_0^4)=\frac{i}{2}((1-2\eta^2)^2+4qs\eta_0^2)=i4qs\eta_0^2$
- $f'=-8\eta_0(1+qs+\frac{1}{2}(q/s+s/q-4)\eta_0^2$

- $\phi = -2\,s\,\beta + 2\,\beta\,\eta$ ArcCosh(η) (transverse part).

In our case the last terms are exponentially small and imaginary. The first term already corresponds to the perturbative solution. Expanding around η gives a purely imaginary correction.

Viktorov's correction becomes

$$\begin{aligned} Im(\eta) &= (e^{2(s-lArcCosh(\frac{l}{\beta a}))} + (c_L/c_T)^2 e^{2(q-lArcCosh(\frac{l}{\alpha a}))} \\ &\times \frac{4\eta_0^2\sqrt{\eta_0^2-1}\sqrt{\eta_0^2-(c_T/c_L)^2}}{8\eta_0(1+\sqrt{\eta_0^2-1}\sqrt{\eta_0^2-(c_T/c_L)^2} + \frac{1}{2}\eta_0^2(\frac{\sqrt{\eta_0^2-1}}{\sqrt{\eta_0^2-(c_T/c_L)^2}} + \frac{\sqrt{\eta_0^2-(c_T/c_L)^2}}{\sqrt{\eta_0^2-1}} - 4))}, \end{aligned} \tag{4.14}$$

where $l = \beta(\eta_0 + \frac{\eta_1}{\beta a} + \ldots)$ is the current best *real* approximation. We remark that this result is essentially non-perturbative and for high frequencies exponentially small.

4.2 Green's function in the presence of a single cavity

The motivation for studying a single cavity Green's function is that from this elementary case one can get many insights about the high frequency behaviour in elastodynamics. We shall extract from this case the ray dynamics, including detailed evolution of phases and amplitudes.

4.2.1 Sommerfeld-Watson transformation

In analogy with the scalar treatment for a disc we define the Green's function for a cavity in elastodynamics as

$$\begin{aligned} \mathbf{G}(r_>, r_<) &= \frac{1}{8i\rho\omega^2}\sum_l \left(\psi_l^+(r_>) \otimes (\psi_l^{-\sim}(r_<) + \mathbf{S}_l^{(1)}\psi_l^{+\sim}(r_<))\right) \\ &= [G(r_>, r_<)_{ab}] \\ &= \frac{1}{8i\rho\omega^2}\sum_{l,\pi}\left[\psi_{la\pi}^+(r_>)(\psi_{lb\pi}^{-\sim}(r_<) + \sum_\sigma S_{l\pi\sigma}^{(1)}\psi_{lb\sigma}^{+\sim}(r_<))\right] \\ &= \frac{1}{8i\rho\omega^2}\sum_l [\psi_l^+(r_>)] \cdot ([\psi_l^{-\sim}(r_<)]^t + [S_l^{(1)}] \cdot [\psi_l^{+\sim}(r_<)]^t) \end{aligned} \tag{4.15}$$

Here the terms $[\psi]$ refer to the vector components of the displacement field in global coordinates, and greek indices $\pi, \sigma \in \{P, S\}$ refer to the pressure, shear components. The displacement matrices can be found from a local expression:

$$[\psi] = \mathbf{R}^{G\,loc} \cdot [\psi]^{(loc)} \tag{4.16}$$

with

$$\mathbf{R}^{G\,loc} = \begin{pmatrix} \cos(\theta) & -\sin(\theta) \\ \sin(\theta) & \cos(\theta) \end{pmatrix} =: \mathbf{R}_\theta \tag{4.17}$$

and for resp. $e^{\pm il\theta}$-dependence

$$[\psi]_l^{(loc)+(\ )/\sim} = e^{\pm il\theta} \begin{pmatrix} \partial_a H_l^{(1)}(a\alpha) & \pm\frac{il}{a} H_l^{(1)}(a\beta) \\ \pm\frac{il}{a} H_l^{(1)}(a\alpha) & -\partial_a H_l^{(1)}(a\beta) \end{pmatrix} \tag{4.18}$$

Remark: Above the one-cavity S-matrix is unspecified. We shall concentrate on the traction free cavity with the S-matrix given by (3.41). (4.15) can be obtained from the *free* Green's function (3.9) by modifying the regular part

$$\psi_l^{\wedge\sim} = \frac{1}{2}(\psi_l^{-\sim} + \psi_l^{+\sim}) =: \frac{1}{2}(\psi_l^{-\sim} + \mathbf{S}_l^{(1)} \cdot \psi_l^{+\sim}). \tag{4.19}$$

The motivation is here that only the outgoing wave functions are affected by the cavity. The scattering matrix is chosen with respect to the given boundary conditions such that (4.15) itself satisfies the boundary conditions. Since the scattering matrix is diagonal in angular momentum it only depends on one index.

To simplify the notation we shall put $\mathbf{\Psi} := [\psi^{(loc)\sim}]|_{\theta=0}$ in the following. We shall sometimes refer to the scattering matrix as

$$\mathbf{S}_\nu^{(1)} = -\frac{\begin{pmatrix} \tilde{A} & \tilde{B} \\ \tilde{C} & \tilde{D} \end{pmatrix}}{\mathrm{Det}[H_\nu^{(1)}]} \equiv \frac{N}{\mathrm{Det}[H_\nu^{(1)}]}. \tag{4.20}$$

Here the matrix N is minus the transpose of the cofactor of the outgoing traction matrix times the incoming traction matrix whereas the denominator $\mathrm{Det}[H_\nu^{(1)}]$ is the determinant of the outgoing traction matrix.

We put $\Delta\theta = \theta' - \theta$ and rewrite (4.15) as a contour integral

$$\begin{aligned}\mathbf{G}(r_>, r_<) = & \frac{1}{8i\rho\omega^2}\oint_C d\nu \frac{e^{i\nu\Delta\theta}}{e^{2\pi i\nu}-1}\mathbf{R}_{\theta'}\mathbf{\Psi}^+_\nu(r')(\mathbf{\Psi}^-_\nu(r)+\mathbf{S}^{(1)}_\nu\mathbf{\Psi}^+_\nu(r))\mathbf{R}^{-1}_\theta \\ = & \mathbf{R}_{\theta'}\{\frac{1}{8i\rho\omega^2}\oint_C d\nu \frac{e^{i\nu(\Delta\theta-\pi)}}{2i\sin\nu\pi}\mathbf{\Psi}^+_\nu(r')(\mathbf{\Psi}^-_\nu(r)+\mathbf{S}^{(1)}_\nu\mathbf{\Psi}^+_\nu(r))^t\}\mathbf{R}^{-1}_\theta. \quad (4.21)\end{aligned}$$

Here the contour C runs counter-clockwise slightly above and below the real axis. Cauchy's theorem ensures that we pick up the correct contribution from every integer. By transforming to another contour which goes slightly above the real axis we get for a general function f

$$\oint_C d\nu\, f(\nu) = \int_{-\infty+i\epsilon}^{\infty+i\epsilon} d\nu\,(f(-\nu)-f(\nu)). \quad (4.22)$$

Now the effect of reversing the (complex) order ν of our basis functions will besides phase factors also involve a linear transformation σ that flips off-diagonal elements in $\mathbf{\Psi}$

$$\mathbf{\Psi}^\pm_{-\nu} = e^{\pm i\pi\nu}\sigma(\mathbf{\Psi}^\pm_\nu). \quad (4.23)$$

Hence the scattering matrix will transform as

$$\mathbf{S}^{(1)}_{-\nu} = e^{-2\pi i\nu}\sigma(\mathbf{S}^{(1)}_\nu). \quad (4.24)$$

The integrand as a function of the complexified angular momentum ν will be split in a regular part and a part that has poles on the real axis. The former can be evaluated on the real axis by the stationary phase method. The latter, however, is calculated in the upper ν-plane at the poles of the scattering determinant. Here we focus on the leading poles corresponding to the Rayleigh surface waves, whereas the stationary phase integral will lead to geometrical, "body", rays. In this case ("insonified" or "light" case) we shall *choose* to write the functional dependence ("Watson factors") as

$$e^{i\nu\Delta\theta} + \frac{e^{i\nu(2\pi+\Delta\theta)}}{1-e^{2\pi i\nu}} + \sigma\frac{e^{i\nu(2\pi-\Delta\theta)}}{1-e^{2\pi i\nu}}\,, \quad (4.25)$$

where by abuse of notation σ is 1 for diagonal elements and -1 for off-diagonal.

There are cases where the Green's function does not have a geometrical contribution (the "shadow" case) or where the distinction between surface and geometric

contributions breaks down ("penumbra"). The penumbra case will not be considered here. The shadow case, however, is written *without* a regular part

$$\frac{e^{i\nu(\Delta\theta)}}{1-e^{2\pi i\nu}} + \sigma\frac{e^{i\nu(2\pi-\Delta\theta)}}{1-e^{2\pi i\nu}}\,. \tag{4.26}$$

We shall only consider the light case which is the most general. Thus splitting the Green's function into a geometric and diffractive part

$$\mathbf{G}(r'=r_>, r=r_<) = \mathbf{G}(r',r)_{geo} + \mathbf{G}_{diff}(r',r) \tag{4.27}$$

is accomplished by

$$\mathbf{G}_{geo}(r',r) = \mathbf{R}_{\theta'}\{\frac{1}{8i\rho\omega^2}\int_{-\infty+i\epsilon}^{\infty+i\epsilon} d\nu\, e^{i\nu\Delta\theta}\,\mathbf{\Psi}_\nu^+(r')(\mathbf{\Psi}_\nu^-(r)+\mathbf{S}_\nu^{(1)}\mathbf{\Psi}_\nu^+(r))^t\}\mathbf{R}_\theta^{-1} \tag{4.28}$$

and

$$\begin{aligned}\mathbf{G}_{diff}(r',r) &= \mathbf{R}_{\theta'}\{\frac{1}{8i\rho\omega^2}\int_{-\infty+i\epsilon}^{\infty+i\epsilon} d\nu\,\frac{e^{i\nu(2\pi+\Delta\theta)}+\sigma e^{i\nu(2\pi-\Delta\theta)}}{1-e^{2\pi i\nu}}\,\mathbf{\Psi}_\nu^+(r') \\ &\quad\times(\mathbf{\Psi}_\nu^-(r)+\mathbf{S}_\nu^{(1)}\mathbf{\Psi}_\nu^+(r))^t\}\mathbf{R}_\theta^{-1}.\end{aligned} \tag{4.29}$$

4.2.2 Geometrical contributions to the Green's function

As mentioned above we consider the light case where the positions r, r' are connected with a geometrical straight line not passing through the cavity. We thus look for the following contributions:

1. A straight path from r to r'.
2. A reflected path for each polarization, here longitudinal to longitudinal and transverse to transverse.
3. A refracted or wave splitting path: longitudinal to transverse and vice versa.

We shall here treat only the straight path and the wave splitting, since the reflected case is quite similar to the latter.

Free path

For the straight path we shall distinguish between two cases: Define the point of closest encounter on the straight line connecting r, r' with the cavity. It is from here the impact parameter is measured. The points r, r' are either on the same side with respect to this point or on the opposite sides. We shall show that the first case is obtained from the term without the scattering matrix in (4.28), whereas latter case follows from the term with the scattering matrix included. In the following we shall denote these saddles by ν_{L1}, ν_{T1} and ν_{L2}, ν_{T2} .

The asymptotic expansion of $H_l(z)$ when $z > l$ is given by the oscillatory Debye's expansion

$$\begin{aligned} H_\nu^{(1)}(z) &\sim \sqrt{\frac{2}{\pi Q}} \exp(iQ - i\nu \arccos\frac{\nu}{z} - i\frac{\pi}{4}) \\ H_\nu^{(2)}(z) &\sim \sqrt{\frac{2}{\pi Q}} \exp(-iQ + i\nu \arccos\frac{\nu}{z} + i\frac{\pi}{4}) \\ H_\nu^{(1)'}(z) &\sim i\,Q\,H_\nu^{(1)}(z)\,, \end{aligned} \tag{4.30}$$

using the same symbols as in (4.4)

$$\begin{aligned} Q(\nu, z) &= \sqrt{z^2 - l^2} \\ q = Q_L &= Q(\nu, k_L r) \\ s = Q_T &= Q(\nu, k_T r) \end{aligned} \tag{4.31}$$

and similarly for the arguments r' and a $(q', q_a, \ldots)$.

In the first case we get

$$\begin{aligned} \mathbf{G}_{geo}(r', r) &\sim \mathbf{R}_{\theta'} \{ \frac{1}{8i\rho\omega^2} \int_{-\infty+i\epsilon}^{\infty+i\epsilon} d\nu\, e^{i\nu\Delta\theta}\, \frac{i}{r'} \begin{pmatrix} q' & \nu \\ \nu & -s' \end{pmatrix} \\ &\quad \times \begin{pmatrix} H_\nu^{(1)}(k_L r') & 0 \\ 0 & H_\nu^{(1)}(k_T r') \end{pmatrix} \begin{pmatrix} H_\nu^{(2)}(k_L r) & 0 \\ 0 & H_\nu^{(2)}(k_T r) \end{pmatrix} \\ &\quad \times \frac{-i}{r} \begin{pmatrix} q & \nu \\ \nu & -s \end{pmatrix} \} \mathbf{R}_\theta^{-1} \\ &\sim \mathbf{R}_{\theta'} \begin{pmatrix} q'/r' & \nu/r' \\ \nu/r' & -s'/r' \end{pmatrix} \\ &\quad \times \frac{1}{4i\rho\omega^2} \sqrt{\frac{2}{\pi}} \begin{pmatrix} \frac{e^{ik_L L_{L1} - i\pi/4}}{\sqrt{k_L L_{L1}}} & 0 \\ 0 & \frac{e^{ik_T L_{T1} - i\pi/4}}{\sqrt{k_T L_{T1}}} \end{pmatrix} \\ &\quad \times \begin{pmatrix} q/r & \nu/r \\ \nu/r & -s/r \end{pmatrix} \mathbf{R}_\theta^{-1}\,, \end{aligned} \tag{4.32}$$

where the saddle point conditions for each polarization are

$$\begin{aligned} 0 &= \Delta\theta - \arccos\frac{\nu_{L1}}{k_L r'} + \arccos\frac{\nu_{L1}}{k_L r} \\ 0 &= \Delta\theta - \arccos\frac{\nu_{T1}}{k_T r'} + \arccos\frac{\nu_{T1}}{k_T r}\,. \end{aligned} \tag{4.33}$$

These equations have real solutions ν_{i1} and can be intepreted if we define $\nu_i = k_i b$ with b as the *impact* parameter and $i \in \{\mathrm{L}, \mathrm{T}\}$.

In the phase factor evaluated at the saddle only the terms of type q, s-survive. Thus for the lengths L_{i1} we have

$$k_L L_{L1} = q' - q \qquad k_T L_{T1} = s' - s, \tag{4.34}$$

which corresponds to

$$L_{L1} = L_{T1} = |\mathbf{r}' - \mathbf{r}| = \sqrt{r'^2 - b^2} - \sqrt{r^2 - b^2}, \tag{4.35}$$

since Q_i/k_i is the projection of the length of the vector $\vec{r}$ onto the tangent plane of the point of closest contact. We postpone the discussion of the overall amplitude to the wave splitting case below.

The final step is to intepret the matrices sandwiched between the rotation matrices $\mathbf{R}_\theta, \mathbf{R}_{\theta'}$. We describe the impact vector as $\mathbf{r}_0 = b\,\hat{\mathbf{r}}(\theta_0)$, where θ_0 is the angle in the global coordinate system. Then $L_{S1} = r'\sin(\theta' - \theta_0) - r\sin(\theta - \theta_0)$. Therefore e.g. $\frac{\partial}{\partial_{r'}}(k' L_{S1}) = k'\sin(\theta' - \theta_0) = q'/r'$ and $\frac{1}{r'}\frac{\partial}{\partial_{\theta'}}(k' L_{S1}) = k'\cos(\theta' - \theta_0) = k' b/r' = \nu/r'$. Thus

$$\begin{aligned} \mathbf{G}_{geo}(r', r) \;\sim\; & \overrightarrow{\nabla}_{\mathbf{r}'}\,\frac{1}{4i\rho\omega^2}\sqrt{\frac{2}{\pi}}\frac{\exp\left(ik_L L_{S1} - i\frac{\pi}{4}\right)}{\sqrt{k_L L_{S1}}} \otimes \overleftarrow{\nabla}_{\mathbf{r}} \\ & + \overrightarrow{\nabla}_{\mathbf{r}'}\times\hat{\mathbf{z}}\frac{1}{4i\rho\omega^2}\sqrt{\frac{2}{\pi}}\frac{\exp\left(ik_T L_{S1} - i\frac{\pi}{4}\right)}{\sqrt{k_T L_{S1}}} \otimes \overleftarrow{\nabla}_{\mathbf{r}}\times\hat{\mathbf{z}} \\ = & \overrightarrow{\nabla}_{\mathbf{r}'}\,\frac{1}{\rho\omega^2} G_{\mathrm{sc}}(k_L L_{S1}) \otimes \overleftarrow{\nabla}_{\mathbf{r}} + \overrightarrow{\nabla}_{\mathbf{r}'}\times\hat{\mathbf{z}}\frac{1}{\rho\omega^2} G_{\mathrm{sc}}(k_T L_{S1}) \otimes \overleftarrow{\nabla}_{\mathbf{r}}\times\hat{\mathbf{z}}, \end{aligned} \tag{4.36}$$

where

$$G_{\mathrm{sc}}(kL) = \frac{1}{4i}\frac{\exp\left(ikL - i\frac{\pi}{4}\right)}{\sqrt{kL}} \tag{4.37}$$

is the semiclassical free propagator for the two-dimensional scalar problem.

In the case where the point of impact is between the points r, r', both saddles ν_{L2}, ν_{T2} are larger than the arguments $k_L a, k_T a$. The scattering matrix becomes

$$\begin{aligned} S_\nu^{(1)} &= -[t(\psi_\nu^{+\sim})]^{-1} \cdot [t(\psi_\nu^{-\sim})] \\ &= \mathbf{1} - 2\,[t(\psi_\nu^{+\sim})]^{-1} \cdot [t(\psi_\nu^{\wedge\sim})] \\ &\sim \mathbf{1}\,, \end{aligned} \tag{4.38}$$

where we used (4.3) in the end to eliminate the regular functions. Thus this case is similar to the first.

The saddle point condition is

$$0 = \Delta\theta - \arccos(\frac{\nu_{i2}}{k_i r'}) - \arccos(\frac{\nu_{i2}}{k_i r}) \tag{4.39}$$

and leads similarly to

$$\mathbf{G}_{geo}(r', r) = \vec{\nabla}_{\mathbf{r}'}\, \frac{1}{\rho\omega^2} G_{\rm sc}(k_L L_{S2}) \otimes \overleftarrow{\nabla}_{\mathbf{r}} + \vec{\nabla}_{\mathbf{r}'}\, \times\hat{\mathbf{z}} \frac{1}{\rho\omega^2} G_{\rm sc}(k_T L_{S2}) \otimes \overleftarrow{\nabla}_{\mathbf{r}}\, \times\hat{\mathbf{z}}. \tag{4.40}$$

For a given pair of points r, r' typically only one saddle will be dominant and therefore there will only be one free path contribution.

Reflection and refraction

The wave splitting case is by far the most interesting geometrical contribution. We shall focus on an incoming transverse ray and calculate the outgoing longitudinal ray. The reflection/refraction part of the Green's function is

$$\begin{aligned} \mathbf{G}_{geo}(r', r) \sim\; & \mathbf{R}_{\theta'} \{ \frac{1}{8i\rho\omega^2} \int_{-\infty+i\epsilon}^{\infty+i\epsilon} d\nu\, e^{i\nu\Delta\theta}\, \frac{i}{r'} \begin{pmatrix} q' & \nu \\ \nu & -s' \end{pmatrix} \\ & \times \begin{pmatrix} H_\nu^{(1)}(k_L r') & 0 \\ 0 & H_\nu^{(1)}(k_T r') \end{pmatrix} \mathbf{S}_\nu^{(1)} \begin{pmatrix} H_\nu^{(2)}(k_L r) & 0 \\ 0 & H_\nu^{(2)}(k_T r) \end{pmatrix} \\ & \times \frac{i}{r} \begin{pmatrix} q & -\nu \\ -\nu & -s \end{pmatrix} \} \mathbf{R}_\theta^{-1}\,. \end{aligned} \tag{4.41}$$

The scattering matrix will be calculated in the oscillating Debye approximation (4.30):

$$\begin{aligned}
\mathrm{Det}[H_\nu^{(1)}] \;&\sim \frac{2}{\pi}\left(q_a s_a\right)^{-\frac{1}{2}} \exp\left(iq_a - i\nu\arccos\left(\frac{\nu}{\alpha}\right) + is_a - i\nu\arccos\left(\frac{\nu}{\beta}\right) - i\frac{\pi}{2}\right) \\
&\quad \times \left\{-(2\nu^2-\beta^2)^2 + 4\nu^2 - i2\beta^2\left(q_a+s_a\right) - 4(\nu^2-1)q_a s_a\right\}, \qquad (4.42) \\
\widetilde{A} \;&\sim \frac{2}{\pi}\left(q_a s_a\right)^{-\frac{1}{2}} \exp\left(-iq_a + i\nu\arccos\left(\frac{\nu}{\alpha}\right) + is_a - i\nu\arccos\left(\frac{\nu}{\beta}\right)\right) \\
&\quad \times \left\{-(2\nu^2-\beta^2)^2 + 4\nu^2 - i2\beta^2\left(-q_a+s_a\right) + 4(\nu^2-1)q_a s_a\right\}, \qquad (4.43) \\
\widetilde{D} \;&\sim \frac{2}{\pi}\left(q_a s_a\right)^{-\frac{1}{2}} \exp\left(iq_a - i\nu\arccos\left(\frac{\nu}{\alpha}\right) - is_a + i\nu\arccos\left(\frac{\nu}{\beta}\right)\right) \\
&\quad \times \left\{-(2\nu^2-\beta^2)^2 + 4\nu^2 - i2\beta^2\left(q_a-s_a\right) + 4(\nu^2-1)q_a s_a\right\}, \qquad (4.44) \\
\widetilde{B} \;&\sim -\frac{2}{\pi}\,4\nu\left\{2\nu^2-\beta^2-2\right\} \qquad (4.45) \\
&\sim -\widetilde{C}\,, \qquad (4.46)
\end{aligned}$$

such that

$$\begin{aligned}
\frac{\widetilde{A}}{\mathrm{Det}[H_\nu^{(1)}]} \;&\sim\; \exp\left(-2iq_a + 2i\nu\arccos\left(\frac{\nu}{\alpha}\right) + i\frac{\pi}{2}\right) \\
&\quad \times \left\{-(2\nu^2-\beta^2)^2 + 4\nu^2 - i2\beta^2\left(-q_a+s_a\right) + 4(\nu^2-1)q_a s_a\right\} \\
&\quad \times \left\{-(2\nu^2-\beta^2)^2 + 4\nu^2 - i2\beta^2\left(q_a+s_a\right) - 4(\nu^2-1)q_a s_a\right\}^{-1} \qquad (4.47) \\
\frac{\widetilde{D}}{\mathrm{Det}[H_\nu^{(1)}]} \;&\sim\; \exp\left(-2is_a + 2i\nu\arccos\left(\frac{\nu}{\beta}\right) + i\frac{\pi}{2}\right) \\
&\quad \times \left\{-(2\nu^2-\beta^2)^2 + 4\nu^2 - i2\beta^2\left(q_a-s_a\right) + 4(\nu^2-1)q_a s_a\right\} \\
&\quad \times \left\{-(2\nu^2-\beta^2)^2 + 4\nu^2 - i2\beta^2\left(q_a+s_a\right) - 4(\nu^2-1)q_a s_a\right\}^{-1} \qquad (4.48) \\
\frac{\widetilde{B}}{\mathrm{Det}[H_\nu^{(1)}]} \;&\sim\; \exp\left(-iq_a + i\nu\arccos\left(\frac{\nu}{\alpha}\right) - is_a + i\nu\arccos\left(\frac{\nu}{\beta}\right) + i\frac{\pi}{2}\right) \\
&\quad \times 4\nu\left\{2\nu^2-\beta^2-2\right\}\sqrt{q_a s_a} \\
&\quad \times \left\{(2\nu^2-\beta^2)^2 - 4\nu^2 + i2\beta^2\left(q_a+s_a\right) + 4(\nu^2-1)q_a s_a\right\}^{-1} \\
&\sim\; -\frac{\widetilde{C}}{\mathrm{Det}[H_\nu^{(1)}]}\,. \qquad (4.49)
\end{aligned}$$

There will be a saddle for each component in the matrix. Their equations are:

$$
\begin{aligned}
0 &= \Delta\theta - \arccos\left(\frac{\nu_A}{k_L r'}\right) + 2\arccos\left(\frac{\nu_A}{k_L a}\right) - \arccos\left(\frac{\nu_A}{k_L r}\right) , && (4.50)\\
0 &= \Delta\theta - \arccos\left(\frac{\nu_B}{k_L r'}\right) + \arccos\left(\frac{\nu_B}{k_L a}\right) + \arccos\left(\frac{\nu_B}{k_T a}\right) - \arccos\left(\frac{\nu_B}{k_T r}\right) , && (4.51)\\
0 &= \Delta\theta - \arccos\left(\frac{\nu_C}{k_T r'}\right) + \arccos\left(\frac{\nu_C}{k_T a}\right) + \arccos\left(\frac{\nu_C}{k_L a}\right) - \arccos\left(\frac{\nu_C}{k_L r}\right) , && (4.52)\\
0 &= \Delta\theta - \arccos\left(\frac{\nu_D}{k_T r'}\right) + 2\arccos\left(\frac{\nu_D}{k_T a}\right) - \arccos\left(\frac{\nu_D}{k_T r}\right) . && (4.53)
\end{aligned}
$$

Thus e.g. $\nu_B =: \nu_{LT}$ corresponds to the transverse $k := k_T$ to longitudinal conversion $k' := k_L$. The relevant impact parameters are

$$
b = b_{LT} = \nu_{LT}/k_T \quad \text{and} \quad b' = b'_{LT} = \nu_{LT}/k_L \, . \tag{4.54}
$$

The flight lengths d from a point r or r' to point of impact

$$
\begin{aligned}
d' = d'_{LT} &= \sqrt{r'^2 - {b'_{LT}}^2} - \sqrt{a^2 - {b'_{LT}}^2} \, , \\
d = d_{LT} &= \sqrt{r^2 - b_{LT}^2} - \sqrt{a^2 - b_{LT}^2} \, . && (4.55)
\end{aligned}
$$

At the stationary point the phase will contain

$$
(q' - q_a) + (s - s_a) = k'd' + kd. \tag{4.56}
$$

Except from the amplitudes collected in the $\mathbf{S}^{(1)}_\nu$-matrix we have contributions from the amplitude of the Hankel functions and the amplitude arising from the second derivative of the total phase. Ignoring numerical factors their product is

$$
\begin{aligned}
-q's\,(\frac{1}{q'} - \frac{1}{q_a} + \frac{1}{s} - \frac{1}{s_a}) &= (k'd'\frac{s_a}{q_a} + kd\frac{q_a}{s_a} + (k'd')(kd)(\frac{1}{q_a} + \frac{1}{s_a})) \\
&\equiv \sqrt{k_L k_T} R_{LT} \, , && (4.57)
\end{aligned}
$$

where

$$
R_{LT} = \frac{\sqrt{\frac{k}{k'}}\, d'\, \rho}{\rho'} + \frac{\sqrt{\frac{k'}{k}}\, d\, \rho'}{\rho} + \left(\frac{\sqrt{\frac{k}{k'}}}{\rho'} + \frac{\sqrt{\frac{k'}{k}}}{\rho}\right) d'\, d \, . \tag{4.58}
$$

Here the projected rays, ρ, ρ', onto the tangent plane are related to

$$q_a = \sqrt{(k_L a)^2 - \nu^2} = k'\rho' \tag{4.59}$$

and

$$s_a = \sqrt{(k_T a)^2 - \nu^2} = k\rho\,. \tag{4.60}$$

and the velocity ratio:

$$\kappa = c_L/c_T = k_T/k_L \tag{4.61}$$

In (4.57) we use the geometrical mean of the wave vectors to get a symmetric expression.

This result agrees with what one calculates from *stability* matrices, as we shall see below. These matrices correspond to the ray matrices in geometrical optics. From these one can calculate the stability of a given (optical) ray system. For their derivation see Appendix H. They are linearized flows mapping initial to final tangent vectors in phase space:

$$(dz_-, d\theta_-) \mapsto (dz_+, d\theta_+),$$

where dz is the transverse displacement of a ray and $d\theta$ the shift in its direction.

Stability matrices for trajectory segments

Flight

$$\mathbf{F} = \begin{pmatrix} 1 & d \\ 0 & 1 \end{pmatrix} \tag{4.62}$$

Reflection

$$\mathbf{R} = -\begin{pmatrix} 1 & 0 \\ \frac{2}{\rho} & 1 \end{pmatrix} \tag{4.63}$$

Wave splitting from T to L -waves:

$$\mathbf{R}_{LT} = -\begin{pmatrix} \frac{\rho'}{\rho} & 0 \\ \frac{\kappa}{\rho'} + \frac{1}{\rho} & \kappa\frac{\rho}{\rho'} \end{pmatrix}, \tag{4.64}$$

where κ is the velocity ratio (4.61). The opposite case from L- to T-waves has $\kappa := 1/\kappa$. We note that

$$\rho = a\cos\phi, \tag{4.65}$$

where ϕ is the *angle of incidence*. So $\rho = \sqrt{a^2 - b^2}$ with b the impact parameter.

The amplitude for a point source in geometrical optics decrease radially as

$$\frac{1}{\sqrt{kR^{eff}}}\,. \tag{4.66}$$

This radius of a wave front is called the *effective length*. It evolves discontinuously at reflection/refraction and is conveniently described using ray matrices. Thus the effective length w.r.t. the final momentum $k' = k_L$ can be read off in the $d\theta$ to dz-position of products of stability matrices [2]. Why is that? Assume an initial infinitesimal volume element initially near the point source in configuration space. It will have a cross section proportional to its angular spread $d\theta$. Upon flight and reflection the element will acquire a new cross section. The ratio of these is the effective length and given by the element $(1,2)$ in the stability matrix: in the T to L case we have

$$\mathbf{F}' \cdot \mathbf{R}_{LT} \cdot \mathbf{F} = -\begin{pmatrix} \star & R^{eff}_{LT} \\ \star & \star \end{pmatrix}\,, \tag{4.67}$$

with

$$R^{eff}_{LT} = d\,\frac{\rho'}{\rho} + d'\,\frac{\rho}{\rho'}\kappa + (\frac{\kappa}{\rho'} + \frac{1}{\rho})\,d\,d' \tag{4.68}$$

Now this latter length gives the attenuation upon multiplication with the *final* wave number:

$$\sqrt{k_L k_T}R_{LT} = k_L R^{eff}_{LT}\,, \tag{4.69}$$

in agreement with the stationary phase calculation. Similarly for the L to T conversion using the right hand side of (4.58).

The amplitudes are given by

$$
\begin{aligned}
Z_{LL} \equiv & \left\{ (2b_R^2 - \frac{c_L^2}{c_T^2}\, a^2)^2 - \frac{4b_R^2}{k_L^2} - i\frac{2c_L^2 a^2}{c_T^2 k_L} \left[\sqrt{a^2 - b_R^2} - \sqrt{\frac{c_L^2}{c_T^2}\, a^2 - b_R^2} \right] \right. \\
& \left. -4(b_R^2 - \frac{1}{k_L^2}) \sqrt{a^2 - b_R^2} \sqrt{\frac{c_L^2}{c_T^2} a^2 - b_R^2} \right\} \left\{ (2b_R^2 - \frac{c_L^2}{c_T^2}\, a^2)^2 - \frac{4b_R^2}{k_L^2} \right. \\
& \left. + i\frac{2c_L^2 a^2}{c_T^2 k_L} \left[\sqrt{a^2 - b_R^2} + \sqrt{\frac{c_L^2}{c_T^2}\, a^2 - b_R^2} \right] + 4(b_R^2 - \frac{1}{k_L^2}) \sqrt{a^2 - b_R^2} \sqrt{\frac{c_L^2}{c_T^2}\, a^2 - b_R^2} \right\}^{-1} \\
\approx & \left\{ (2b_R^2 - \frac{c_L^2}{c_T^2}\, a^2)^2 - 4b_R^2 \sqrt{a^2 - b_R^2} \sqrt{\frac{c_L^2}{c_T^2}\, a^2 - b_R^2} \right\} \\
& \times \left\{ (2b_R^2 - \frac{c_L^2}{c_T^2}\, a^2)^2 + 4b_R^2 \sqrt{a^2 - b_R^2} \sqrt{\frac{c_L^2}{c_T^2}\, a^2 - b_R^2} \right\}^{-1}, \qquad (4.70)
\end{aligned}
$$

$$
\begin{aligned}
Z_{LT} \equiv & \, 4b_{LT} \{2b_{LT}^2 - a^2 - \frac{2}{k_T^2}\} \left\{ (\frac{c_T^2}{c_L^2}\, a^2 - b_{LT}^2)(a^2 - b_{LT}^2) \right\}^{\frac{1}{4}} \left\{ (2b_{LT}^2 - a^2)^2 - \frac{4b_{LT}^2}{k_T^2} \right. \\
& \left. + i\frac{2a^2}{k_T} \left[\sqrt{\frac{c_T^2}{c_L^2}\, a^2 - b_{LT}^2}\, v + \sqrt{a^2 - b_{LT}^2} \right] + 4(b_{LT}^2 - \frac{1}{k_T^2}) \sqrt{\frac{c_T^2}{c_L^2}\, a^2 - b_{LT}^2} \sqrt{a^2 - b_{LT}^2} \right\}^{-1} \\
\approx & \, 4b_{LT} \{2b_{LT}^2 - a^2\} \left\{ (\frac{c_T^2}{c_L^2}\, a^2 - b_{LT}^2)(a^2 - b_{LT}^2) \right\}^{\frac{1}{4}} \\
& \times \left\{ (2b_{LT}^2 - a^2)^2 + 4b_{LT}^2 \sqrt{\frac{c_T^2}{c_L^2}\, a^2 - b_{LT}^2} \sqrt{a^2 - b_{LT}^2} \right\}^{-1}, \qquad (4.71)
\end{aligned}
$$

$$
\begin{aligned}
Z_{TL} \equiv & -4b_{TL} \{2b_{TL}^2 - \frac{c_L^2}{c_T^2}\, a^2 - \frac{2}{k_L^2}\} \left\{ (a^2 - b_{TL}^2)(\frac{c_L^2}{c_T^2}\, a^2 - b_{TL}^2) \right\}^{\frac{1}{4}} \left\{ (2b_{TL}^2 - \frac{c_L^2}{c_T^2}\, a^2)^2 - \frac{4b_{TL}^2}{k_L^2} \right. \\
& \left. + i\frac{2c_L^2 a^2}{c_T^2 k_L} \left[\sqrt{a^2 - b_{TL}^2} + \sqrt{\frac{c_L^2}{c_T^2}\, a^2 - b_{TL}^2} \right] + 4(b_{TL}^2 - \frac{1}{k_L^2}) \sqrt{a^2 - b_{TL}^2} \sqrt{\frac{c_L^2}{c_T^2}\, a^2 - b_{TL}^2} \right\}^{-1} \\
\approx & -4b_{TL} \{2b_{TL}^2 - \frac{c_L^2}{c_T^2}\, a^2\} \left\{ (a^2 - b_{TL}^2)(\frac{c_L^2}{c_T^2}\, a^2 - b_{TL}^2) \right\}^{\frac{1}{4}} \\
& \times \left\{ (2b_{TL}^2 - \frac{c_L^2}{c_T^2}\, a^2)^2 + 4b_{TL}^2 \sqrt{a^2 - b_{TL}^2} \sqrt{\frac{c_L^2}{c_T^2}\, a^2 - b_{TL}^2} \right\}^{-1}, \qquad (4.72)
\end{aligned}
$$

$$
\begin{aligned}
Z_{TT} \equiv & \left\{ (2b_R^2 - a^2)^2 - \frac{4b_R^2}{k_T^2} + i\frac{2a^2}{k_T} \left[\sqrt{\frac{c_T^2}{c_L^2}\, a^2 - b_R^2} - \sqrt{a^2 - b_R^2} \right] \right. \\
& \left. -4(b_R^2 - \frac{1}{k_T^2}) \sqrt{\frac{c_T^2}{c_L^2}\, a^2 - b_R^2}\, \sqrt{a^2 - b_R^2} \right\} \left\{ (2b_R^2 - a^2)^2 - \frac{4b_R^2}{k_T^2} \right. \\
& \left. + i\frac{2a^2}{k_T} \left[\sqrt{\frac{c_T^2}{c_L^2}\, a^2 - b_R^2} + \sqrt{a^2 - b_R^2} \right] + 4(b_R^2 - \frac{1}{k_T^2}) \sqrt{\frac{c_T^2}{c_L^2}\, a^2 - b_R^2}\, \sqrt{a^2 - b_R^2} \right\}^{-1} \qquad (4.73) \\
\approx & \left\{ (2b_R^2 - a^2)^2 - 4b_R^2 \sqrt{\frac{c_T^2}{c_L^2}\, a^2 - b_R^2}\, \sqrt{a^2 - b_R^2} \right\} \left\{ (2b_R^2 - a^2)^2 + 4b_R^2 \sqrt{\frac{c_T^2}{c_L^2}\, a^2 - b_R^2}\, \sqrt{a^2 - b_R^2} \right\}^{-1},
\end{aligned}
$$

where the subscript R refers to reflection. Note that the off-diagonal terms Z_{LT}

and Z_{TL} vanish in the case of vanishing angle of impact, i.e., $b_{LT} = 0$ and $b_{TL} = 0$, respectively. Thus there is no mode conversion for normal incidence as is well known for the infinite half plane. We see that the constants Z_{ij} fullfill relations like $Z_{TT}^2 + Z_{LT}^2 = 1$ expressing the unitarity of the scattering matrix which again reflects energy conservation.

The semiclassical approximation to the second term of the geometrical contribution (4.41) at the lower saddles (i.e. with impact parameter smaller than the radius) corresponding to reflection and refraction is

$$
\begin{aligned}
& \mathbf{R}_{\theta'}\, i \begin{pmatrix} q'_R/r' & \nu_R/r' \\ \nu_R/r' & -s'_R/r' \end{pmatrix} \\
& \qquad \times \frac{1}{4i\rho\omega^2}\sqrt{\frac{2}{\pi}} e^{-i\frac{\pi}{4}} \begin{pmatrix} -Z_{LL}\frac{e^{ik_L(d'+d)}}{(k_L R_{\text{eff}})^{1/2}} & 0 \\ 0 & -Z_{TT}\frac{e^{ik_T(d'+d)}}{(k_T R_{\text{eff}})^{1/2}} \end{pmatrix} \\
& \qquad \times\, i \begin{pmatrix} q_R/r & -\nu_R/r \\ -\nu_R/r & -s_R/r \end{pmatrix} \mathbf{R}_\theta^{-1} \\
+ \quad & \mathbf{R}_{\theta'}\, i \begin{pmatrix} q'_{LT}/r' & \nu_{TL}/r' \\ \nu_{LT}/r' & -s'_{TL}/r' \end{pmatrix} \\
& \qquad \times \frac{1}{4i\rho\omega^2}\sqrt{\frac{2}{\pi}} e^{-i\frac{\pi}{4}} \begin{pmatrix} 0 & -Z_{LT}\frac{e^{ik_L d'_{LT}+ik_T d_{LT}}}{(\sqrt{k_T k_L} R_{LT})^{1/2}} \\ -Z_{TL}\frac{e^{ik_T d'_{TL}+ik_L d_{TL}}}{(\sqrt{k_T k_L} R_{TL})^{1/2}} & 0 \end{pmatrix} \\
& \qquad \times\, i \begin{pmatrix} q_{TL}/r & -\nu_{TL}/r \\ -\nu_{LT}/r & -s_{LT}/r \end{pmatrix} \mathbf{R}_\theta^{-1} \\
= \quad & \overrightarrow{\nabla}_{\mathbf{r}'} \left\{ -Z_{LL}\, \frac{1}{4i\rho\omega^2}\sqrt{\frac{2}{\pi}}\, \frac{e^{ik_L(d+d')-i\pi/4}}{\sqrt{k_L R_{\text{eff}}}} \right\} \otimes \overleftarrow{\nabla}_{\mathbf{r}} \\
& + \overrightarrow{\nabla}_{\mathbf{r}'} \times\hat{\mathbf{z}} \left\{ -Z_{TT}\, \frac{1}{4i\rho\omega^2}\sqrt{\frac{2}{\pi}}\, \frac{e^{ik_T(d+d')-i\pi/4}}{\sqrt{k_T R_{\text{eff}}}} \right\} \otimes \overleftarrow{\nabla}_{\mathbf{r}} \times\hat{\mathbf{z}} \\
& + \overrightarrow{\nabla}_{\mathbf{r}'} \left\{ -Z_{LT}\, \frac{1}{4i\rho\omega^2}\sqrt{\frac{2}{\pi}}\, \frac{e^{ik_L d'_{LT}+ik_T d_{LT}-i\pi/4}}{\sqrt{\sqrt{k_T k_L} R_{LT}}} \right\} \otimes \overleftarrow{\nabla}_{\mathbf{r}} \times\hat{\mathbf{z}} \\
& + \overrightarrow{\nabla}_{\mathbf{r}'} \times\hat{\mathbf{z}} \left\{ -Z_{TL}\, \frac{1}{4i\rho\omega^2}\sqrt{\frac{2}{\pi}}\, \frac{e^{ik_T d'_{TL}+ik_L d_{TL}-i\pi/4}}{\sqrt{\sqrt{k_T k_L} R_{TL}}} \right\} \otimes \overleftarrow{\nabla}_{\mathbf{r}} \quad . \qquad (4.74)
\end{aligned}
$$

4.2.3 Diffractive contributions in the Green's function

We now proceed with the final contribution to the Green's function. In the following we shall put the cavity radius $a = 1$. Evaluating the residue integral (4.29)

$$\mathbf{G}_{\rm diff}(k_T,k_L;\mathbf{r}',\mathbf{r}) \sim \frac{1}{8i\rho\omega^2}\sum_l 2\pi i\,\mathbf{R}_{\theta'}\frac{e^{i\nu_l(2\pi+\theta'-\theta)}+\sigma_{\nu_l}e^{i\nu_l(2\pi-\theta'+\theta)}}{1-e^{i2\nu_l\pi}} \times\begin{pmatrix}\frac{\partial}{\partial r'}H^{(1)}_{\nu_l}(k_Lr') & \frac{i\nu_l}{r'}H^{(1)}_{\nu_l}(k_Tr')\\ \frac{i\nu_l}{r'}H^{(1)}_{\nu_l}(k_Lr') & -\frac{\partial}{\partial r'}H^{(1)}_{\nu_l}(k_Tr')\end{pmatrix}\frac{\mathbf{N}}{\frac{\partial}{\partial\nu}\mathrm{Det}[H^{(1)}_\nu]|_{\nu=\nu_l}} \times\begin{pmatrix}\frac{\partial}{\partial r}H^{(1)}_{\nu_l}(k_Lr) & \frac{-i\nu_l}{r}H^{(1)}_{\nu_l}(k_Lr)\\ \frac{-i\nu_l}{r}H^{(1)}_{\nu_l}(k_Tr) & -\frac{\partial}{\partial r}H^{(1)}_{\nu_l}(k_Tr)\end{pmatrix}\mathbf{R}_\theta^{-1}. \tag{4.75}$$

Here the sum over l is a sum over poles. The residue in (4.29) is calculated from

$$\frac{\mathbf{N}}{\frac{\partial}{\partial\nu}\mathrm{Det}[H^{(1)}_\nu]|_{\nu=\nu_l}}\,. \tag{4.76}$$

We calculate this ratio using the exponential Debye expansion. As in (4.4) we use variables q,s. So

$$\begin{aligned}
\mathrm{Det}[H^{(1)}_\nu] \sim&\frac{2}{\pi}(q_as_a)^{-\frac12}\exp\left(iq_a-i\nu\arccos\left(\frac{\nu}{\alpha}\right)+is_a-i\nu\arccos\left(\frac{\nu}{\beta}\right)-i\frac{\pi}{2}\right)\\
&\times\left\{-(2\nu^2-\beta^2)^2+4\nu^2-i2\beta^2\left[q_a+s_a\right]-4(\nu^2-1)q_as_a\right\}, &(4.77)\\
\widetilde{A} \sim&\frac{2}{\pi}(q_as_a)^{-\frac12}\exp\left(-iq_a+i\nu\arccos\left(\frac{\nu}{\alpha}\right)+is_a-i\nu\arccos\left(\frac{\nu}{\beta}\right)\right)\\
&\times\left\{-(2\nu^2-\beta^2)^2+4\nu^2-i2\beta^2\left[-q_a+s_a\right]+4(\nu^2-1)q_as_a\right\}, &(4.78)\\
\widetilde{D} \sim&\frac{2}{\pi}(q_as_a)^{-\frac12}\exp\left(iq_a-i\nu\arccos\left(\frac{\nu}{\alpha}\right)-is_a+i\nu\arccos\left(\frac{\nu}{\beta}\right)\right)\\
&\times\left\{-(2\nu^2-\beta^2)^2+4\nu^2-i2\beta^2\left[q_a-s_a\right]+4(\nu^2-1)q_as_a\right\}, &(4.79)\\
\widetilde{B} \sim&-\frac{2}{\pi}4\nu\left\{2\nu^2-\beta^2-2\right\} &(4.80)\\
\sim&-\widetilde{C} &(4.81)
\end{aligned}$$

and therefore

$$\frac{\widetilde{A}}{\frac{\partial}{\partial\nu_{Ra}}\mathrm{Det}H^{(1)}_{\nu_{Ra}}} \sim\exp\left(2q_a-2\nu_{Ra}\mathrm{ArcCosh}\frac{\nu_{Ra}}{\alpha}+\mathrm{i}\frac{\pi}{2}\right)$$

$$
\begin{aligned}
&\times\left\{-(2{\nu_{Ra}}^2-\beta^2)^2+4{\nu_{Ra}}^2-2\beta^2\left[q_a-s_a\right]-4({\nu_{Ra}}^2-1)q_a s_a\right\}\\
&\times\left\{-8\nu_{Ra}(2{\nu_{Ra}}^2-\beta^2)+8\nu_{Ra}+2\beta^2\left[\frac{\nu_{Ra}}{q_a}+\frac{\nu_{Ra}}{s_a}\right]+8\nu_{Ra}q_a s_a\right.\\
&\qquad\left.+4\nu_{Ra}({\nu_{Ra}}^2-1)\left(\frac{q_a}{s_a}+\frac{s_a}{q_a}\right)\right\}^{-1}\\
\sim&\exp\left(2q_a-2\nu_{Ra}\mathrm{ArcCosh}\frac{\nu_{Ra}}{\alpha}+\mathrm{i}\frac{\pi}{2}\right)\\
&\times\left\{-(2{\nu_{Ra}}^2-\beta^2)^2-4{\nu_{Ra}}^2q_a s_a\right\}\\
&\times\frac{1}{8\nu_{Ra}}\left\{-(2{\nu_{Ra}}^2-\beta^2)+q_a s_a+\tfrac{1}{2}{\nu_{Ra}}^2\left(\frac{q_a}{s_a}+\frac{s_a}{q_a}\right)\right\}^{-1}
\end{aligned}
\tag{4.82}
$$

$$
\begin{aligned}
\frac{\widetilde{D}}{\frac{\partial}{\partial\nu_{Ra}}\mathrm{Det}H^{(1)}_{\nu_{Ra}}}\sim&\exp\left(2s_a-2\nu_{Ra}\mathrm{ArcCosh}\frac{\nu_{Ra}}{\beta}+\mathrm{i}\frac{\pi}{2}\right)\\
&\times\left\{-(2{\nu_{Ra}}^2-\beta^2)^2+4{\nu_{Ra}}^2+2\beta^2\left[q_a-s_a\right]-4({\nu_{Ra}}^2-1)q_a s_a\right\}\\
&\times\left\{-8\nu_{Ra}(2{\nu_{Ra}}^2-\beta^2)+8\nu_{Ra}+2\beta^2\left[\frac{\nu_{Ra}}{q_a}+\frac{\nu_{Ra}}{s_a}\right]+8\nu_{Ra}q_a s_a\right.\\
&\qquad\left.+4\nu_{Ra}({\nu_{Ra}}^2-1)\left(\frac{q_a}{s_a}+\frac{s_a}{q_a}\right)\right\}^{-1}\\
\sim&\exp\left(2s_a-2\nu_{Ra}\mathrm{ArcCosh}\frac{\nu_{Ra}}{\beta}+\mathrm{i}\frac{\pi}{2}\right)\\
&\times\left\{-(2{\nu_{Ra}}^2-\beta^2)^2-4{\nu_{Ra}}^2q_a s_a\right\}\\
&\times\frac{1}{8\nu_{Ra}}\left\{-(2{\nu_{Ra}}^2-\beta^2)+q_a s_a+\tfrac{1}{2}{\nu_{Ra}}^2\left(\frac{q_a}{s_a}+\frac{s_a}{q_a}\right)\right\}^{-1}
\end{aligned}
\tag{4.83}
$$

$$
\begin{aligned}
\frac{\widetilde{B}}{\frac{\partial}{\partial\nu_{Ra}}\mathrm{Det}H^{(1)}_{\nu_{Ra}}}\sim&-\frac{\widetilde{C}}{\frac{\partial}{\partial\nu_{Ra}}\mathrm{Det}H^{(1)}_{\nu_{Ra}}}\\
\sim&\exp\left(q_a-\nu_{Ra}\mathrm{ArcCosh}\frac{\nu_{Ra}}{\alpha}+\mathrm{s_a}-\nu_{Ra}\mathrm{ArcCosh}\frac{\nu_{Ra}}{\beta}\right)\\
&\times 4\nu_{Ra}\left\{2{\nu_{Ra}}^2-\beta^2-2\right\}\left(q_a s_a\right)^{\frac{1}{2}}\\
&\times\left\{-8\nu_{Ra}(2{\nu_{Ra}}^2-\beta^2)+8\nu_{Ra}+2\beta^2\left[\frac{\nu_{Ra}}{q_a}+\frac{\nu_{Ra}}{s_a}\right]+8\nu_{Ra}q_a s_a\right.\\
&\qquad\left.+4\nu_{Ra}({\nu_{Ra}}^2-1)\left(\frac{q_a}{s_a}+\frac{s_a}{q_a}\right)\right\}^{-1}\\
\sim&\exp\left(q_a-\nu_{Ra}\mathrm{ArcCosh}\frac{\nu_{Ra}}{\alpha}+\mathrm{s_a}-\nu_{Ra}\mathrm{ArcCosh}\frac{\nu_{Ra}}{\beta}\right)\\
&\times\left\{{\nu_{Ra}}^2-\tfrac{1}{2}\beta^2\right\}\left(q_a s_a\right)^{\frac{1}{2}}
\end{aligned}
$$

$$\times \left\{ -(2{\nu_{Ra}}^2 - \beta^2) + q_a s_a + \tfrac{1}{2}{\nu_{Ra}}^2 \left(\frac{q_a}{s_a} + \frac{s_a}{q_a} \right) \right\}^{-1}$$

. (4.84)

From this we read off the diffraction *matrix* in the Rayleigh case

$$\left\{ \widetilde{\mathbf{D}}_R^2 \right\} \sim 4\pi(k_T a) \begin{pmatrix} i\widetilde{Z}_{\rm diag}\, e^{-2\lambda(\nu_{Ra},\alpha)} & -\widetilde{Z}_{\rm off} e^{-\lambda(\nu_{Ra},\alpha)-\lambda(\nu_{Ra},\beta)} \\ \widetilde{Z}_{\rm off}\, e^{-\lambda(\nu_{Ra},\alpha)-\lambda(\nu_{Ra},\beta)} & i\widetilde{Z}_{\rm diag} e^{-2\lambda(\nu_{Ra},\beta)} \end{pmatrix} , \tag{4.85}$$

where

$$\widetilde{Z}_{\rm diag} \equiv \left\{ \frac{1}{8\eta_R}(2{\eta_R}^2 - 1)^2 + \tfrac{1}{2}\eta_R \sqrt{{\eta_R}^2 - \left(\frac{c_T}{c_L}\right)^2}\sqrt{{\eta_R}^2 - 1} \right\}$$
$$\times \left\{ (2{\eta_R}^2 - 1) - \sqrt{{\eta_R}^2 - \left(\frac{c_T}{c_L}\right)}\sqrt{{\eta_R}^2 - 1} - \tfrac{1}{2}{\eta_R}^2 \left[\sqrt{\frac{{\eta_R}^2 - \left(\frac{c_T}{c_L}\right)^2}{{\eta_R}^2 - 1}} + \sqrt{\frac{{\eta_R}^2 - 1}{{\eta_R}^2 - \left(\frac{c_T^2}{c_L^2}\right)}} \right] \right\}^{-1} , \tag{4.86}$$

$$\widetilde{Z}_{\rm off} = \frac{1}{2}\{2{\eta_R}^2 - 1\} \sqrt{\sqrt{{\eta_R}^2 - \left(\frac{c_T}{c_L}\right)^2}\sqrt{{\eta_R}^2 - 1}}$$
$$\times \left\{ (2{\eta_R}^2 - 1) - \sqrt{{\eta_R}^2 - \left(\frac{c_T}{c_L}\right)}\sqrt{{\eta_R}^2 - 1} - \tfrac{1}{2}{\eta_R}^2 \left[\sqrt{\frac{{\eta_R}^2 - \left(\frac{c_T}{c_L}\right)^2}{{\eta_R}^2 - 1}} + \sqrt{\frac{{\eta_R}^2 - 1}{{\eta_R}^2 - \left(\frac{c_T^2}{c_L^2}\right)}} \right] \right\}^{-1} , \tag{4.87}$$

$$\lambda(\nu, X) \equiv -\sqrt{\nu^2 - X^2} + \nu \mathrm{ArcCosh}\frac{\nu}{\mathrm{X}} . \tag{4.88}$$

Similarly we define a diffraction matrix with flipped signs in the off-diagonal elements corresponding to negative ν:

$$\left\{ \sigma_R \widetilde{\mathbf{D}}_R^2 \right\} \sim 4\pi(k_T a) \begin{pmatrix} i\widetilde{Z}_{\rm diag}\, e^{-2\lambda(\nu_{Ra},\alpha)} & \widetilde{Z}_{\rm off} e^{-\lambda(\nu_{Ra},\alpha)-\lambda(\nu_{Ra},\beta)} \\ -\widetilde{Z}_{\rm off}\, e^{-\lambda(\nu_{Ra},\alpha)-\lambda(\nu_{Ra},\beta)} & i\widetilde{Z}_{\rm diag} e^{-2\lambda(\nu_{Ra},\beta)} \end{pmatrix} . \tag{4.89}$$

The exterior "legs" of the Green's function will be replaced as above by their oscillating Debye expansion (4.30). This is valid when $k_L r' > k_L r \gg k_R a = \eta_R k_T a$, that is when $r \gg \frac{c_L}{c_T} a \eta_R$. Thus for polyethylene $r \gg 3.611a$. For *shear* legs the situation is less restrictive with $r \gg \eta_R a$.

Thus the Rayleigh contribution of (4.75) reads

$$\mathbf{G}_{\rm Rayl}(k_T, k_L; \mathbf{r}', \mathbf{r}) = \frac{1}{\sqrt{\rho}\omega} \begin{pmatrix} \cos\theta' & -\sin\theta' \\ \sin\theta' & \cos\theta' \end{pmatrix} \begin{pmatrix} \frac{\vec{\partial}}{\partial r'} & \frac{1}{r'}\frac{\vec{\partial}}{\partial \theta'} \\ \frac{1}{r'}\frac{\vec{\partial}}{\partial \theta'} & -\frac{\vec{\partial}}{\partial r'} \end{pmatrix}$$

$$\times \frac{1}{4i}\sqrt{\frac{2}{\pi}} \begin{pmatrix} \frac{e^{i\sqrt{k_L^2 r'^2-\nu_{Ra}^2}-i\nu_{Ra}\arccos(\frac{\nu_{Ra}}{k_L r'})-i\frac{\pi}{4}}}{\left(k_L^2 r'^2-\nu_{Ra}^2\right)^{1/4}} & 0 \\ 0 & \frac{e^{i\sqrt{k_T^2 r'^2-\nu_{Ra}^2}-i\nu_{Ra}\arccos(\frac{\nu_{Ra}}{k_T r'})-i\frac{\pi}{4}}}{\left(k_T^2 r'^2-\nu_{Ra}^2\right)^{1/4}} \end{pmatrix}$$

$$\times \left\{ \{\mathbf{D}_R^2\} \frac{e^{i\nu_{Ra}(2\pi+\theta'-\theta)}}{1-e^{i2\nu_{Ra}\pi}} + \{\sigma_{\nu_{Ra}}\mathbf{D}_R^2\} \frac{e^{i\nu_{Ra}(2\pi-\theta'+\theta)}}{1-e^{i2\nu_{Ra}\pi}} \right\}$$

$$\times \frac{1}{4i}\sqrt{\frac{2}{\pi}} \begin{pmatrix} \frac{e^{i\sqrt{k_L^2 r^2-\nu_{Ra}^2}-i\nu_{Ra}\arccos(\frac{\nu_{Ra}}{k_L r})-i\frac{\pi}{4}}}{\left(k_L^2 r^2-\nu_{Ra}^2\right)^{1/4}} & 0 \\ 0 & \frac{e^{i\sqrt{k_T^2 r^2-\nu_{Ra}^2}-i\nu_{Ra}\arccos(\frac{\nu_{Ra}}{k_T r})-i\frac{\pi}{4}}}{\left(k_T^2 r^2-\nu_{Ra}^2\right)^{1/4}} \end{pmatrix}$$

$$\times \begin{pmatrix} \frac{\overleftarrow{\partial}}{\partial r} & \frac{1}{r}\frac{\overleftarrow{\partial}}{\partial\theta} \\ \frac{1}{r}\frac{\overleftarrow{\partial}}{\partial\theta} & -\frac{\overleftarrow{\partial}}{\partial r} \end{pmatrix} \begin{pmatrix} \cos\theta & \sin\theta \\ -\sin\theta & \cos\theta \end{pmatrix} \frac{1}{\sqrt{\rho}\omega} \,. \tag{4.90}$$

We now think of the Cauchy denominator as $\frac{1}{1-e^{2\pi i\nu}} = \sum_{n=0}^{\infty} e^{i2\pi n\nu}$. Here ν is evaluated at a Rayleigh pole and the sum represents revolutions of surface waves.

Further the first and last line corresponds to the usual factors from the points r, r'. Ignoring those i.e. focusing on the elastic potentials we can write the four different types of Rayleigh paths in terms of a 2×2 matrix

$$\begin{pmatrix} G_{\text{Rayl}}(L,L) & G_{\text{Rayl}}(L,T) \\ G_{\text{Rayl}}(L,T) & G_{\text{Rayl}}(T,T) \end{pmatrix} \tag{4.91}$$

by introducing a general element labelled by $X, Y \in \{L, T\}$:

$$\begin{aligned} \mathbf{G}_{\text{Rayl}}(X,Y) \;=\; & \sum_{n=0}^{\infty} \sum_{\sigma=-,+} G_{\text{sc}}\left(k_T\eta_R \sqrt{\left(\frac{r'}{\frac{c_X}{c_T}\eta_R}\right)^2 - a^2} \right) \\ & \times 4\pi(k_T a) \begin{pmatrix} i\widetilde{Z}_{\text{diag}} & ie^{i\frac{\pi}{2}\sigma}\widetilde{Z}_{\text{off}} \\ ie^{-i\frac{\pi}{2}\sigma}\widetilde{Z}_{\text{off}} & i\widetilde{Z}_{\text{diag}} \end{pmatrix}_{XY} e^{-\lambda(k_T\eta_R a, \frac{c_X}{c_T}k_T)-\lambda(k_T\eta_R a, \frac{c_Y}{c_T}k_T)} \\ & \times \exp\left(ik_T\eta_R\, a \left[2\pi + \sigma(\theta'-\theta) - \arccos\left(a\frac{\frac{c_X}{c_T}\eta_R}{r'}\right) - \arccos\left(a\frac{\frac{c_Y}{c_T}\eta_R}{r}\right) + 2n\pi \right] \right) \\ & \times G_{\text{sc}}\left(k_T\eta_R \sqrt{\left(\frac{r}{\frac{c_Y}{c_T}\eta_R}\right)^2 - a^2} \right) \,. \end{aligned} \tag{4.92}$$

Note that we have end point factors with rescaled lengths (see fig. 4.2) , for example $r'/(\eta_R c_L/c_T)$. It is as if we send a Rayleigh wave from the corresponding rescaled point $\mathbf{r}'/(\eta_R c_L/c_T)$ to hit the cavity tangentially. This is also seen in the angular factors. Here the n counts the number of revolutions and the phase obtained from

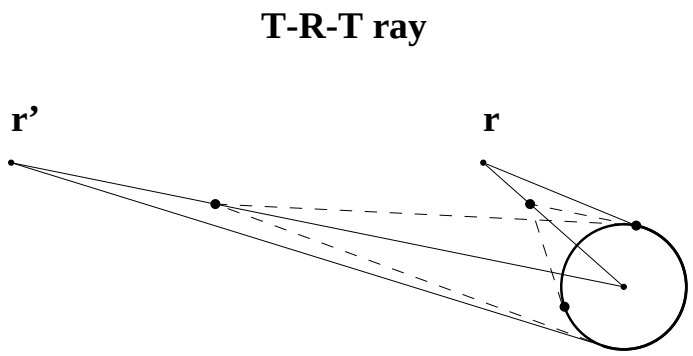

Figure 4.2: A shear ray getting diffracted at a cavity. The dashed lines indicates the geometrical construction of a reduced length from which tangential contact is obtained.

the cavity is the one given by the Rayleigh wave number $k_R = \eta_R k_T$ times the total length traversed. The effect of the rescaling is that the physical orbits do not hit tangentially. If the rescaling is close to unity the orbits appear to be almost tangential. This happens e.g. for shear waves coupling to Rayleigh waves in polyethylene. Finally the coupling of longitudinal rays to Rayleigh segments is suppressed exponentially by the corresponding factor $e^{-\lambda(\nu_{Ra},\alpha)}$ with λ given by (4.88) .

For our material in question we can say that the connection to the cavity is *almost tangential* (about 0.5 percent in radians for the orbits later on in the two cavity system).

Remark: we have not found the roots of the diffraction matrix (4.85) above. This would be interesting, however, if one want to know the surface field for say subsequent treatment of cracks at the cavity.

Résumé

The surface resonances of one cavity were studied following [45] with emphasis on the attenuation. Next the Green's function was investigated by the Sommerfeld-Watson transformation following [3]. This lead to a ray picture corresponding to *classical* dynamics, albeit with inclusion of surface rays.

Chapter 5

Numerics

In this chapter we employ the machinery of chapter 3 to calculate resonances and the Wigner delay time, investigating both the modulus and the phase of the scattering determinant.

All numerical calculations have been done for polyethylene for which the longitudinal and transversal velocities are

$$c_L = 1950 m/s \qquad \text{and} \qquad c_T = 540\, m/s$$

as this is a material for which there exist scattering results for a single cavity [13]. We will state most results in terms of the dimensionless size parameter $k_L a$. We have used the NAG-library in our calculations.

5.1 One-cavity

I have found a good numerical agreement with the resonances first computed in [13]. As my formula (3.41) differ slightly from those of refs. [19, 18] it is a comforting check that we find the same resonances, fig. 4.1. In addition, these authors claim that a family of poles different from the Franz and the Rayleigh poles is present; we confirm their claim. These unanticipated resonances are to be associated with the *complex* roots of the Rayleigh equation. However, the large attenuation renders these pseudo-Rayleigh resonances physically uninteresting, and we have not investigated them further. We can also locate various creeping resonances of Franz type (longitudinal and transversal) but again we omit those because of their strong attenuation. I have not studied the phase and time delay for this simple one-cavity case, and have concentrated instead on the multi-cavity case to whcich we turn now.

5.2 Multi-cavity

The case of several cavities was implemented using the formulas derived in Sect. 3. The geometry was fixed to $R/a = 6$. This is the ratio between cavity centers and the radius of a single cavity. When the ratio is $R/a = 2$, the cavities touch and for smaller ratios the method breaks down. We remark that the calculation uses a truncation of the exact cluster matrix which strictly speaking is infinite dimensional. The size of this matrix has to be sufficiently big for higher frequencies. Empirically we have found that one should at least use angular momenta of order $N \approx 5(k_L a)_{max}$. This is worse than in the scalar case where the order $N \approx 1.5(k_L a)_{max} + \cdots$. That, however, is problematic since the matrix then involves Hankel functions of very high order which are hard to compute.

For general shapes the elastodynamic litterature typically resorts to methods like finite and boundary elements. Such calculations are carried out for *real* frequencies ("harmonic forcing"). An independent numerical check of the scattering determinant for complex frequencies using a method different than the scattering states would be reassuring, but has not been performed here.

The high frequency limit of the cluster determinant is attacked by studying its cumulants in terms of traces (3.52). Currently we work on the first cumulant. Instead of calculating the full determinant the traces are calculated numerically and therefore (3.52) can be constructed up to desired order.

5.2.1 Scattering resonances

Calculations based on the **M**-matrix formalism derived in chapter 3 have been implemented by Andreas Wirzba [3]. I have included here a plot fig. 5.1 of the scattering resonances calculated by Wirzba. These exact results are an essential benchmark for gauging the validity of high-frequency approximations, just as Wirzba's exact quantum resonances were essential for the development of the theory of creeping and $\hbar$-corrections for quantum mechanics [2].

The resonances are found by searching for the zeroes of the cluster determinant in the complex $k_L a$-plane. There is a very irregular band of resonances close to the real axis, and further down in the complex plane at $Im(k_L a) \sim -0.29$ we have a regularly spaced band. The latter corresponds to the shortest geometrical orbit bouncing back and forth between the two cavities. These resonances are described to three significant digits using a classical longitudinally polarized periodic orbit. We call this orbit P in the following. In the quantum mechanical, scalar case surface resonances give a complicated structure only deep in the complex $k_L a$-plane whereas the regular structure given by the geometrical orbit close to the real axis dominates the spectrum. Thus in elastodynamics the situation is qualitatively very different.

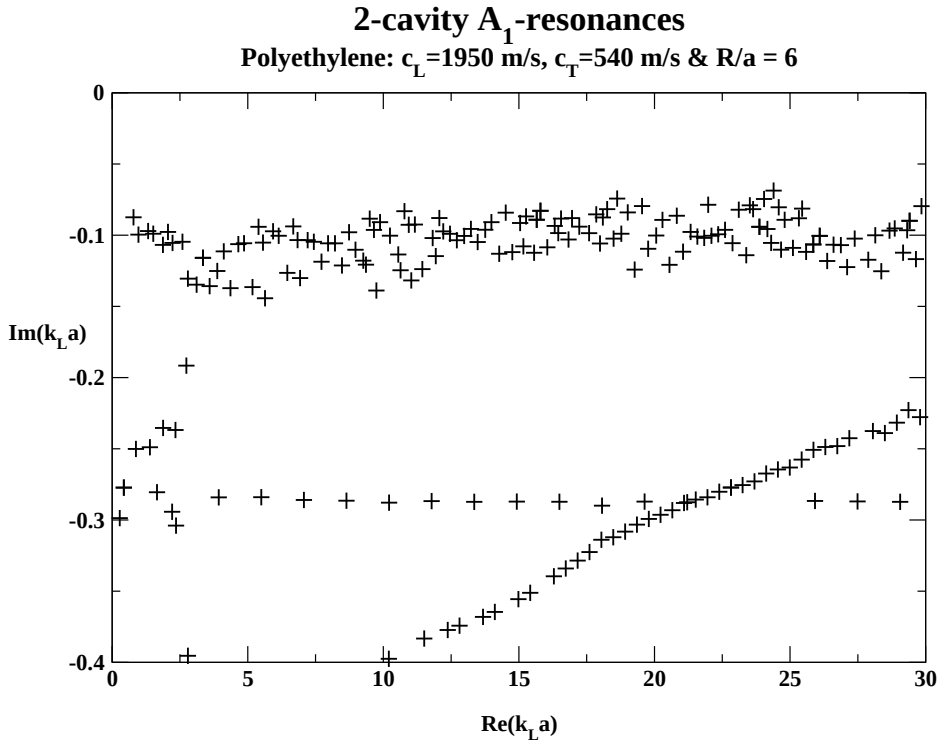

Figure 5.1: A_1 scattering resonances (A. Wirzba [3]).

5.2.2 Time delay

A more direct calculation is the evaluation of the phase of the scattering determinant for *real* frequencies. Physically this corresponds to a harmonic forcing of the system. As explained in sect. 3.6 the scattering determinant factorizes and it suffices to study the phase of the individual factors. A priori we understand the single cavity determinant and we can therefore focus entirely on the multi-cavity determinant. It turns out that the phase itself shows little variation compared to its derivative which again is related to the Wigner time delay. This quantity measures the time delay of a wave packet sent into the scattering system, see Appendix G.

We have calculated the derivative of the multi-cavity determinant as a function of the size parameter $k_L a$, see fig. 5.2 . The plot shows that the delay from the cluster attains both positive and negative values : the delay seems to oscillate but not with a single frequency. The main period of oscillation in the representations A_1 and B_1 is bigger than the period for A_2, B_2. To investigate the origin of these oscillations we perform a Fourier transform, and switching to time variables with the cavity radius a chosen as $1\,cm$ we obtain the corresponding *time spectrum*. This is the equivalent of a length spectrum in ordinary quantum billiards. Here, however, we have two kinds of wave vectors: longitudinal and transversal of *different* geometrical length and the correct quantity to consider is the angular velocity ω, dual to time. The same can be done for quantum billiards if one knows the wave velocity but for theoretically purposes one works equally well with the length spectrum.

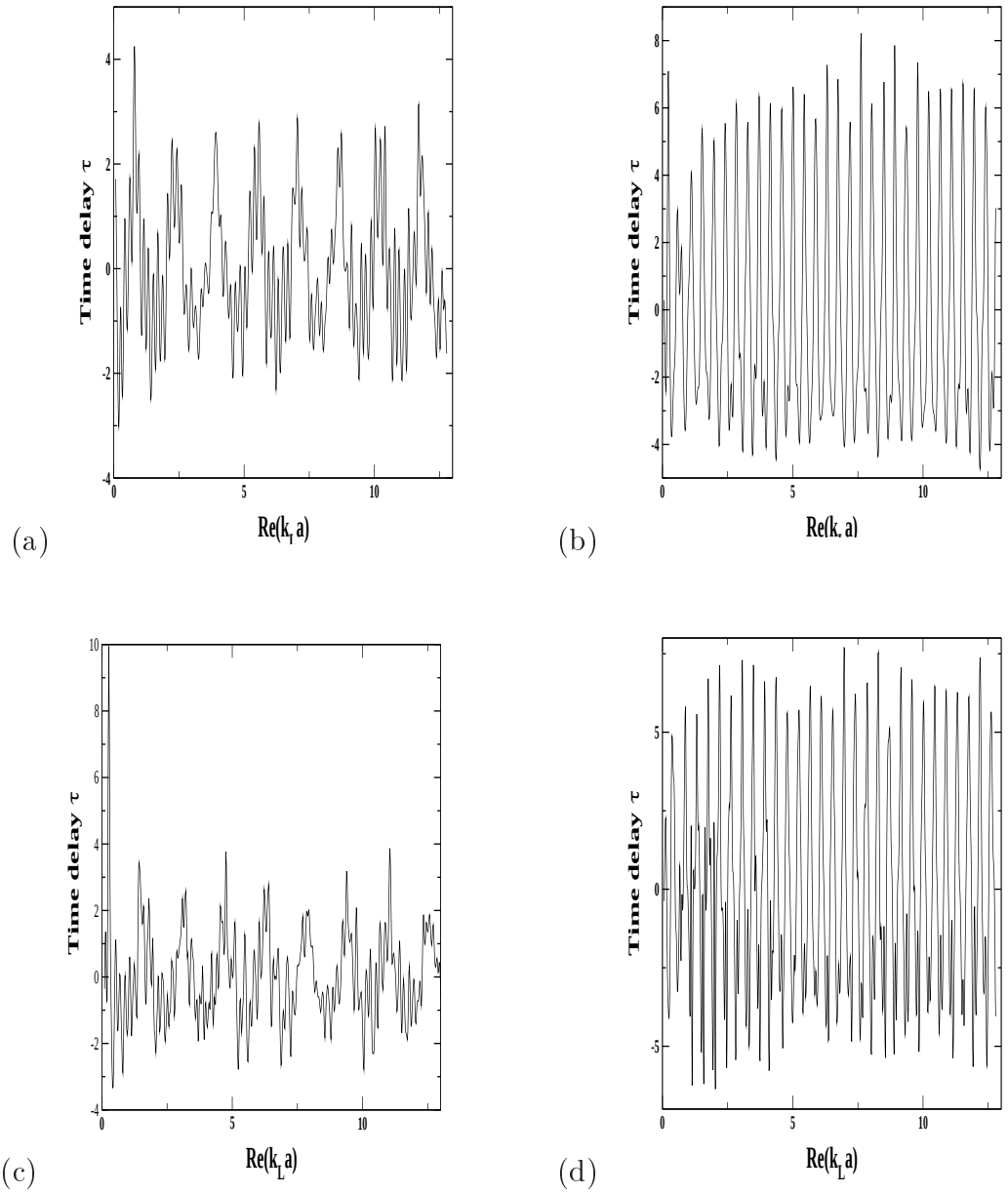

Figure 5.2: Delay as a function of frequency (delay in units of $2a/c_L$): (a) Representation A_1; (b) Representation A_2 ;(c) Representation B_1;(d) Representation B_2;

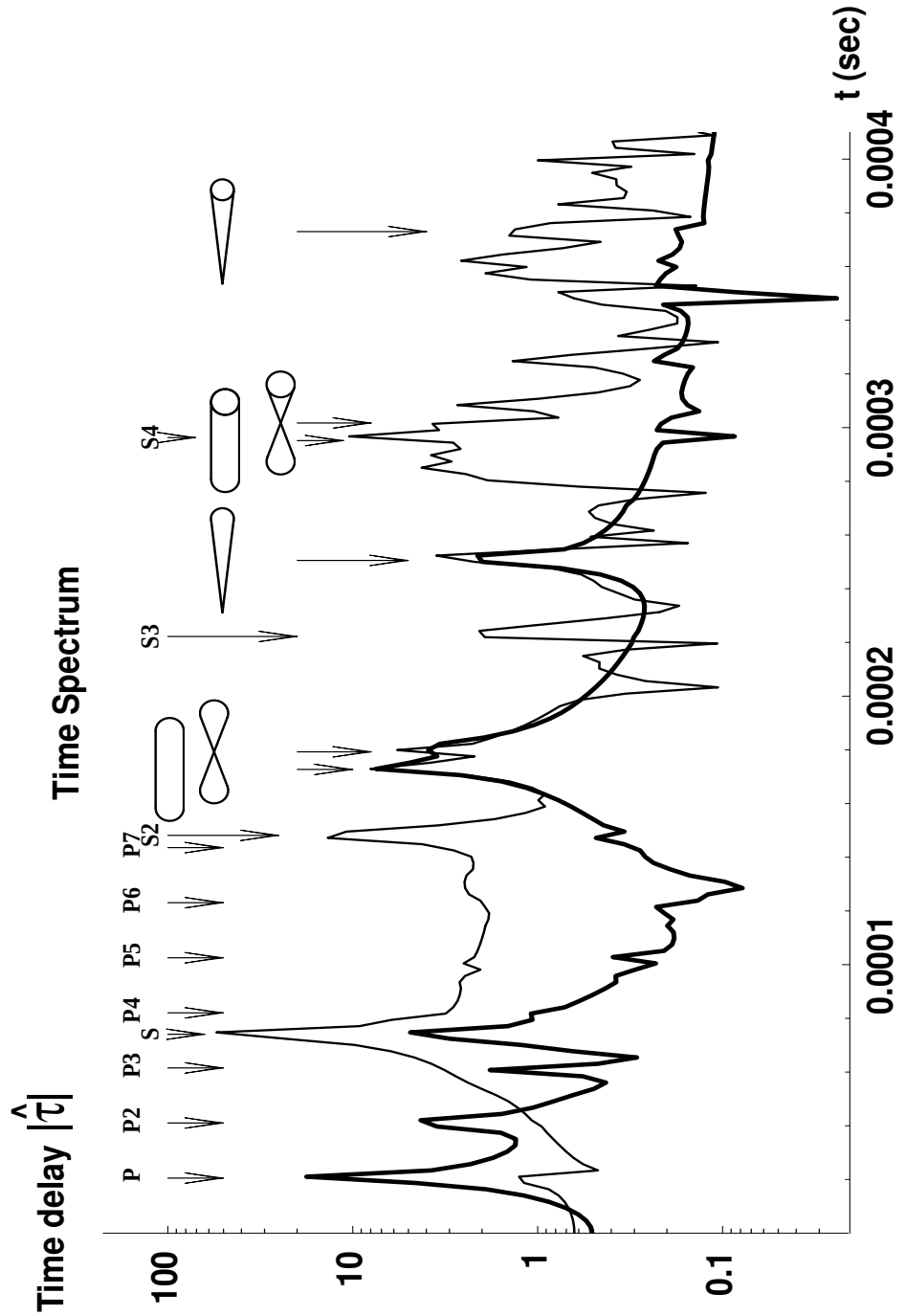

Figure 5.3: Time spectrum with a few orbits indicated for the two cavity system with $a = 1\,cm$ and cavity distance $R = 6\,cm$. Symbols P, S refer to geometrical orbits. Curved segments are of Rayleigh type and connect to transversal geometric rays. The thick line corresponds to the A_1-representation; the thin line B_2.

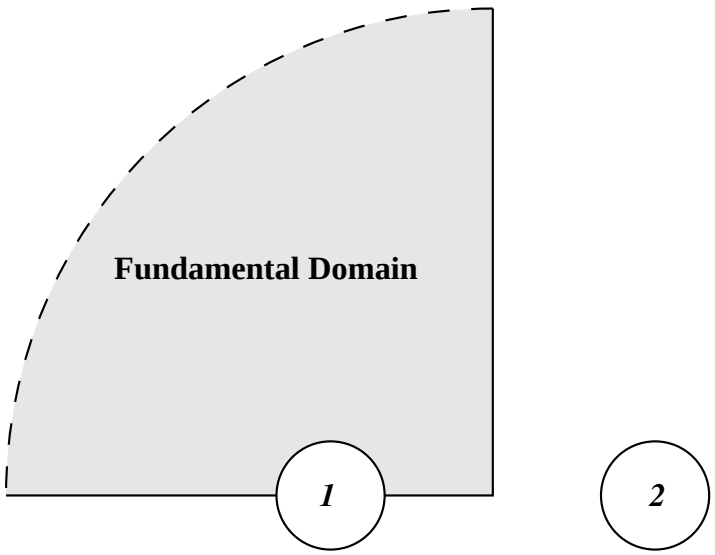

Figure 5.4: The fundamental domain is the shaded area, one quarter of the full physical domain.

The striking and encouraging result is the agreement between the prominent peaks and the periods of the periodic orbits in the two cavity system. The times measured correspond to the periodic orbits in the symmetry reduced domain of fig. 5.4. This *fundamental* domain is a quarter of the two cavity system in the sense that by applying the symmetry group C_{2v} one *tiles* the full physical domain, see sect. 3.6. We have plotted the time spectrum for two of the four irreducible representations of C_{2v}. The other two representations show similar peaks as those shown.

We find the shortest orbits using the ray dynamics derived in chapter 4. First there are the simple geometric orbits called P and S and their iterates $P^2, S^2, \cdots$. The P-orbit has a shorter period than the S-orbit and is seen in the representations A_1 and B_1. By the inverse Fourier transform this gives a larger period of oscillation in fig. 5.2. It is worth noting that both the P-orbit and S-orbit have the same geometrical orbit and yet they do not seem to occur with the same weight in the representations. Second are the orbits with surface segments which can contribute with multiple revolutions as well. As one can see from the decrease of peak heights, in contradistinction to the quantum case, repeats of geometrical orbits are far more inhibited than taking an extra repeat around a cavity. In general different orbits may have nearly the same periods; this complicates the interpretation of the time spectrum. This can be investigated by varying system parameters $R/a, c_L/c_T$ and improving the resolution by going to higher size parameters $k_L a$. We should mention that we have only constructed a few orbits which do not include the longitudinal polarization except for the purely geometric orbit. Thus there are many things to

improve on: finding more orbits and varying the parameters of the system.

The above calculation of the time delay spectrum can be helpful in the process of searching for orbits. However, the real achievement is that they explain the wave-mechanical scattering determinant in terms of classical dynamics. The analysis demonstrates that the multi-cavity determinant is dominated by phases associated with periodic orbits. Their actual amplitudes and the widths of the peaks in the time delay spectrum are still under investigation. We mention that the situation is already understood in the scalar case. Thus Wirzba [2] finds directly to leading order in the saddle point expansion for the geometrical orbits:

$$\mathrm{Det}\,\mathbf{M} = \exp\left(-\sum_{p}\sum_{r=1}^{\infty}\frac{z^{rn_p}}{r}\frac{e^{ir(\oint_p \mathbf{k}\cdot\mathbf{dx}+s_p)}}{|\mathbf{1}-\mathbf{J}_p^r|^{\frac{1}{2}}}\right) \tag{5.1}$$

with $s_p = -n_p\pi$ or 0 for Dirichlet, respectively Neumann boundary conditions.

Résumé

The resonances and the Wigner time delays were found for the two cavity system using the multi-cavity determinant $\mathrm{Det}\,(\mathbf{M})$. The irregular frequency behavior was shown to arise from a multitude of periodic orbits of the associated high frequency dynamics.

Chapter 6

Summary and outlook

The ultimate goal of the research undertaken here was to develop a short-wavelength approximation theory of wave chaos in elastodynamics, paralleling the Gutzwiller semiclassical periodic orbit theory of quantal spectra of systems whose classical dynamics is chaotic.

Following the strategy of Keller's geometrical theory of diffraction we have considered a system which is a combination of simpler geometries, a system of cylindrical cavities in plane strain elastodynamics.

For this I have derived the exact scattering determinant, generalizing the Wirzba method for the case of the scalar Helmholtz equation [2].

Using recent ideas of Wirzba [3] we have discussed the high-frequency limit of the Green's function in the presence of a single cavity. Wirzba treats scattering resonances, individual cumulants and the Wigner delay time. In this thesis I have focused on the Wigner delay and the corresponding time spectrum.

The main unexpected result of our investigation is the realization that a system of only two cavities in elastodynamics has a chaotic ray dynamics, contrary to the scalar case. This fact is due to the apparently harmless but experimentally prefered free boundary condition which facilitates an infinity of unstable periodic orbits of creeping nature. Remarkably, the creeping of Rayleigh type is only slightly attenuated for high frequencies. For the scalar systems studied previously the infinity of orbits have been of *bulk* nature and all other orbits of creeping type have been strongly suppressed. The less welcome surprise in this thesis has been the unexpected difficulty of extending the high frequency theoretical treatment to low frequencies, in contrast to the success of Franz creeping rays in the scalar case.

In collaboration with Predrag Cvitanović, Gabor Vattay, Gergely Palla, Carl P. Dettmann and André Voros [30, 39] a part of my thesis research has also been to investigate high order noise corrections for stochastic dynamical systems. This line

of research aims to improve periodic orbit theory in stochastic and wave systems by including corrections to the classical contribution [43, 37, 28, 29]. Methods to calculate many corrections and to understand their asymptotics using *resurgence* have been achieved. These developments have not been reported in this thesis.

6.1 What is new in this thesis

We have developed a numerical method to calculate the scattering determinant for finitely many cylindrical cavities in an elastic medium. We have applied these methods specifically to plane strain elastodynamics with free boundary conditions. The multiple scattering wave problem has a ray approximation which includes surface rays of Rayleigh type. These are of major importance, also at high frequencies in contrast to the previous work in quantum chaos on the scalar Helmholtz equation. It appears difficult to extend the high-frequency approximation to lower frequencies as for the Franz creeping rays. Now already the two cylindrical cavity system has an infinite number of orbits and is in that sense chaotic. Contributions to the spectral function from a few periodic orbits have been identified.

6.2 Outlook

The preceding analysis has shown the relevance of periodic orbits in the elastodynamic multi-cavity system. To proceed one should next concentrate on the *weights* of these orbits. With this we mean to calculate all higher traces of the corresponding Fredholm determinant in the limit of high frequencies and thereby establish the specific form of a zeta function (5.1), as in the scalar case. To prove Fredholm properties would imply the shadowing results previously obtained in scalar quantum mechanics and classical hyperbolic systems; in particular in elastodynamics also for the important surface orbits. The next step would be to study the three cavity system or higher, since there effects of the mode conversion would be more prominent. The wave splitting seems to be suppressed for the two cavity system. The reason is that most conversions happen close to normal incidence and hence are inhibited. For certain geometries one should also expect interesting contributions from penumbra effects and its generalization in the wave splitting case: at critical incidence angles a transversally polarized ray converting to a longitudinal ray gracing the boundary. Further it would be useful to extend the ray description of Rayleigh waves to lower frequencies, in particular with respect to their attenuation. The case where the cavities almost touch would be interesting too and require full knowledge of all the various wave types in elastodynamics. More general methods both theoretical and numerical also applicable to anisotropic materials would be of practical importance. For instance single crystal quartz which is anisotropic has a higher Q-value than the isotropic fused quartz.

As the reader already realizes, there are plenty of possible extensions and applications of this work just in the field of elastodynamics. Other wave problems in optics, piezo-electricity and bandgap structures would similarly benefit from an understanding of the underlying classical structure.

These systems show complicated features and we can at this point say that they are in part the result of the existence of several classical orbits in the system. It is now possible to handle these elegantly when the classical dynamics is strongly chaotic by expressing the corresponding spectral functions as generalized zeta functions. The detail of whether the system is classical, quantum, stochastic or as indicated elastodynamic only enters in the specific weights of the orbits. To further extend this general framework in a particular field will therefore benefit many other domains. Here we mention in particular the improvement of the asymptotical calculation of orbit weights and the still open problem of mixed phase space.

Appendix A

Counting elasticity tensor parameters

A short discussion can be found in [17]. The 4-tensor c_{iklm} is called the elasticity tensor and because of the symmetries of the strain field we see that it effectively can be described by a 4-tensor with the following symmetries:

$$c_{iklm} = c_{kilm} = c_{ikml} = c_{lmik}. \tag{A.1}$$

Here the symmetries are with respect to exchange of the indices in one of the pairs (12) respectively (34), and finally exchange of the pair (12) with the pair (34). By a counting argument it is not difficult to see that in three dimensions this gives 21 independent components of the elasticity tensor. First because of the exchange symmetry in each pair one labels (Voigt notation) each type of pair with a number from 1 to 6: xx=1,yy=2,zz=3,yz=4, xz=5, xy=6. There are indeed $\frac{3(3+1)}{2} = 6$ labelings. Second because of the symmetry of the exchange of pair (12) with (34) we will have say $c_{25} = c_{52}$. So using exactly the same argument as the first we find $\frac{6(6+1)}{2} = 21$ different components. However, if further symmetries are present, the number of components is further reduced. Let us now consider the important case of an isotropic medium.

Suppose we transform to coordinates:

$$x'_i = O^j_i x_j, \tag{A.2}$$

where O^j_i are the components of an orthogonal matrix. This corresponds to a rotation plus perhaps a reflection (depending on the sign of $Det(O) = \pm 1$). The elastic tensor c_{ijkl} transforms as follows:

$$c'_{ijkl} = c_{abcd} O^a_i O^b_j O^c_k O^d_l. \tag{A.3}$$

In an isotropic body we demand that any tensor should be invariant under orthogonal transformations, hence

$$c_{ijkl} = c_{abcd}\, O_i^a O_j^b O_k^c O_l^d. \tag{A.4}$$

As an example of such a tensor we mention the identity transformation as an invariant 2-tensor:

$$\delta'_{rs} = \delta_{ab}\, O_r^a O_s^b = O_r^a O_s^a = \delta_{rs}, \tag{A.5}$$

since the rows are orthonormal in an orthogonal matrix. Using this tensor as a building block we arrive at the following isotropic candidate :

$$c_{rsmn} = \lambda\, \delta_{rs}\delta_{mn} + \mu\, \delta_{rm}\delta_{ns} + \nu\, \delta_{rn}\delta_{sm}. \tag{A.6}$$

Further all isotropic 4-tensors have this form [44]. Then we invoke the symmetries of the elasticity tensor to reduce the above expression: By the symmetry of the last two indices, $c_{rsmn} = c_{rsnm}$:

$$\lambda\, \delta_{rs}\delta_{mn} + \mu\delta_{rm}\delta_{ns} + \nu\, \delta_{rn}\delta_{sm} = \lambda\, \delta_{rs}\delta_{nm} + \mu\, \delta_{rn}\delta_{ms} + \nu\, \delta_{rm}\delta_{sn} \tag{A.7}$$

and we conclude that $\mu = \nu$. The elasticity tensor in the isotropic case therefore depends only on 2 parameters, the so-called Lamé constants λ and μ:

$$c_{ijkl} = \lambda\, \delta_{ij}\delta_{kl} + \mu\, (\delta_{ik}\delta_{jl} + \delta_{il}\delta jk). \tag{A.8}$$

Appendix B

Green's function using scattering states

For a derivation of the fundamental solution in both 2 and 3 dimensions see [27].

B.1 Asymptotic behavior at infinity

We shall utilize the boundary relations expressing orthogonality of the wave functions:

$$\int_{\partial_\infty} (\psi_l^+ \cdot t(\psi_m^{-\sim}) - t(\psi_l^+) \cdot \psi_m^{-\sim})\, dS = 8\, i\, \rho\, \omega^2\, \delta_{lm}$$

and likewise

$$\int_{\partial_\infty} (\psi_l^\pm \cdot t(\psi_m^{\wedge\sim}) - t(\psi_l^\pm) \cdot \psi_m^{\wedge\sim})\, dS = 4\, i\, \rho\, \omega^2\, \delta_{lm}\,.$$

This suggests we put

$$G^\sim = \frac{1}{4i\rho\omega^2} \sum_n \psi_n^+(r_>) \otimes \psi_n^{\wedge\sim}(r_<)\,.$$

Thus for a sufficiently large disc Ω of radius R ($\partial\Omega = \partial_\infty$):

$$\int \left((\Delta^* + \rho\omega^2)(G^\sim) \cdot \psi\right)\, dV = \lim_{R\to\infty} \int_\Omega \left((\Delta^* + \rho\omega^2)(G^\sim) \cdot \psi\right)\, dV,$$

where ψ is any (regular) basis function.

Betti's third theorem now gives

$$\begin{aligned}\int_\Omega \left((\Delta^* + \rho\omega^2)(G^\sim)\cdot\psi\right)\, dV &= \int_\Omega \Big((\Delta^* + \rho\omega^2)(G^\sim)\cdot\psi \\ &\quad -G^\sim\cdot(\Delta^* + \rho\omega^2)(\psi)\Big)\, dV \\ &= \int_\Omega (\Delta^*(G^\sim)\cdot\psi - G^\sim\cdot\Delta^*(\psi))\, dV \\ &= \int_{\partial_\infty} (t(G^\sim)\cdot\psi - G^\sim\cdot t(\psi))\, dS \\ &= \psi\,.\end{aligned}$$

Here we used that we can add $\int ((\Delta^* + \rho\omega^2)(\psi)\cdot G^\sim)\, dV$ since ψ is regular and annihilated by $\Delta^* + \rho\omega^2$ and at the last equality sign orthogonality at infinity. Hence $(\Delta^* + \rho\omega^2)G^\sim = \delta$ on regular basis functions, i.e. like a delta function kernel. Thus $G^\sim$ is a candidate for a Green's function.

B.2 Derivation using transverse gradient

Let us in the following put $\mathbf{\Delta r} = \mathbf{r_2} - \mathbf{r_1}$. Assume $r_> = r_2$ and $r_< = r_1$. The gradient will be $\nabla = \nabla_2 = \nabla_>$.

First notice that:

$$\mathbf{G}(\mathbf{\Delta r}) = \frac{1}{4i\rho\omega^2}\left((k_T^2\mathbf{1} + \nabla\otimes\nabla)H_0^{(1)}(k_T\Delta r) - \nabla\otimes\nabla H_0^{(1)}(k_L\Delta r)\right)\,. \tag{B.1}$$

Second that (A. Wirzba):

$$(k_T^2\mathbf{1} + \nabla\otimes\nabla)H_0^{(1)}(k_T\Delta r) = -(\nabla\times\hat{z})\otimes(\nabla\times\hat{z})H_0^{(1)}(k_T\Delta r)\,. \tag{B.2}$$

This can be seen in Cartesian components (and hence in all other coordinate systems) as follows:

$$\begin{aligned}-(\nabla\times\hat{z})\otimes(\nabla\times\hat{z})_{af}H_0^{(1)}(k_T\Delta r) &= -\epsilon_{abc}\partial_b z_c\,\epsilon_{fgh}\partial_g z_h H_0^{(1)}(k_T\Delta r) \\ &= -\epsilon_{ab3}\partial_b\epsilon_{fg3}\,\partial_g H_0^{(1)}(k_T\Delta r)\,, \end{aligned}\tag{B.3}$$

which in matrix form is

$$\begin{pmatrix} -\partial_2^2 & \partial_1\partial_2 \\ \partial_1\partial_2 & -\partial_1^2 \end{pmatrix} H_0^{(1)}(k_T\Delta r)\,. \tag{B.4}$$

Now the statement (B.2) holds iff:

$$\begin{pmatrix} -\partial_2^2 & \partial_1\partial_2 \\ \partial_1\partial_2 & -\partial_1^2 \end{pmatrix} H_0^{(1)}(k_T\Delta r) = \left(k_T^2 \begin{pmatrix} 1 & 0 \\ 0 & 1 \end{pmatrix} + \begin{pmatrix} \partial_1^2 & \partial_1\partial_2 \\ \partial_1\partial_2 & \partial_2^2 \end{pmatrix}\right) H_0^{(1)}(k_T\Delta r). \tag{B.5}$$

Here the non-diagonal elements are identical and the diagonal elements are the same iff:

$$(\Delta + k_T^2)H_0^{(1)}(k_T\Delta r) = 0\,. \tag{B.6}$$

This, however, is known from scattering theory.

Summarizing we get:

$$\begin{aligned} \mathbf{G}(\mathbf{\Delta r}) &= \frac{1}{4i\rho\omega^2} \\ &\quad \times \left(-(\nabla\times\hat{z})\otimes(\nabla\times\hat{z})H_0^{(1)}(k_T\Delta r) - (\nabla\otimes\nabla)H_0^{(1)}(k_L\Delta r)\right)\,. \end{aligned} \tag{B.7}$$

Next we decompose the Hankel function using again results from the scalar case:

$$\begin{aligned} G_{scalar}(\Delta r) &= \frac{1}{4i}H_0^{(1)}(k\Delta r) \\ &= \frac{1}{4i}\sum_{m=-\infty}^{\infty} J_m(kr_<)H_m^{(1)}(kr_>)e^{\pm im\Delta\phi}\,, \end{aligned} \tag{B.8}$$

with $\Delta\phi = \phi_2 - \phi_1$.

Since the gradient acts on a function of Δr we can trade off $\nabla = \nabla_> = -\nabla_<$. Hence we can also decompose the differential operator in the vector case such that the part with $\nabla_>$ acts on $r_>$ etc. :

$$\begin{aligned}
\mathbf{G}(\mathbf{\Delta r}) &= \frac{1}{4i\rho\omega^2}\sum_{m=-\infty}^{\infty}\nabla_<(J_m(k_L r_<)e^{-im\phi_<})\otimes\nabla_>(H_m^{(1)}(k_L r_>)e^{im\phi_>}) \\
&+ (\nabla_<\times\hat{z}J_m(k_T r_<)e^{-im\phi_<})\otimes(\nabla_>\times\hat{z}H_m^{(1)}(k_T r_>)e^{im\phi_>}) \\
&= \frac{1}{4i\rho\omega^2}\sum_n \psi_{\mathbf{n}}^{\wedge\sim}(\mathbf{r}_<)\otimes\psi_{\mathbf{n}}^{(+)}(\mathbf{r}_>)\,. \qquad \text{(B.9)}
\end{aligned}$$

The last equality sign is by definition of the basis functions. Here n is a multi index describing the angular momentum and the polarization.

Appendix C

Translation matrices and their composition

The following concepts are introduced for practical convenience. Several times we consider the normal modes in new coordinate systems. Physically this corresponds to a unitary transformation.

To write a normal mode of a given polarization (wave vector k) in system $S \in \{j, j', G\}$ to a disc system j we find from the addition theorem for Bessel functions:

$$\psi_n^{(Z)}(X^{(S)}) = \sum_l T_{nl}^{(Z)Sj}\, \psi_l^{\wedge}(X^{(j)})\,, \tag{C.1}$$

where $Z \in \{\wedge, +, -\}$ and

$$T_{nl}^{(Z)Sj} = (-1)^l Z_{n-l}(kR_{Sj})\, e^{i(n\theta_j^{(S)} - l\theta_S^{(j)})} \tag{C.2}$$

with

$$Z_n = \begin{cases} J_n & \text{for } Z = \wedge \\ H_n^{(1)} & \text{for } Z = (+) \\ H_n^{(2)} & \text{for } Z = (-) \end{cases} . \tag{C.3}$$

Here R_{Sj} indicates the distance between the origins of the two coordinate systems.

Typically one chooses the angle of the global coordinate system in any of the local systems to be equal π:

$$\theta_G^{(j)} = \pi. \tag{C.4}$$

From any system to the global system G:

$$\psi_n^{(Z)}(X^{(S)}) = \sum_l T_{nl}^{(Z)SG}\, \psi_l^{(Z)}(X^{(G)})\,, \tag{C.5}$$

where

$$T_{nl}^{(Z)SG} = (-1)^l J_{n-l}(kR_S)\, e^{i(n\theta_j^{(S)} - l\theta_S^{(j)})}\,. \tag{C.6}$$

Also composition is possible e.g.:

$$T^{+jG} \cdot T^{\wedge Gj} = 1 \tag{C.7}$$

and

$$T^{+jG} \cdot T^{\wedge Gj'} = T^{\wedge jj'}\,. \tag{C.8}$$

Appendix D

Calculation of boundary integrals

Below we shall suppress the polarization indices. Thus in some cases " l" may refer to angular momentum l and either pressure or shear and is thus a multi-index. $\mathbf{B}_m$ does not carry a polarization index whereas a_m, ψ_l and T_{nl} do. Finally the condensed matrix representation uses the brackets [].

I_j^j :

$$\begin{aligned} I_j^j &= \int_{\partial_j} ds\, u(s) \cdot t(G(s, X^{(j)})) \\ &= \frac{1}{4i\rho\omega^2} \int_{\partial_j} ds \sum_{m,l} \mathbf{B}_m^{(j)} e^{im\theta} \cdot \mathbf{t}(\psi_l^{(+)\sim}(s))\, \psi_l^{\wedge}(X^{(j)}) \\ &= \frac{\pi a_j}{2i\rho\omega^2} \sum_l \mathbf{B}_l^{(j)} \cdot \mathbf{t}(\psi_l^{(+)\sim}(a_j, \theta = 0))\, \psi_l^{\wedge}(X^{(j)}) \\ &= \frac{\pi a_j}{2i\rho\omega^2} \mathbf{B}_l^{(j)} \cdot [\mathbf{t}(\psi_l^{(+)\sim}(a_j))] \cdot [\psi_l^{\wedge}(X^{(j)})]^t. \end{aligned} \tag{D.1}$$

Above the reader may put $l = (l\,\alpha)$ on the second and third line. Here we used the dyadic form of the Green's function. We notice that we can put the "$\sim$" on either the regular or the outgoing part of the Green's tensor. The traction operator must act on the outgoing part (C. Chandre: $|X| = r_<$, since X is just inside the cavity). Next we can integrate over the boundary using the orthonormality of the Fourier basis giving a factor $2\pi a_j\, \delta_{lm}$.

$I_{j'}^j$:

Now the traction operator, $\mathbf{t} = \mathbf{t}_s$, has to act on the regular part. This is because the point at the disc j, $X^{(j)}$, can be assumed further away than the initial integration

point $s = s^{(j')}$ as seen from the disc j' . That is $r_< = s$ in the regular part.

$$\begin{aligned} I^j_{j'} &= \int_{\partial_{j'}} ds\, u(s) \cdot t(G(s, X^{(j')})) \\ &= \frac{1}{4i\rho\omega^2} \int_{\partial_{j'}} ds \sum_{m,l} \mathbf{B}^{(j')}_m e^{im\theta} \cdot \mathbf{t}(\psi^{(\wedge)\sim}_l(s))\, \psi^+_l(X^{(j')}) \\ &= \frac{\pi a_{j'}}{2i\rho\omega^2} \sum_{l,n} \mathbf{B}^{(j')}_l \cdot \mathbf{t}(\psi^{\wedge\sim}_l(a_{j'}, \theta' = 0)) T^{+j'j}_{ln} \psi^\wedge_n(X^{(j)}) \\ &= \frac{\pi a_{j'}}{2i\rho\omega^2} \mathbf{B}^{(j')}_l \cdot [\mathbf{t}(\psi^{\wedge\sim}_l(a_{j'}))] \cdot T^{+j'j}_{ln} \cdot [\psi^\wedge_n(X^{(j)})]^t . \end{aligned} \tag{D.2}$$

Above the reader may put $l = (l\,\alpha)$ $n = (n\,\beta)$ on the second and third line. For the third equality we applied a translation operator. Thus if the (multi-) index corresponds to a pressure state:

$$T^{+Pj'j}_{ln} = (-1)^n H^{(1)}_{l-n}(\alpha R_{j'j}) e^{i(l\phi^{(j')}_j - n\phi^{(j)}_{j'})}. \tag{D.3}$$

I^j_∞ :

Inserting the expansion at infinity and the Green's function we get

$$\begin{aligned} I^j_\infty &= \int_{\partial_\infty} ds\, (u(s) \cdot t(G(s, X^{(G)})) - t(u(s)) \cdot G(s, X^{(G)})) \\ &= \frac{1}{8i\rho\omega^2} \sum_{i,l} a_i \int_{\partial_\infty} ds\ ((\delta_{il}\psi^{(-)}_l + S_{il}\, \psi^{(+)}_l)(s) \cdot \mathbf{t}(\psi^{(+)\sim}_l(s))\, \psi^\wedge_l(X^{(G)}) \\ &\quad -((\delta_{il}\mathbf{t}(\psi^{(-)}_l) + S_{il}\, \mathbf{t}(\psi^{(+)}_l))(s) \cdot \psi^{(+)\sim}_l(s))\, \psi^\wedge_l(X^{(G)})) \\ &= \sum_i a_i \psi^\wedge_i(X^{(G)}) \\ &= \sum_{i,l} a_i T^{\wedge Gj}_{il} \psi^\wedge_l(X^{(j)}) \\ &= a_i \cdot T^{\wedge Gj}_{il} \cdot [\psi^\wedge_l(X^{(j)})]^t . \end{aligned} \tag{D.4}$$

For this situation $s = r_>$ and therefore the traction has to act on the outgoing part. Orthogonality at infinity was used at the third equality sign.

I^r_j :

The calculation is similar to $I^j_{j'}$. Here the final point goes to infinity so $X^{(j)} = r = r_>$ whereas $s = r_<$. However, now we just translate to the global coordinate system in

the end.

$$\begin{aligned} I_j^r &= \int_{\partial_j} ds\, u(s)\cdot t(G(s,X^{(j)}=r)) \\ &= \frac{1}{4i\rho\omega^2}\int_{\partial_j} ds\, \sum_{m,l}\mathbf{B}_m^{(j)} e^{im\theta}\cdot \mathbf{t}(\psi_l^{(\wedge)\sim}(s))\,\psi_l^+(X^{(j)}) \\ &= \frac{\pi a_j}{2i\rho\omega^2}\sum_{l,n}\mathbf{B}_l^{(j)}\cdot \mathbf{t}(\psi_l^{\wedge\sim}(a_j,\theta=0))T_{ln}^{+jG}\psi_n^+(X^{(G)}) \\ &= \frac{\pi a_j}{2i\rho\omega^2}\,\mathbf{B}_l^{(j)}\cdot[\mathbf{t}(\psi_l^{\wedge\sim}(a_j))]\cdot T_{ln}^{+jG}\cdot[\psi_n^{(+)}(X^{(G)})]^t. \end{aligned} \tag{D.5}$$

I_∞^r **:**

Here the calculation is just like I_∞^j. The only simplification is that we do not translate in the end to the j-system but stay in the global system.

$$\begin{aligned} I_\infty^r &= \int_{\partial_\infty} ds\,(u(s)\cdot t(G(s,X^{(G)})) - t(u(s))\cdot G(s,X^{(G)})) \\ &= \frac{1}{8i\rho\omega^2}\sum_{i,l} a_i \int_{\partial_\infty} ds\ ((\delta_{il}\psi_l^{(-)} + S_{il}\,\psi_l^{(+)})(s)\cdot \mathbf{t}(\psi_l^{(+)\sim}(s))\,\psi_l^\wedge(X^{(G)}) \\ &\quad -(\delta_{il}\mathbf{t}(\psi_l^{(-)}) + S_{il}\,\mathbf{t}(\psi_l^{(+)}))(s)\cdot\psi_l^{(+)\sim}(s))\,\psi_l^\wedge(X^{(G)})) \\ &= \sum_i a_i\psi_i^\wedge(X^{(G)}) \\ &= a_i\cdot[\psi_i^\wedge(X^{(G)})]^t\,. \end{aligned} \tag{D.6}$$

Assembly of the M-matrix :

First we have the relationship

$$I_\infty^j - (I_j^j + \sum_{j'\neq j} I_{j'}^j) = 0 \tag{D.7}$$

among discs. The difference in signs come from the boundary normal vector being opposite. Including all indices we get in the basis of $\psi^\wedge$:

$$\begin{aligned} \sum_{l\pi} a_{l\pi} T_{l\pi;n\sigma}^{\wedge Gj} &= \frac{\pi a_j}{2i\rho\omega^2}\sum_{l\pi}\mathbf{B}_l^{(j)}\cdot\mathbf{t}(\psi_{l\pi}^{(+)\sim}(a_j,\theta=0))\delta_{l\pi;n\sigma} \\ &+ \sum_{j'\neq j}\frac{\pi a_{j'}}{2i\rho\omega^2}\sum_{l\pi}\mathbf{B}_l^{(j')}\cdot\mathbf{t}(\psi_{l\pi}^{\wedge\sim}(a_{j'},\theta'=0))T_{l\pi;n\sigma}^{+j'j}\,. \end{aligned} \tag{D.8}$$

That is

$$\begin{aligned} a_l \cdot T_{ln}^{\wedge Gj} &= \frac{\pi a_j}{2i\rho\omega^2}\,\delta_{ln}\mathbf{B}_l^{(j)} \cdot [\mathbf{t}(\psi_{l\pi}^{(+)\sim}(a_j))] \\ &+ \sum_{j'\neq j} \frac{\pi a_{j'}}{2i\rho\omega^2} \sum_{l\pi} \mathbf{B}_l^{(j')} \cdot [\mathbf{t}(\psi_l^{\wedge\sim}(a_{j'}))] \cdot T_{ln}^{+j'j}\,. \end{aligned} \tag{D.9}$$

In the above the traction $\mathbf{t}$ as the boundary data $\mathbf{B}$ refer actual physical vectors and hence are coordinate free. We now write everything in say global coordinates. Normalizing gives us a matrix equation:

$$\mathbf{a} \cdot \mathbf{C}^{\mathbf{j}} = \sum_{\mathbf{j}'} \mathbf{B}^{\mathbf{j}'} \cdot \mathbf{M}^{\mathbf{j}'\mathbf{j}} \tag{D.10}$$

with

$$\begin{aligned} \mathbf{M}_{na;lb}^{jj'} &= \delta_{jj'}\delta_{ln}\delta_{ab} + (1-\delta_{jj'}) \\ &\times \frac{a_j}{a_{j'}} \sum_{\sigma,\pi\in\{P,S\}} ([\mathbf{t}(\psi_{n\sigma}^{\wedge\sim})(a_j)] \cdot \mathbf{T}_{n\sigma;l\pi}^{+jj'} \cdot [\mathbf{t}(\psi_{l\pi}^{+\sim}(a_{j'})]^{-1})_{ab}\,. \end{aligned} \tag{D.11}$$

The next chapter explains further the $[\mathbf{t}(\psi)]$-terms.

Appendix E

Traction matrices

In the actual calculation of the traction of the basis functions we use polar coordinates. Therefore we use the covariant derivative. In these coordinates the basis vectors no longer are constants:

$$\nabla\hat{\mathbf{r}} = \frac{1}{r}\,\hat{\theta}\,\hat{\theta} \tag{E.1}$$

$$\nabla\hat{\theta} = -\frac{1}{r}\,\hat{\mathbf{r}}\,\hat{\theta}\,. \tag{E.2}$$

whereas on functions

$$\nabla f = \partial_r f\,\hat{\mathbf{r}} + \frac{1}{r}\partial_\theta f\,\hat{\theta}\,. \tag{E.3}$$

For a displacement field $\mathbf{u}$ the traction on a circular boundary ($\hat{\mathbf{r}} = \mathbf{n}$) is:

$$\mathbf{t} = \sigma\cdot\hat{\mathbf{r}} = (\lambda\nabla\cdot\mathbf{u}\,\mathbf{1} + \mu(\nabla\mathbf{u} + \mathbf{u}\nabla))\cdot\hat{\mathbf{r}}\,, \tag{E.4}$$

with $\mathbf{1} = \hat{\mathbf{r}}\,\hat{\mathbf{r}} + \hat{\theta}\,\hat{\theta}$.

Assuming the displacement field given by potentials $\mathbf{u} = \nabla\phi + \nabla\times(\hat{\mathbf{z}}\psi)$ the traction vector is found after some calculation to be

$$\begin{aligned}\mathbf{t} &= \begin{pmatrix}\sigma_{rr}\\ \sigma_{r\theta}\end{pmatrix}\\ &= \begin{pmatrix}\lambda\Delta\phi + 2\mu(\frac{\partial^2\phi}{\partial r^2} + \partial_r(\frac{1}{r}\partial_\theta\psi))\\ \mu(2(\frac{\partial_r\partial_\theta\phi}{r} - \frac{\partial_\theta\phi}{r^2}) + \frac{\frac{\partial^2\psi}{\partial\theta^2}}{r^2} - r\partial_r(\frac{1}{r}\partial_r\psi))\end{pmatrix}.\end{aligned} \tag{E.5}$$

Next we use partial waves as pressure and shear potentials. Calculating for an outgoing state with angular dependence $e^{-im\theta}$ using recurrence relations for the Bessel functions [35]:

$$
\begin{aligned}
[\mathbf{t}(\psi)_m^{+\sim}] &= \begin{pmatrix} t(P_m)_r^{+\sim} & t(S_m)_r^{+\sim} \\ t(P_m)_\theta^{+\sim} & t(S_m)_\theta^{+\sim} \end{pmatrix} = \frac{2\mu}{a^2} \qquad \text{(E.6)} \\
\times &\begin{pmatrix} (m^2+m-\frac{1}{2}a^2\beta^2)H_m^{(1)}(a\alpha) - a\alpha H_{m-1}^{(1)}(a\alpha) & im((m+1)H_m^{(1)}(a\beta) - a\beta H_{m-1}^{(1)}(a\beta)) \\ im((m+1)H_m^{(1)}(a\alpha) - a\alpha H_{m-1}^{(1)}(a\alpha)) & a\beta H_{m-1}^{(1)}(a\beta) - (m^2+m-\frac{1}{2}a^2\beta^2)H_m^{(1)}(a\beta) \end{pmatrix}.
\end{aligned}
$$

Here we have posed $\theta = 0$ in the end. In $[\mathbf{t}(\psi_m)] = [\mathbf{t}(\psi_m)_{a\pi}]_{a\in\{r,\theta\},\pi\in\{P,S\}}$ has a spatial index a and a polarization index π.

This can also be expressed in terms of the derivative of a Hankel function as follows:

$$
\begin{aligned}
[\mathbf{t}(\psi)_m^{+\sim}] &= \frac{2\mu}{a^2} \\
\times &\begin{pmatrix} (m^2-\frac{1}{2}a^2\beta^2)H_m^{(1)}(a\alpha) - a\alpha H_m^{(1)'}(a\alpha) & im(H_m^{(1)}(a\beta) - a\beta H_m^{(1)'}(a\beta)) \\ im(H_m^{(1)}(a\alpha) - a\alpha H_m^{(1)'}(a\alpha)) & a\beta H_m^{(1)'}(a\beta) - (m^2-\frac{1}{2}a^2\beta^2)H_m^{(1)}(a\beta) \end{pmatrix}. \qquad \text{(E.7)}
\end{aligned}
$$

Thus changing $m \to -m$ gives a besides a factor $(-1)^m$ also a sign change on the off-diagonal elements.

Appendix F

Symmetry factorization

We shall use the presence of a symmetry group to reduce the calculation of the spectral determinants into factors each belonging to irreducible representations.

Thus for two cavities of equal size the the symmetry group is that of a rectangle C_{2v} whereas three-cavities aranged in an equilateral triangle will obey C_{3v}-symmetry. These symmetries will be reflected on the level of the spectrum for the scattering matrix. The former decomposes into parts belonging to irreducible representations for the group. The character table is given by table 3.1.

We shall assume the cavities symmetrically arranged with respect to a given origo. For the two cavity system we assume the *centers on the x-axis*. Furthermore the cavity-radii are equal ($= a$). For the group considered there is one rotation and two reflections. The rotation C_2 will be around the global point of center whereas the reflections σ_i will be along the coordinate axes.

The translation matrix from one cavity to another will have the form:

$$\begin{aligned} [T_{ml}^{+12}] &= (-1)^m \begin{pmatrix} H_{m-l}^{(1)}(\alpha R) & 0 \\ 0 & H_{m-l}^{(1)}(\beta R) \end{pmatrix} \\ &\equiv (-1)^m [T_{m-l}] \end{aligned}$$

The vectorial boundary data will transform under the symmetry group. With respect to reflections along the x-axis we find

$$B_m e^{im\theta} \mapsto B_m \cdot \sigma_z \; e^{-im\theta} \, .$$

Here

$$\sigma_z = \begin{pmatrix} 1 & 0 \\ 0 & -1 \end{pmatrix}$$

is a Pauli-matrix and B the coordinates of the vector data.

Symmetrizing the expansion of the wave function $\mathbf{u}$ with respect to σ_x:

$$\begin{aligned} u &= \sum_m \frac{1}{2} \left(B_m \, e^{im\theta} \pm B_m \cdot \sigma_z \, e^{-im\theta} \right) \\ &\equiv \sum_m b_m e^{im\theta} \, , \end{aligned} \tag{F.1}$$

where in general

$$b^{(1)}_{-m} = \chi(\sigma_x) \, b^{(2)}_m \cdot \sigma_z = \pm \, b^{(1)}_m \cdot \sigma_z \tag{F.2}$$

with e.g. plus for a symmetric configuration.

Likewise the action of C_2 allows us to relate boundary data on different cavities:

$$b^{(2)}_m = \chi(C_2) \, b^{(1)}_m \, . \tag{F.3}$$

To calculate the inter-cavity matrix we use (3.4) and calculate the boundary integrals I^j_j and $I^j_{j'}$ with $j' \neq j$. We remark that we do not have to consider the boundary at infinity. The results will be sums over basis functions. Let us assume the final cavity, $j = 2$. We shall calculate the coupling of the boundary data with index m to the displacement field basis vector of index l. We consider the main case with l, m positive using the results of chapter D:

From the opposite cavity, cavity 1:

$$b^1_m \cdot [t^{1\wedge}_m] \cdot [T_{ml}] \cdot [\psi^2_l]^t \, .$$

From the opposite cavity with negative angular momentum:

$$b^1_{-m} \cdot [t^{1\wedge}_{-m}] \cdot [T_{-ml}] \cdot [\psi^2_l]^t \, .$$

From itself

$$b_m^2 \cdot \delta_{lm} [t_l^{2+}] \cdot [\psi_l^2]^t \,.$$

Here we have omitted $\sim$ in the traction matrices. To reverse the order in the traction matrix $m := -m$ gives besides $(-1)^m$ also a minus sign in the off-diagonal elements. The action of flipping these elements can be obtained as follows:

$$\mathbf{t} \mapsto \sigma_z \cdot \mathbf{t} \cdot \sigma_z \,. \tag{F.4}$$

The coefficient from the cavities of the basis function with index $l > 0$ becomes:

$$(-1)^m [t_m^{1\wedge}] \cdot T_{m-l} + (-1)^{(l+m)} \sigma_z \cdot (\sigma_z \cdot [t_m^{1\wedge}] \cdot \sigma_z) \cdot T_{m+l} + [t_l^{2+}] \delta_{lm} \,. \tag{F.5}$$

By dividing and using $\sigma_z^2 = \mathbf{1}$ we find the inter-cavity matrix (3.50):

$$\delta_{lm} + (-1)^m \, \chi(C_2) \, [t_m^{1\wedge}] \cdot \Big(T_{m-l} + \chi(\sigma_x) \, (-1)^l \, T_{m+l} \cdot \sigma_z \Big) \cdot [t_l^{2+}]^{-1} \,, \tag{F.6}$$

since in coordinates $[t_l^{2+}] = [t_l^{1+}] = [t_l^+]$ and likewise for $[t_l^{1\wedge}]$.

We remark that if we had aligned the cavities along the y-axis we would have the character of σ_y instead. Therefore there is a certain ambiguity between the B_i-representations which are symmetric along one axis and anti-symmetric along another. The A_i-representations, however, are either fully symmetric or fully anti-symmetric and the results for these are independent of the alignment of the cavities. For (3.50) in the main text we use $\sigma_1 = \chi(C_2)$ and $\sigma_2 = \chi(\sigma_x)$ corresponding to x-axis alignment.

Appendix G

Wigner's time delay

Below we shall discuss the delays of wave packets for the two-cavity scattering system.

G.1 Delay of plane wave

This so-called Wigner delay is defined as

$$\begin{aligned} d(k) &= \frac{d}{dk}\mathrm{Arg}\left(\mathrm{Det}\left(\mathbf{S}(k)\right)\right) \\ &= -i\frac{d}{dk}\log\left(\mathrm{Det}\left(\mathbf{S}(k)\right)\right) \\ &= -i\,\mathrm{Tr}\left(\mathbf{S}^{\dagger}(k)\frac{d\mathbf{S}}{dk}(k)\right) \end{aligned} \tag{G.1}$$

and can be shown to equal the total delay of a wave packet in a scattering system [46, 47]. We shall review this fact below.

A related quantity is the total scattering *phase shift* $\Theta(k)$ defined as

$$\det\mathbf{S}(k) = e^{+i\,\Theta(k)}\,,$$

so that $d(k) = \frac{d}{dk}\Theta(k)$.

The time delay may be both positive and negative, reflecting attractive respectively repulsive features of the scattering system.

To elucidate the connection between the scattering determinant and the time delay we study a plane wave:

The phase of a wave packet will have the form:

$$\phi = \vec{k} \cdot \vec{x} - \omega\, t \ (+\Theta)\,.$$

Here the term in the parenthesis refers to the phase shift that will occur if scattering is present. The center of the wave packet will be determined by the principle of stationary phase:

$$0 = d\phi = d\vec{k} \cdot \vec{x} - d\omega\, t \ (+d\Theta)\,.$$

Hence the packet is located at

$$\vec{x} = \frac{\partial \omega}{\partial \vec{k}}\, t \ \left(-\frac{\partial \Theta}{\partial \vec{k}} \right) .$$

The first term is just the group velocity times the given time t. Thus the the packet is retarded by a length given by the derivative of the phase shift with respect to the wave vector $\vec{k}$. The arrival of the wave packet at the position $\vec{x}$ will therefore be delayed. This *time delay* can similarly be found as

$$\tau(\omega) = \frac{\partial \Theta(\omega)}{\partial \omega}.$$

To show this we introduce the *slowness* of the phase $\vec{s} = \vec{k}/\omega$ for which $\vec{s} \cdot \vec{v}_g = 1$, where $\vec{v}_g$ is the group velocity to get

$$d\vec{k} \cdot \vec{x} = \vec{s} \cdot \vec{x}\, d\omega = \frac{x}{v_g}\, d\omega\,,$$

since we may assume $\vec{x}$ is parallel to the group velocity (consistent with the above). Hence the arrival time becomes

$$t = \frac{x}{v_g} \ \left(+\frac{\partial \Theta(\omega)}{\partial \omega} \right) .$$

If the scattering matrix is non-diagonal one next interprets

$$\Delta t_{ij} = Re(-i\, S_{ij}^{-1} \frac{\partial S_{ij}}{\partial \omega}) =: Re(\, \frac{\partial \Theta_{ij}}{\partial \omega})$$

as the delay in the j'th scattering channel after an injection in the i'th. The probability for appearing in channel j goes as $|S_{ij}|^2$ and therefore the average delay for the incoming states in channel i is

$$\begin{aligned} < \Delta t_i > &= \sum_j |S_{ij}|^2 \Delta t_{ij} \\ &= Re(-i \sum_j S_{ij}^* \frac{\partial S_{ij}}{\partial \omega}) \\ &= Re(-i\, \mathbf{S}^\dagger \cdot \frac{\partial \mathbf{S}}{\partial \omega})_{ii} \\ &= (-i\, \mathbf{S}^\dagger \cdot \frac{\partial \mathbf{S}}{\partial \omega})_{ii}\,, \end{aligned}$$

where we have used the derivative, $\partial/\partial\omega$, of the unitarity relation $\mathbf{S} \cdot \mathbf{S}^\dagger = \mathbf{1}$ valid for real frequencies. This discussion can in particular be made for wave packets related to partial waves and superpositions of these like an incoming plane wave corresponding to free motion (3.14). The total Wigner delay therefore corresponds to the sum over all channel delays (G.1).

G.2 Excess level density

For another interpretation of the Wigner Delay [2, 7], consider the Krein-Friedel-Lloyd formula in terms of the wave number:

$$\mathrm{Im\,Tr}\,(\mathbf{S}^\dagger \cdot \frac{\partial \mathbf{S}}{\partial \mathrm{k}}) = 2\pi\,(g(k) - g_0(k)) =: 2\pi\,\Delta g(k)$$

which expresses the change of level density $g(k)$ from a free system to a system with a potential. In our case the perturbation comes from the cavities. The right hand side of the above is calculated in the limit of an enclosing box going to infinity, followed by taking the limit $k \equiv k + i\epsilon \to k$ for $\epsilon \to 0+$. This result is also referred to as the spectral shift theorem.

G.3 Cluster delay and symmetries

As we have shown, the total scattering determinant factorizes into a product of the individual single cavity scattering determinants and an inter-cavity or *cluster* determinant. Each of these functions will contribute to the total phase shift additively. The single cavity is already understood and its contribution can be taken out, both

theoretically and experimentally. The latter is achieved by measuring the phase shift for single cavities before the multi-cavity case is considered. We emphasize that in the following we study the delay from the cluster and *not* the total delay. In our resonance search in the complex $k_L a$-plane we focused on the modulus of this function (poles). By studying the Wigner time delay, however, the emphasis is on the *phase*.

The effect of a symmetry group will be the following: The total time delay can be written as a sum over delays for the irreducible representations (counted with their multiplicities). This follows from above since the scattering determinant will factorize over each irreducible representation.

Experimentally one can measure the total phase shift and hence calculate the time delay. Further one can measure the phase shift and time delay for each of the irreducible representations by placing detectors and/or transmitters symmetrically. For the two cavity system it suffices to perform the measurements with say one transmitter and four receivers. One measures the response (amplitude and phase) at the four symmetrically positioned receivers. Next, one constructs the response at a given detector for a symmetrized incoming wave packet. Using the already measured fields this response can be found by applying the corresponding symmetry operations on the fields. Finally the phase shift at the given point is extracted.

Numerically we have access to the symmetry reduced phase shift and in our calculation we present the associated delay for each irreducible representation. Using the formula above we approximate the derivative with a centered difference. In chapter 5 we have shown plots for each irreducible representation where the abscissa is the longitudinal size parameter $k_L a$ and the ordinate the delay.

Appendix H

Ray matrices

H.1 Refraction and reflection

We consider a ray incident on a surface fig. 2.2. The outgoing ray has in general a different angle of incidence as described by Snell' s law. We investigate the result of a variation of the in going wave in order to find the corresponding differential. For definiteness we think of an incoming S-wave refracting to a P-wave.

Some notation: We use the index "$-$" to describe the incoming wave and "$+$" the outgoing. The direction of the waves are given by a unit vector $\mathbf{e}$ and the normal of the surface is given by a unit vector $\mathbf{n}$. The linear operation of rotating 90° counter-clockwise vectors is denoted by a "cech" , e.g.. $\check{\mathbf{n}}$ is now a vector lying in the tangent plane of the surface. The direction of the wave is now parametrized by some angle, i.e..

$$\mathbf{e} = \begin{pmatrix} \cos(\theta) \\ \sin(\theta) \end{pmatrix} \tag{H.1}$$

and therefore a variation of the direction is

$$d\mathbf{e} = \begin{pmatrix} -\sin(\theta) \\ \cos(\theta) \end{pmatrix} d\theta = \check{\mathbf{e}}\, d\theta\,. \tag{H.2}$$

A variation in the transverse direction of the ray will be described by the vector

$$d\mathbf{z} = dz\, \check{\mathbf{e}}\,. \tag{H.3}$$

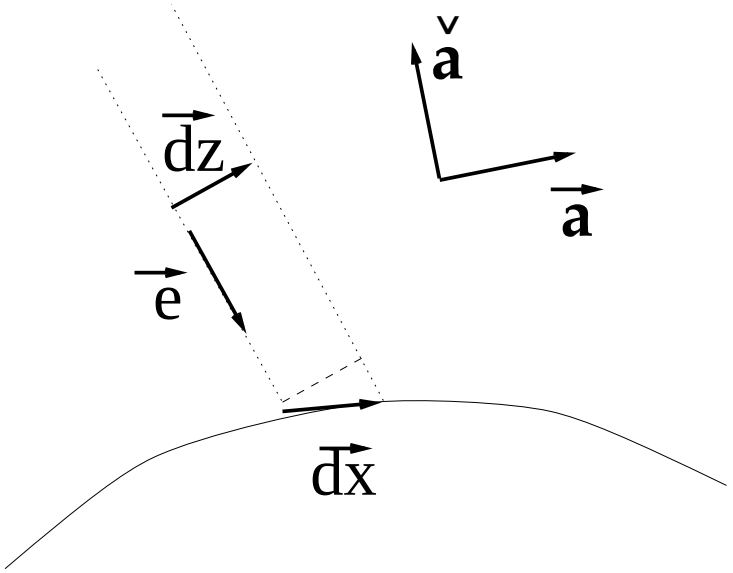

Figure H.1: The shadow of the transverse displacement on the boundary

By considering fig. H.1 it is clear that this variation is related to a variation of the point of incidence on the boundary (i.e.. a tangent vector) $d\mathbf{x}$ in the following way (dyadic notation):

$$\check{\mathbf{e}}\check{\mathbf{e}} \cdot d\mathbf{x} = d\mathbf{z} \,. \tag{H.4}$$

Thus $dz = \check{\mathbf{e}} \cdot d\mathbf{x}$. Since $d\mathbf{x}$ is a tangent vector we have

$$d\mathbf{x} = \check{\mathbf{n}}(\check{\mathbf{n}} \cdot d\mathbf{x}) \tag{H.5}$$

implying

$$dz = \check{\mathbf{e}} \cdot \check{\mathbf{n}}(\check{\mathbf{n}} \cdot d\mathbf{x}) = (\mathbf{e} \cdot \mathbf{n})(\check{\mathbf{n}} \cdot d\mathbf{x}) \,. \tag{H.6}$$

Thus

$$d\mathbf{x} = \check{\mathbf{n}} \frac{dz}{(\mathbf{n} \cdot \mathbf{e})} \,. \tag{H.7}$$

The change in the normal vector is given by

$$d\mathbf{n} = \frac{d\mathbf{x}}{R} \,, \tag{H.8}$$

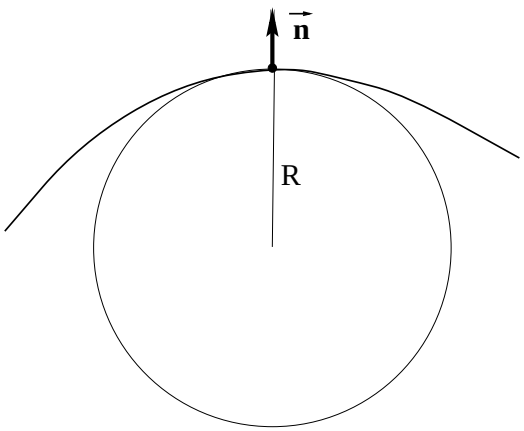

Figure H.2: Local curvature

where R is the local radius of curvature :

Therefore

$$d\mathbf{n} = \check{\mathbf{n}} \frac{dz}{(\mathbf{n}\cdot\mathbf{e})R} \,. \tag{H.9}$$

This gives

$$dz_+ = \frac{(\mathbf{n}\cdot\mathbf{e}_+)}{(\mathbf{n}\cdot\mathbf{e}_-)}\, dz_- = -\frac{\cos(\theta_+)}{\cos(\theta_-)}\, dz_- \,. \tag{H.10}$$

Furthermore

$$d\check{\mathbf{n}} = -\mathbf{n} \frac{dz}{(\mathbf{n}\cdot\mathbf{e})R} \,, \tag{H.11}$$

since $\check{\check{\mathbf{a}}} = -\mathbf{a}$ for any vector $\mathbf{a}$.

Let us derive Snell's law. The projected slowness on the border has to be conserved, i.e..

$$\check{\mathbf{n}}\check{\mathbf{n}}\cdot\mathbf{s}_- = \check{\mathbf{n}}\check{\mathbf{n}}\cdot\mathbf{s}_+ \,, \tag{H.12}$$

where the slowness vector is

$$\mathbf{s} = s\,\mathbf{e} \,. \tag{H.13}$$

Thus

$$(\check{\mathbf{n}} \cdot \mathbf{e}_-)s_- = (\check{\mathbf{n}} \cdot \mathbf{e}_+)s_+ \tag{H.14}$$

or when expressed in terms of angles

$$\frac{\sin(\phi_+)}{\sin(\phi_-)} = \frac{v_+}{v_-}\,, \tag{H.15}$$

where $v_\pm$ is the velocity.

Varying the projected slowness and using the expression for $d\check{\mathbf{n}}$ we find

$$d((\check{\mathbf{n}} \cdot \mathbf{e})\, s) = (-\frac{dz}{R} + (\mathbf{n} \cdot \mathbf{e})\, d\theta)\, s\,. \tag{H.16}$$

This differential element,1-form, is conserved allowing us to solve for the end angular variation $d\theta_+$. Defining $\kappa = \frac{v_+}{v_-}$ we get

$$d\theta_+ = -\left(\frac{\kappa}{\cos(\phi_+)} + \frac{1}{\cos(\phi_-)}\right)\frac{dz_-}{R} - \kappa\frac{\cos(\phi_-)}{\cos(\phi_+)}\, d\theta_-\,. \tag{H.17}$$

The differential $((dz_-, d\theta_-) \mapsto (dz_+, d\theta_+))$ therefore becomes

$$-\begin{pmatrix} \frac{\cos(\phi_+)}{\cos(\phi_-)} & 0 \\ \frac{1}{R}(\frac{\kappa}{\cos(\phi_+)} + \frac{1}{\cos(\phi_-)}) & \kappa\frac{\cos(\phi_-)}{\cos(\phi_+)} \end{pmatrix}\,. \tag{H.18}$$

This differential is the familiar reflection differential, when $\kappa = 1$:

$$-\begin{pmatrix} 1 & 0 \\ \frac{2}{R\cos(\phi_-)} & 1 \end{pmatrix}\,. \tag{H.19}$$

To find the differential when we have the opposite conversion, i.e.. from P-wave to S-wave, we just have to change the velocity ratio κ to $1/\kappa$ With wave split the differential has determinant κ respectively $1/\kappa$ ([10] find a similar result but in other coordinates). In a closed orbit however every time we have a conversion from S to P we also has to have the opposite, so the product of the differentials for the orbit will still have a determinant equal to 1.

H.2 Flight differential

An initial phase space point $(\mathbf{x}_-, \mathbf{v}_-)$ evolves during the time t to the point

$$(\mathbf{x}_+, \mathbf{v}_+) = (\mathbf{x}_- + \mathbf{v}_- t, \mathbf{v}_-). \tag{H.20}$$

Then it is not hard to find the differential

$$\begin{pmatrix} 1 & \Delta x \\ 0 & 1 \end{pmatrix}, \tag{H.21}$$

when we consider transverse displacements of the ray and angular variations of the velocity as above. Here Δx is the total flight length.

Bibliography

[1] P. Cvitanović, et al., *Classical and Quantum Chaos*, `www.nbi.dk/ChaosBook/` (Niels Bohr Institute, Copenhagen 2000).

[2] A. Wirzba, *Quantum Mechanics and Semiclassics of Hyperbolic n-Disk Scattering*, *Physics Reports* **309**, 1-116 (1999); `chao-dyn/9712015`.

[3] A. Wirzba, private communication.

[4] E.P. Wigner, *Proc. Fourth Can. Math. Congress*, (1957).

[5] G.S. Ezra, K. Richter, G. Tanner and D. Wintgen, *J. Phys. B,* **24**, L413 (1991).

[6] V. de Alfaro and T. Regge, *Potential Scattering* (North-Holland, Amsterdam 1965).

[7] W. Thirring, *A course in mathematical physics 3* (Springer, Wien 1979).

[8] V.I. Arnold, *Mathematical Methods of Classical Mechanics* (Springer, Berlin 1978).

[9] A. I. Borisenko and I. E. Tarapov, *Vector and tensor analysis with applications* (Dover, New York 1968).

[10] L. Couchmann, E. Ott and T.M. Antonsen, Jr., *"Quantum chaos in systems with ray splitting"*, *Phys. Rev. A* **46**, 6193 (1992).

[11] C.A. Brebbia, J.C.F. Telles and L.C. Wrobel, *Boundary Element Techniques* (Springer, Berlin 1984).

[12] Delsanto et al., in *Army Conference on applied mathematics and computing* , Transactions of the first Army conference on applied mathematics and computing, 773 (Research Triangle Park, N.C., U.S. Army Research Office 1984).

[13] J.L. Izbicki, J. M. Conoir, N. Veksler, *New results for Franz and Rayleigh waves propagationg around a cylindrical vacuum/solid interface*, *Wave Motion* **28**, 227 (1998).

[14] W. Franz, *Theorie der Beugung Elektromagnetischer Wellen*, (Springer, Berlin, 1954); Über die Greenschen Funktionen des Zylinders und der Kugel, *Z. Naturforschung* **9a**, 705 (1954).

[15] J.B. Keller and F.C. Karal, Jr., *Surface Wave Excitation and Propagation,J. Appl. Phys.* **31**, 1039 (1960).

[16] J.B. Keller and F.C. Karal, Jr., *Geometrical Theory of Elastic Surface-Wave Excitation and Propagation*, *J. Acoust. Soc. Am.* **36**, 32 (1964).

[17] L.D. Landau and E.M. Lifshitz, *Theory of Elasticity* (Pergamon, Oxford 1959).

[18] A.D. Pierce, R.N. Thurston and W.P. Mason eds., *Physical Acoustics* XV, XXI and XXII (Academic Press, New York 1981, 1992 and 1993).

[19] Y.H. Pao and C.C. Mow, *Diffraction of Elastic Waves and Dynamic Stress Concentrations* (Rand Corporation, New York 1971).

[20] J. Miklowitz and J.D. Achenbach, eds., *Modern Problems in Elastic Wave Propagation* (Wiley, New York 1978).

[21] M.J.P. Musgrave, *Crystal Acoustics* (Holden-Day, San Fransisco 1970).

[22] H. M. Nussenzveig, *Diffraction Effects in Semiclassical Scattering* (Cambridge, New York 1992).

[23] C. Ellegaard, T. Guhr, K. Lindemann, J. Nygaard and M. Oxborrow, *Symmetry Breaking and Spectral Statistics of Acoustic Resonances in Quartz Blocks*, *Phys. Rev. Lett.* **77**, 4918 (1996).

[24] L.E. Reichl, *The Transition to Chaos*, (Springer, New York 1992).

[25] B. Rulf, *Rayleigh Waves on Curved Surfaces*, *J. Acoust. Soc. Am.* **45**, 493 (1969).

[26] A. Selberg, *J. Indian Math. Soc.* **20**, 47 (1956).

[27] J.D. Achenbach, A.K. Gautesen and H. McMaken, *Ray Methods for Waves in Elastic Solids* (Pitman, Boston 1982).

[28] P. Cvitanović, C.P. Dettmann, R. Mainieri and G. Vattay, *Trace formulas for stochastic evolution operators: Weak noise perturbation theory*, *J. Stat. Phys.* **93**, 981 (1998); `chao-dyn/9807034`.

[29] P. Cvitanović, C.P. Dettmann, R. Mainieri and G. Vattay, *"Trace formulas for stochastic evolution operators: Smooth conjugation method"*, Nonlinearity **12**, 939 (1999); `chao-dyn/9811003`.

[30] P. Cvitanović, N. Søndergaard, C.P. Dettmann, G. Palla and G. Vattay, *"Spectrum of stochastic evolution operators: Local matrix representation approach"*, Phys. Rev. E **60**, 3936 (1999); `chao-dyn/9904027`.

[31] M.C. Gutzwiller, *J. Math. Phys.* **12**, 343 (1971).

[32] A. Holle, J. Main, G. Weibusch, H. Rottke and K.H. Welge, *Phys. Rev. Lett.* **61**, 161 (1988).

[33] B. Eckhardt and D. Wintgen: *J. Phys. B* **20**, 355 (1990).

[34] M.C. Gutzwiller, *Chaos in Classical and Quantum Mechanics* (Springer, New York 1990).

[35] M. Abramowitz and I. A. Stegun, *Handbook of mathematical functions with formulas, graphs and mathematical tables* (Dover, New York 1972).

[36] H.H. Rugh, "The Correlation Spectrum for Hyperbolic Analytic Maps", *Nonlinearity* **5**, 1237 (1992).

[37] G. Vattay and P.E. Rosenqvist, *Phys. Rev. Lett.* **76**, 335 (1996), `chao-dyn/9509015`; G. Vattay, *Phys. Rev. Lett.* **76**, 1059 (1996).

[38] R.B. Dingle, *Asymptotic Expansions: their Derivation and Interpretation* (Academic Press, London, 1973).

[39] N. Søndergaard, G. Vattay, G. Palla and A. Voros, *"Asymptotics of high order noise corrections"*, to appear in *J. Stat. Phys.* **101**; `chao-dyn/9911016` .

[40] A. Boström, *"Multiple scattering of elastic waves by bounded obstacles"*, *J. Acoust. Soc. Am.* **67**, 399 (1980).

[41] B. Peterson and S. Ström, *"Matrix formulation of acoustic scattering from an arbitrary number of scatterers"*, *J. Acoust. Soc. Am.* **56**, 771 (1974).

[42] P. Dahlqvist, *Escape from intermittent repellers - Periodic orbit theory for the crossover from exponential to algebraic decay*, *Phys. Rev. E* **60** , 6639 (1999); `chao-dyn/9903025`.

[43] P. Gaspard and A. Alonso, *"$\hbar$-expansion for the periodic-orbit quantization of hyperbolic systems"*, *Phys. Rev. A* **47**, R3468 (1993).

[44] M. Hamermesh, *Group theory and its application to physical problems* (Addison Wesley, Reading Mass. 1962).

[45] I.A. Viktorov, *Rayleigh and Lamb waves* (Plenum Press, New York, 1967).

[46] E.P. Wigner, *Phys. Rev.* **98**, 145 (1955).

[47] F.T. Smith, *Phys. Rev.* **118**, 349 (1960).